Technische Universität München

Fakultät für Medizin

Thioredoxin reductase 1 (Txnrd1) and Glutathione system are central to pancreatic homeostasis

Bailing Li

Vollständiger Abdruck der von der Fakultät für Medizin der Technischen Universität München zur Erlangung des akademischen Grades einer

Doktorin der Medizin (Dr. Med.)

genehmigten Dissertation.

Vorsitz: Prof. Dr. Wolfgang A. Weber

Prüfer*innen der Dissertation:

1. Prof. Dr. Roland M. Schmid

2. apl. Prof. Dr. Dr. Ihsan Ekin Demir

Die Dissertation wurde am 13.01.2023 bei der Fakultät für Medizin der Technischen Universität München eingereicht und durch die Fakultät für Medizin am 16.05.2023 angenommen.

Parts of this thesis were presented at the following scientific conferences:

1. Oral Presentation

Conference name: 28th United European Gastroenterology (UEG) Week Virtual 2020

Conference organizer: United European Gastroenterology

Conference date: October 11-13, 2020

Conference location: Virtual

Title: *Txnrd1* modulates the course of acute experimental pancreatitis by influencing NF-κB activity

Presenting author: Bailing Li

2. Oral Presentation

Conference name: II Med Retreat 2022

Conference organizer: Prof. Dr. Roland M. Schmid

Conference date: September 29-30, 2022

Conference location: Kloster Irsee

Title: Thioredoxin and glutathione systems are central to pancreatic recovery after experimental pancreatitis

Presenting author: Bailing Li

Table of Contents

LIST OF ABBREVIATIONS 5

ABSTRACT 7

ZUSAMMENFASSUNG 8

1. INTRODUCTION 9

1.1 Acute pancreatitis 9
1.1.1 Acute pancreatitis in human 10
1.1.2 Murine models of acute pancreatitis 11

1.2 Oxidants and antioxidants 13
1.2.1 Oxidative stress 13
1.2.2 Oxidants 13
1.2.3 Antioxidants 14

1.3 Oxidative stress in acute pancreatitis 17

1.4 Thioredoxin and thioredoxin reductases 18

1.5 Thioredoxin reductase 1 in the pancreas 20

1.6 Aim of this thesis 22

2. MATERIALS AND METHODS 23

2.1 Materials 23
2.1.1 Chemicals and Reagents 23
2.1.2 Buffers and Solutions 26
2.1.3 Antibodies used in the experiment and their usage 29
2.1.4 Kits 31
2.1.5 Laboratory devices and equipment 31
2.1.6 Software and algorithms 32

2.2 Methods 33
2.2.1 Generation of Txnrd1$^{\Delta panc}$ mouse model 33
2.2.2 Acute Pancreatitis of Pancreas-specific knockout mouse model 34
2.2.2.1 Mouse husbandry 34
2.2.2.2 Induction of acute pancreatitis in mice by caerulein 35
2.2.2.3 Dose and time point-finding of BSO treatment in wild-type mice . 36
2.2.2.4 Induction of glutathione depletion in mice by BSO treatment 36
2.2.2.5 Tissue harvesting and preparation of organs 37
2.2.2.6 Serum analysis 38
2.2.2.7 Preparation for paraffin-embedded organ sections 38
2.2.3 Polymerase chain reaction (PCR) 38
2.2.4 Acini and 3D acinar cell culture 40
2.2.5 Western blots 44

2.2.6 Histological analysis 46
2.2.6.1 Hemalaun-Eosin (H&E) Staining 46
2.2.6.2 Immunohistochemistry (IHC) Staining 47
2.2.7 Enzymatic assays 48
2.2.7.1 GSH / GSSG assay 48
2.2.7.2 Lactate dehydrogenase (LDH) assay 50
2.2.8 Statistical analysis 50

3. RESULTS 51

3.1 Experimentally induced acute pancreatitis in *Txnrd1* deficient pancreas .. 51

3.2 The glutathione system is upregulated in *Txnrd1* deficient pancreas 58

3.3 Investigation of the glutathione system as a compensatory mechanism in Txnrd1$^{\Delta panc}$ mice 61
3.3.1 Dose and time point finding for BSO treatment in wild-type mice 61
3.3.2 Investigation of the potential role of GSH in *Txnrd1* deficient pancreas 63

3.4 Glutathione in *Txnrd1* deficient pancreas protects against pancreatitis-induced injury. 72

3.5 In vitro glutathione depletion does not influence acinar integrity in Txnrd1$^{\Delta panc}$ animals 81

3.6 In vitro glutathione depletion inhibited ADM transdifferentiation in *Txnrd1* deficient animals 83

4. DISCUSSION 85

5. SUMMARY 90

6. REFERENCES 92

ACKNOWLEDGES 102

LIST OF ABBREVIATIONS

AP	acute pancreatitis
ADM	acinar-to-ductal metaplasia
BSO	buthionine sulfoximine
CAT	catalase
CCK	cholecystokinin
ER	endoplasmic reticulum
FAEEs	fatty acid ethyl esters
GSH	glutathione
GSSG	glutathione disulfide
GPX	glutathione peroxidase
H_2O_2	hydrogen peroxide
HOCl	hypochlorous acid
HOO	hydroperoxyl radical
MAP	mild acute pancreatitis
MSAP	moderately severe acute pancreatitis
$^{\bullet}NO$	nitric oxide radicals
$^{\bullet}NO_2^-$	nitrogen dioxide radicals
$^{\bullet}OH$	hydroxyl radical
OS	oxidative stress
$O_2^{\bullet -}$	superoxide
PRDX	peroxiredoxin
ROS	reactive oxygen species
RNS	reactive nitrogen species
RSS	reactive sulfur species
ROO	peroxyl radicals
SAP	severe acute pancreatitis
Se	selenium
Sec	selenocysteine

SSA	sulfosalicylic acid
SOD	superoxide dismutase
TGFα	transforming growth factor alpha
Txn	thioredoxin
Txnrd	thioredoxin reductase

ABSTRACT

Acute pancreatitis (AP) is a disease characterized by inflammation and autodigestion in the pancreas. In more severe cases with necrosis and systemic inflammation, it is associated with a high mortality rate. For many years, oxidative stress has been suspected to influence the course of the disease in patients. However, the role of oxidants and antioxidant systems during AP remains poorly understood.

The expression of several components of antioxidant systems during AP in mice was analyzed. It was found that especially thioredoxin reductase 1 and members of the glutathione system changed during AP. To further investigate the role of these antioxidant systems in the disease, our group previously generated mice harboring a pancreas-specific knockout (Txnrd1$^{\Delta panc}$) and found Txnrd1$^{\Delta panc}$ mice showed normal growth, relative pancreatic weight, pancreatic morphology, and exocrine as well as endocrine function.

Interestingly, the glutathione system was upregulated in the *Txnrd1*-deficient pancreata, indicative of a possible compensatory mechanism. We then treated Txnrd1$^{\Delta panc}$ mice with caerulein to induce AP and with BSO to inhibit glutathione synthesis. Both interventions alone only lead to a mild phenotype in Txnrd1$^{\Delta panc}$ mice. However, combined glutathione depletion with acute pancreatitis resulted in a severe phenotype in Txnrd1$^{\Delta panc}$ mice with loss of acinar tissue due to necrosis, increased proliferation, and macrophage infiltration. Taken together, these data suggest that TXNRD1 and the glutathione system are central to pancreatic homeostasis.

ZUSAMMENFASSUNG

Die akute Pankreatitis (AP) ist eine Krankheit, die durch eine Entzündung und Selbstverdauung in der Bauchspeicheldrüse gekennzeichnet ist. In schwereren Fällen mit Nekrose und systemischer Entzündung ist sie mit einer hohen Sterblichkeitsrate verbunden. Seit vielen Jahren wird vermutet, dass oxidativer Stress den Krankheitsverlauf der Patienten beeinflusst. Die Rolle der Oxidantien und der antioxidativen Systeme während der AP ist jedoch nach wie vor unzureichend erforscht.

Daher wurde die Ausprägung verschiedener Komponenten des antioxidativen Systems während der AP bei Mäusen analysiert. Es zeigte sich, dass sich insbesondere die Thioredoxinreduktase 1 und Komponenten des Glutathionsystems im Verlauf der AP verändern. Um die Rolle dieser antioxidativen Systeme bei der Krankheit weiter zu untersuchen, hat unsere Gruppe zuvor Mäuse mit einem pankreasspezifischen Knockout (Txnrd1$^{\Delta panc}$) erzeugt und festgestellt, dass Txnrd1$^{\Delta panc}$-Mäuse keine Auffälligkeiten bezüglich des Wachstums, des relativesn Pankreasgewichts, der Pankreasmorphologie und der exokrine sowie endokrine Funktion aufweisen.

Interessanterweise war das Glutathion-System in der Txnrd1-defizienten Bauchspeicheldrüse erhöht, was auf einen möglichen Kompensationsmechanismus hindeutet. Daraufhin behandelten wir Txnrd1$^{\Delta panc}$-Mäuse mit Caerulein, um eineAP zu induzieren, und mit BSO, um die Glutathionsynthese zu hemmen. Beide Interventionen allein führten nur zu einem milden Phänotyp bei Txnrd1$^{\Delta panc}$-Mäusen. Die kombination aus Glutathiondepletion und akuter Pankreatitis führte jedoch zu einem schweren Phänotyp bei Txnrd1$^{\Delta panc}$-Mäusen mit Verlust von Azinusgewebe aufgrund von Nekrose, erhöhter Proliferation und Makrophageninfiltration. Insgesamt deuten diese Daten darauf hin, dass TXNRD1 und das Glutathionsystem für die Homöostase der Bauchspeicheldrüse von zentraler Bedeutung sind.

1. INTRODUCTION

1.1 Acute pancreatitis

Acute pancreatitis (AP) is an inflammatory disease that causes tissue damage in the exocrine pancreas and is associated with a high rate of morbidity and mortality [1, 2]. A more severe type of disease, which affects around 20% of all AP patients, is linked to significant local and global consequences such as necrosis and systemic inflammation [3].

The pancreas is an organ located behind the stomach in the upper abdomen and is divided into three parts: the head, body, and tail of the pancreas (Figure 1). The pancreas is functionally divided into endocrine and exocrine compartments. Islets of Langerhans define the endocrine section and are composed of 5 different cell types, namely α, β, δ, PP and ε cells. These cells secrete hormones to regulate glucose uptake or release and are involved in the development of metabolic diseases like diabetes, obesity, and others [4-7]. Exocrine pancreas is mainly involved in secretion of proteases for the digestion of proteins, fats, and carbohydrates. Abnormal function or exocrine insufficiency results in digestive or inflammatory complications such as pancreatitis.

For many years, oxidative stress has been suspected to influence the course of the disease in patients [8-10]. A disbalance between ROS and cellular defense mechanisms against ROS is believed to be involved in the pathogenesis of acute pancreatitis since 1984 when it was postulated that the increase in capillary permeability that is seen early in the course of acute pancreatitis might be caused by ROS [11]. The role of free radicals in the development of acute pancreatitis has been popularly discussed [12-15]. There are multiple enzyme systems that remove ROS and oxidation products.

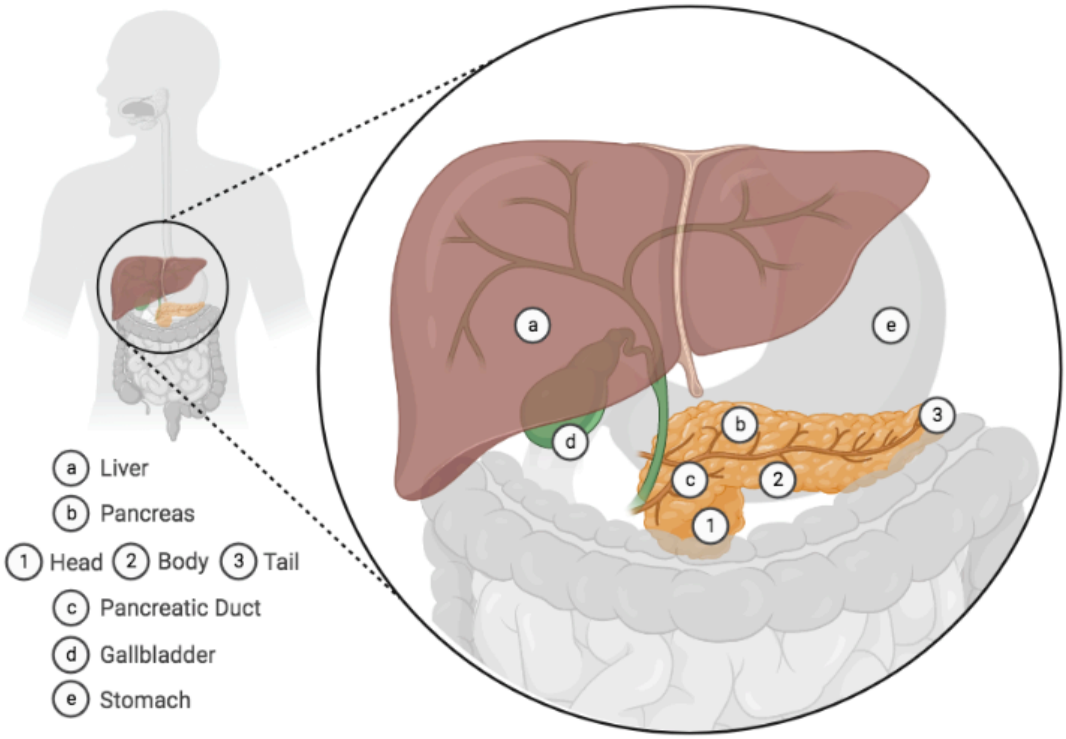

Figure 1 Pancreas Location in Human Body. The image is adapted and modified from "Pancreas", by BioRender.com (2022).

1.1.1 Acute pancreatitis in human

Acute pancreatitis is a common clinical digestive disease with an incidence of about 34 per 100,000 general population per year [16]. It is an inflammatory injury of the pancreas characterized by edema, hemorrhaging, and necrosis caused by self-digestion of pancreatic tissue due to multiple pathogenic factors [17].

Acute pancreatitis (AP) predominantly affects people older than 40 years [18, 19]. It is characterized by acute epigastric pain and elevated blood amylase or lipase levels. Acute pancreatitis is divided into mild acute pancreatitis (MAP), moderately severe acute pancreatitis (MSAP), and severe acute pancreatitis (SAP) according to the

severity of the disease [20]. MAP accounts for the majority of AP, with recovery within 1-2 weeks, and has a low mortality. SAP accounts for about 5% - 10% of AP, with a vicious clinical course and almost always accompanied by persistent organ failure. The etiology of AP is complex, and the reasons for common clinical causes are many: cholestatic diseases, high alcohol consumption, tobacco smoking, and increasing rates of obesity and metabolic disorders, also called hypertriglyceridemia (HTG) [21-25].

1.1.2 Murine models of acute pancreatitis

To further understand the pathogenesis of AP, various mouse models have been generated. In addition, an ideal AP model should be reproducible, with pathological changes, disease step-like changes, and response to therapy similar to human AP.

Claude Bernard invented one AP model in 1856 after injecting bile and olive oil into the pancreatic ducts of mongrel dogs [26]. After more than a century of exploration and development, the following models of *in vivo* pancreatitis are applied in research:

1. Retrograde bile duct injection method: The main pancreatic duct is cannulated after the small pancreatic duct is ligated by dissection, and active pancreatic enzymes or substances that activate pancreatic enzymes such as sodium deoxycholate (DOC) and autologous bile are injected into the pancreatic duct [27].
2. Method of pancreatic duct ligation: ligation of the biliopancreatic duct entering the duodenum and simple pancreatic duct ligation.
3. Acute alcohol-induced pancreatic injury method: fatty acid ethyl esters (FAEEs) are products of the non-oxidative metabolism of ethanol (NOME) from alcohol. And saturated FAEEs were applied to induce AP in rats [28, 29].

4. Choline-deficient ethionine-supplemented (CDE) diet-induced pancreatitis method: administration of CDE to mice [30].

All these pancreatitis models are intended to artificially release pancreatic enzymes that lead to autodigestion of the pancreas. The retrograde bile duct injection and pancreatic duct ligation methods are invasive, difficult to perform, and have a high animal mortality rate, so they are more appropriate for large animals, but not for mice. Therefore, in some cases, dogs and rats were chosen for retrograde bile duct injection and pancreatic duct ligation methods, as well as cats and rabbits in some cases [31]. In the clinical setting, not all patients with alcoholism develop AP, and in pancreatology, a widely accepted model of alcohol-induced AP is lacking [31, 32]. In the CDE diet model, Lombardi et al. and Wang et al. noticed much more hemorrhagic legions appearing in the pancreas [33, 34].

Lampel *et al.* were the first to report the usage of caerulein to establish a non-traumatic AP mouse model [35]. A non-lethal, supramaximal dose of cholecystokinin (CCK) analog caerulein is injected intravenously, subcutaneously, or intraperitoneally to increase pancreatic protein hydrolase secretion to a level that can cause autolysis of pancreatic vesicles [36]. Due to advantages such as ease of operation, stable modeling, reproducibility, and pathology similar to the human AP, this AP model has since been widely used in experimental studies of pancreatitis by many researchers [35].

1.2 Oxidants and antioxidants

1.2.1 Oxidative stress

Oxidative stress (OS) is an imbalance of oxidative and antioxidant entities in the cells. It occurs when the cells are exposed to various harmful stimuli, e.g., air pollution, ultraviolet light (UVA), cigarette smoke, *etc.*, and the level of oxidation exceeds the clearance of the oxidant. Therefore, the cells produce too many reactive oxygen species (ROS), reactive nitrogen species (RNS), and reactive sulfur species (RSS), which are highly reactive molecules, causing inflammatory cell invasion and tissue damage [37-44].

1.2.2 Oxidants

Oxidants are ubiquitous in the environment [37-40], which includes ROS, RNS, RSS, and non-radical derivatives respectively [41-44].

ROS include oxygen ions, peroxides, and oxygen-containing free radicals, which are all byproducts of aerobic metabolism. Usually, ROS are natural products of regular metabolism that play an essential function in cell signaling and organism stability. However, the amount of ROS produced increases considerably with time and under the impact of the external environment (e.g., UV exposure, heat exposure, or ionizing radiation). This alteration can be the result of visible damage to the cell structure.

RNS refers to the interaction of NO with compounds including ROS, resulting in a series of highly oxidizing radicals and nitro compounds including peroxynitrite anions ($ONOO^-$) and its protonated form peroxynitrous acid (HOONO).

Sulfur-based radicals known as RSS can oxidize and inhibit thiol-proteins and enzymes. They are frequently generated when thiols and disulfides are oxidized to higher oxidation states. Persulfides, polysulfides, and thiosulfate are examples of RSS. In Table 1, a summary of the main oxidants is provided [45]. However, the amount of ROS produced increases considerably with time and under the impact of the external environment (e.g., UV exposure, heat exposure, or ionizing radiation).

Table 1 Major oxidants present in the biological systems

ROS	RNS	RSS
Superoxide ($O_2^{\bullet -}$) Hydrogen Peroxide (H_2O_2) Hydroxyl Radical ($^{\bullet}OH$) Peroxynitrite Anion ($ONOO^-$) Hypochlorous Acid (HOCl) Peroxyl Radicals (ROO) Hydroperoxyl Radical (HOO)	Nitric oxide radicals ($^{\bullet}NO$) Peroxynitrite anions ($ONOO^-$) Nitrogen dioxide radicals ($^{\bullet}NO_2^-$)	Persulfides Polysulfides Thiosulfate

1.2.3 Antioxidants

Free radicals are produced as a by-product of the cell during regular metabolic activities. Antioxidants, on the other hand, are produced to neutralize free radicals by providing additional electrons. In most cases, the body can maintain a healthy equilibrium of antioxidants and free radicals and protects the organism from oxidative stress.

There are two main types of antioxidant systems in the body, enzymatic and non-enzymatic antioxidants. Enzymatic antioxidants are a very important class of enzymes, and there are various kinds including thioredoxin (TXN), superoxide

dismutase (SOD), glutathione peroxidase (GPX), catalase (CAT), and peroxiredoxin (PRDX). Non-enzymatic antioxidants are mainly obtained through food and consist of vitamin E, vitamin C, alpha-lipoic acid, thiols, carotenoids, trace elements copper, zinc, selenium (Se), and others [46, 47].

Superoxide Dismutase (SOD):

SODs catalyze the conversion of O_2 to H_2O_2 and O_2. In mammals, there are three isoforms of SOD: SOD1, SOD2, and SOD3 [48-50]. SOD1 is mostly located in cell membranes, but it's also discovered in the nucleus, lysosomes, peroxisomes, and mitochondrial intermembrane spaces on rare occasions [51]. SOD3 is the major SOD of extracellular fluids, such as plasma, lymph, and cerebrospinal fluid. It is also known as the extracellular superoxide dismutase (EC-SOD) [52]. Manganese is a metal cofactor that restricts SOD2 to the mitochondrial matrix, and SOD2 is the only isoform required for aerobic life in physiological settings [53, 54].

Catalase (CAT):

CAT is found in a wide range of aerobic organisms [55]. It catalyzes the breakdown of H_2O_2 into H_2O and O_2. CAT in mammals is a heme-containing enzyme that needs iron as a cofactor. It is found in the peroxisome of most mammals, including humans and mice. In erythrocytes, CAT floats in the cytoplasm due to the lack of cellular organelles [55, 56].

Glutathione (GSH) system:

Glutathione is a tripeptide compound formed by the condensation of cysteine, glycine, and glutamic acid through peptide bonds, which is the most abundant class of compounds containing sulfhydryl groups in cells [57]. It is involved in intracellular amino acid transport, regulation of glucose metabolism, and DNA synthesis. It plays plays an important role in antagonizing exogenous toxins, oxygen radical damage, regulating the immune function of the body, maintaining cellular protein structure and function, and inhibiting apoptosis [58-61]. In mammalian tissues, normal levels

of GSH range from approximately 0.1 to 10 mM and can reach concentrations of up to 10 mM in the liver which is a major site of GSH synthesis [62]. In the liver, GSH is released at high rates into blood plasma and bile, and the bile GSH concentrations can reach 8 to 10 mM. Nearly half of GSH released by rat hepatocytes is transported across the sinusoidal membrane into blood plasma for delivery to other tissues [62, 63].

GSH can scavenge hydrogen peroxide and lipid peroxides by the action of GPX, and it is oxidized to oxidized GSSG, which can be rapidly reduced to GSH by glutathione reductase present in liver and erythrocytes through NADPH hydrogen supply, thus constituting an effective antioxidant system that enables the scavenging reaction of free radicals in the body to be sustained [64]. Moreover, through glutathione s-transferase, GSH can bind to many types of electrophile endogenous compounds and foreign chemicals, enabling their effective and safe excretion from the body [65].

Glutathione Peroxidase (GPX):

The breakdown of H_2O_2 to H_2O and O_2 is catalyzed by GPX. It also transforms organic hydroperoxides into their corresponding alcohols, such as fatty acid hydroperoxides. Furthermore, when compared to CAT, it has a stronger affinity for H_2O_2 when the amount of H_2O_2 is low [55].

GPXs are a type of enzyme that protects cells from oxidative damage caused by ROS. The GPX protein family contains the largest number of selenium-containing proteins in mammals. Five of the eight members in humans have the 21st amino acid selenocysteine (Sec) in their catalytic site instead of the functional counterpart cysteine (Cys). The sequences of all members of this family are extremely similar. GPX1/GPX2, GPX3/GPX5/GPX6, and GPX4/GPX7/GPX8 are three groups that originated from a cysteine-containing progenitor, according to the phylogeny. GPX5 and GPX6 were created via tandem duplication of GPX3, while GPX7 and GPX8 originated from a common GPX4 progenitor. GPX1 is ubiquitously expressed in the cytosol and mitochondria. GPX2 is localized in the gastrointestinal epithelium. GPX2

is related to GPX1 and has the highest levels of expression in the gastrointestinal tract and liver. GPX3 is an extracellular protein that enters the endoplasmic reticulum (ER) for post-translational modification but is released into the bloodstream primarily by kidney proximal tubular cells due to the lack of an ER retention signal. GPX5 is a selenium independent GPX that is found in abundance in epithelial cells and the epididymis lumen. In humans, GPX6 is a selenoprotein, whereas in other species it is a Cys-containing enzyme. GPX7 is protective against ER stress and oxidative stress by promoting the refolding of misfolded proteins. GPX8 is localized in the endoplasmic reticulum membrane. [66, 67].

Peroxiredoxin (PRDX):

PRDX are abundant peroxidases that can make up to 1% of soluble cellular proteins [68]. Six PRDX isoforms are found in mammalian cells. PRDX1 is primarily expressed in the cytosol, nucleus, and peroxisomes. PRDX2 is located in the cytosol and nucleus and binds to cell membranes. PRDX3 is only expressed in the mitochondria. The nucleus and the endoplasmic reticulum both express PRDX4. The cytosol, vesicles, and lysosomes all contain PRDX6. While there are many different types of PRDX, it is far less effective at reducing H_2O_2 than GPX or CAT [69].

1.3 Oxidative stress in acute pancreatitis

Many studies have demonstrated the role of oxidative stress in the acute inflammatory response, particularly in AP-related pancreatic injury [70-72]. The presence of oxidative stress during AP has been verified both in clinical studies and in animal experiments.

In clinical studies, oxidative stress has been reported to be related to the inflammatory process and the severity of AP. T.Solakoglu et al. demonstrated that decreased antioxidant levels were associated with mild AP [73]. In the study of H.

Baser et al., an increase in ischemia-modified albumin (IMA) levels and a decrease in total antioxidant status (TAS) levels were observed in patients with mild AP by the parameters of oxidative stress [74].
In animal experiments studies, Dabrowski et al. [75, 76] and Schoenberg et al. [77, 78] demonstrated that by caerulein injection in an animal model of AP that malondialdehyde (MDA), a biomarker of oxidative stress, increases in concentration after AP and that GSH levels decrease in pancreatic tissue during the early stages of AP. The same results were shown by Neuschwander-Tetri et al. [79].

1.4 Thioredoxin and thioredoxin reductases

The essential trace element selenium [80, 81], discovered by Swedish chemist Jöns Jacob Berzelius in 1817, acts biologically primarily through various selenoenzymes and selenoproteins. Thioredoxin reductases are NAPDH-dependent dimeric selenium-containing enzymes with a flavin adenine dinucleotide (FAD) domain [82, 83].

The thioredoxin (TXN) antioxidant system catalyzes the reduction of intramolecular disulfides and sulfenic acids to their corresponding sulfhydryl moieties and is made up of TXN and thioredoxin reductase (TXNRD). A two-step mechanism governs the reaction: TXN first reduces the substrate, causing it to become oxidized, and then TXNRD recycles TXN back to its reduced state by consuming NADPH. TXN1 and TXN2 are two isoforms of TXN that are particularly important in mammals. Both isoforms are widely expressed in human tissues, TXN1 and its corresponding reductase TXNRD1 are primarily found in the cytosol, whilst TXN2 and TXNRD2 are found in the mitochondria [82, 84-87]. And TXNRDs also contain TXNRD3 (also known as Thioredoxin Glutathione Reductase, TGR) is expressed only in testis tissues in animals [86, 88-90]. TXNRD1 is expressed in a variety of tissues [91-94]. Thioredoxin reduces TXNRD, which is reduced by thioredoxin. TXNRD was utilized because

NADPH breaks the disulfide link between ribonucleotides and deoxyribonucleotides. It's been suggested that it's involved in a variety of pathological and physiological circumstances, including apoptosis, cancer [95], chronic inflammatory and autoimmune diseases [96, 97].

The thioredoxin system consists of thioredoxin (Txn), thioredoxin reductase (Txnrd), and NADPH. Thioredoxin reduces thioredoxin reductase, an thioredoxin reductase uses NADPH to reduce the disulfide bond (Figure 2) [98]. In this process, the reduced thioredoxin is oxidized and the oxidized thioredoxin (Txn-S_2) can be reduced and regenerated by thioredoxin reductases and NADPH, and this cycle completes the redox reactions [99].

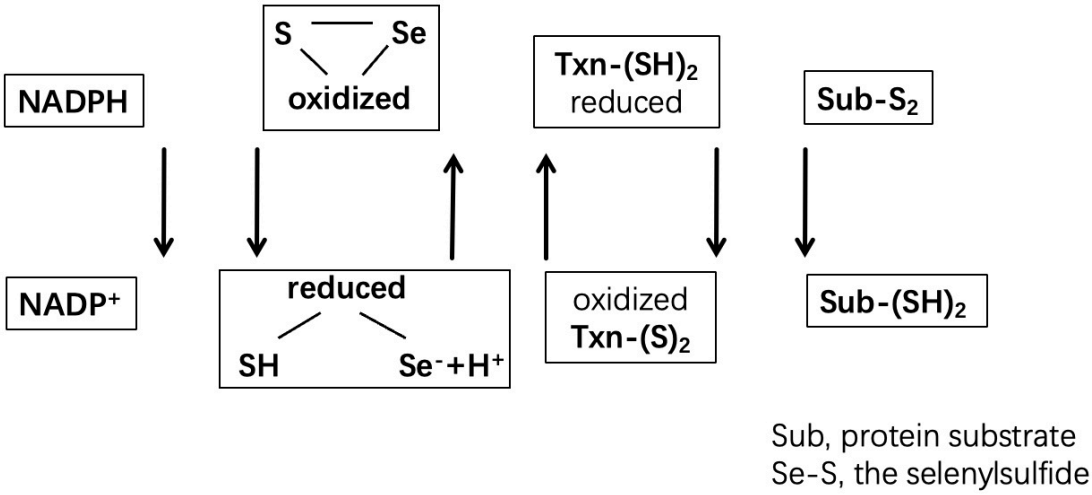

Figure 2 Redox cycling of Txn and Txnrd. The thioredoxin system consists of Txn, Txnrd, and NADPH.

To date, three thioredoxin reductases isoforms have been identified [100-102], all of which have a Sec active site at the C-terminus. Of these three enzymes, thioredoxin reductase 1 is the most studied enzyme and is widely found in the cell plasma of many tissues [93, 94, 103]. Thioredoxin reductase 2 is found primarily in mitochondria and can be purified from rat liver [101] and bovine adrenal cortex [104], where it has important roles in stem cell growth, hematopoiesis, cardiac

growth, and cardiac function [105, 106]. Thioredoxin reductase 3 is found primarily in testicular tissue and catalyzes reduced glutathione thioredoxin [107], which was known as thioredoxin and glutathione reductase (TGR). Thioredoxin reductase 1 and 2 are found in a variety of tissues, particularly in the liver, but thioredoxin reductase 3 is found solely in the testes [102].

1.5 Thioredoxin reductase 1 in the pancreas

Thioredoxin reductase 1 is contained in all human tissues at 0.7 ~ 1.7 g/kg. Its promoter is located between -116 and +168 bp, lacks the TATA and CAAT boxes, and has an increased number of GC bases. Inactivation of *Txnrd1* enzymatic activity leads to early embryonic death [106], highlighting the importance of *Txnrd1* in embryonic development. Bondareva et al. found mouse embryos homozygous for a targeted null mutation of the *Txnrd1* were viable at embryonic day 8.5 (E 8.5) but not at E 9.5 [108]. Jakupoglu et al. found that Cre-mediated knockout of *Txnrd1* leads to early embryonic lethality [106].

In a previous study by our research group, wild-type mice were given injections of caerulein to establish the AP model at short time points. During earlier analysis of Microarray data (Figure 3), it was shown that *Txnrd1* is one of the highest upregulated oxidoreductases during the first 8 hours of AP.

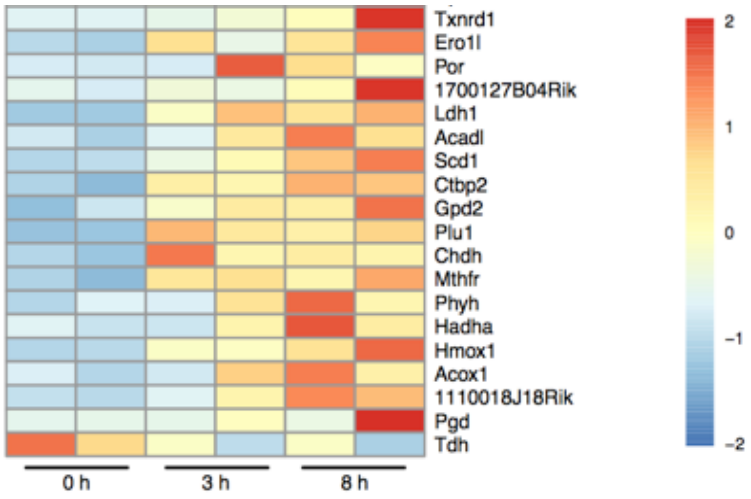

Figure 3 Gene expression as determined by microarray of AP in wild-type mice. All genes were associated with the term "oxidoreductases" and regulated more than 2-fold.

There is little knowledge about the expression and function of thioredoxin reductase in the pancreas. The former members of our group successfully knocked out the thioredoxin reductase 1 gene in the pancreas. They found that in mice with a pancreas-specific thioredoxin reductase 1 deletion thioredoxin reductase 1 activity was significantly decreased, whereas the body weight curves for over one year and the relative pancreatic weight were not different. In terms of exocrine function, when given a high-fat diet, fat droplets didn't change in the control group. Even older mice, 48 weeks, displayed an unchanged pancreatic histology [109]. However, the function of this gene in the pancreas remains to be determined.

1.6 Aim of this thesis

This study aimed to elucidate the role of cytoplasmic *Txnrd1* and the glutathione system during AP.

Firstly, *in vivo* models of Txnrd1$^{\Delta panc}$ and suitable control (wild-type) were analyzed under AP conditions (timepoints: 0 hours, 8 hours, 24 hours, and 1 week) and combined with glutathione depletion (AP condition timepoints: 0 hours, 8 hours, 24 hours, and 1 week).

Subsequently, *in vitro* experiments with pancreatic acinar cells explanted from Txnrd1$^{\Delta panc}$ and wild-type mice were performed to investigate acinar integrity and ADM formation.

In summary, the focus was on *in vivo* and *in vitro* experiments in an attempt to gain insight into the role of *Txnrd1* and the glutathione system in AP development and progression.

2. MATERIALS AND METHODS

2.1 Materials

2.1.1 Chemicals and Reagents

Chemicals and Reagents	Source	Identifier
Amersham ECL Western Blotting Detection Reagent	Cytiva	# RPN2232
Ammonium persulfate (APS)	Sigma-Aldrich	# A7460
ABC kit peroxidase	Vector Laboratories	# PK-4000
Bovine serum albumin	Sigma-Aldrich	# A7030
Bromphenol blue	Carl Roth	# T116.1
Buthionine sulfoximine (BSO)	Enzo Life Sciences	# BML-FR117-0500
Bovine Pituitary Extract	Life Technologies	# 13028-014
5-Bromo-2-deoxyuridine (BrdU)	Sigma-Aldrich	# B5002
Complete protease inhibitor cocktail tablets	Roche Diagnostics	# 04693132001
caerulein	Bachem	# 4030451
Clostridium histolyticum, Type VIII	Sigma-Aldrich	# C2139
Direct PCR®-Tail (Tail lysis buffer)	VWR BDH Chemicals	# 31-102-T
DNA Ladder-Mix	VWR BDH Chemicals	# 732-3282
DAB Peroxidase Substrate Kit	Vector Laboratories	# SK-4100
DTT	Sigma-Aldrich	# D9163
Ethylenediaminetetraacetic acid (EDTA)	Sigma-Aldrich	# 324504
Eosin	Waldeck	# 2C-140
Fermentas Spectra™ Multicolor Broad Range Protein Ladder	ThemoFisher	# 26623
FBS	Life Technologies	# 10499044

Glycine	Sigma-Aldrich	# 50046
Glucose	Sigma-Aldrich	# G8270
GREEN Taq® Ready Mix, PCR Reaction	Promega	# M7123
Hematoxylin solution	Sigma-Aldrich	# 1.05175.2500
30% Hydrogen peroxide	EMSURE	# 1.07209.1000
HEPES	Life Technologies	# 15630
Insulin-Transferrin-Selenium	Life Technologies	# 41400-045
Magnesium Chloride	Sigma-Aldrich	# M1028
Methanol	Carl Roth	# CP43.4
2-Mercaptoethanol	Carl Roth	# 4227.3
Mayer's Hemalum solution	Carl Roth	# 1.09249.2500
McCoy's 5A Medium	Sigma-Aldrich	# M8403
N, N, N', N'-Tetramethyl ethylenediamine (TEMED)	Sigma-Aldrich	# T22500
Nitrocellulose Blotting Membrane (0.2 µm)	Cytiva	# 10600011
N-Acetyl-Lcysteine (NAC)	Sigma-Aldrich	# A7250
Normal goat serum	Dako	# X0907
Novalgin® Tropfen Metamizole-Natrium 1 H_2O	Sanofi	# 01553758
Nonidet™ P 40 Substitute	Sigma-Aldrich	# 74385
$NaHCO_3$	Sigma-Aldrich	# 1.06329.0500
0.9% NaCl solution	B.Braun	# 195148131
Paraformaldehyde 16% solution EM GRADE	Electron Microscopy Sciences	# 15710
PhosSTOP phosphatase inhibitor cocktail tablets	Roche Diagnostics	# 4906837001

Proteinase K, recombinant (20 mg/ml)	Sigma-Aldrich	# 31158440001
PBS	Merck Biochrom^{AG}	# L182-50
pertex embedding medium	Medite	# 41-4012-00
RNA lysis buffer	Promega	# Z3051
Rotiphorese® Gel 30 (37, 5:1)	Carl Roth	# A3029.2
ROTI®-GelStain	Carl Roth	# 3865.2
Rabbit serum	Dako	# X0902
Roti® -Histol	Carl Roth	# 6640.4
Rat Tail Collagen Type I	Corning	# 354236
Skim Milk Powder	Sigma-Aldrich	# 70166
Sodium dodecyl sulfate (SDS)	Sigma-Aldrich	# 11667289001
Sodium Chloride	Sigma-Aldrich	# 71376
10 M Sodium hydroxide	Sigma-Aldrich	# S5881
Sodium Deoxycholate	Sigma-Aldrich	# D6750
Sulfosalicylic acid (SSA)	Sigma-Aldrich	# 5965-83-3 (R8120000-1C)
Soybean Trypsin Inhibitor	Sigma-Aldrich	# T6414
Tween® 20	Sigma-Aldrich	# P1379
Titriplex® III	Sigma-Aldrich	# 1.37004
1-Thioglycerol	Promega	# A208B
Tris-hydrochloride	Carl Roth	# 9090.3
Tris	Carl Roth	# 5429.2
Triton X®-100	Sigma-Aldrich	# T9284
Transforming growth factor (TGFα)	Sigma-Aldrich	# T7924
Unmasking solution citrate	Vector Laboratories	# H3300
Unmasking solution high pH	Vector Laboratories	# H3301
Waymouth's MB 752/1 Medium	Life Technologies	# 31220023

2.1.2 Buffers and Solutions

BrdU solution	
BrdU stock solution	50 mg/µl BrdU dissolved in 10 M NaOH solution. Stored at – 20°C
BrdU working solution	1:10 dilution of BrdU stock solution in 0.9% NaCl. Stored at – 20°C
4% Paraformaldehyde solution	
4% paraformaldehyde	Paraformaldehyde 16% solution EM GRADE diluted in PBS
Hematoxylin and Eosin Staining (H&E Staining)	
Hematoxylin and Eosin Staining (H&E Staining)	0.33% eosin (1:5 with 96% ethanol)
PCR (Polymerase chain reaction)	
Buffer	**Component**
2% Agarose gels	200 ml 1 x TAE buffer 4 g Agarose 10 µg/ml ROTI®-GelStain
TAE Buffer	40 mM Tris 2 mM Titriplex® III 20 mM acetic acid, glacial dilute with deionized water Stored at room temperature
Target	**Primer Sequences**
Cre (324 bp (WT), 199 bp (Cre))	1. 5’-ACCAGCCAGCTATCAACTCG-3’ 2. 5’-TTACATTGGTCCAGCCACC-3’ 3. 5’-CTAGGCCACAGAATTGAAAGATCT-3’ 4. 5’-GTAGGTGGAAATTCTAGCATCATCC-3’

Txnrd1 (66 bp (WT), 130 bp (Txnrd1$^{flox/flox}$)	1. 5'-TCCACCTCACAGGAGTGATCCC-3' 2. 5'-TGCCTAAAGATGAACTCGCAGC-3'
Western blots	
Buffer	**Component**
Lämmli Sample Buffer (6 x SDS)	7 ml Stacking Buffer 3 ml Glycerin (30%) 1 g SDS (10%) 1.2 mg Bromphenol blue 0.93 g DTT (0.6 M) add H_2O to 10 ml Store at - 80℃
RIPA Buffer	150 mM NaCl 50 mM Tris-HCl (PH 7.5) 1% NP40 5% Sodium Deoxycholate 0.1% SDS (20%) fill up to 100 ml with H_2O (Note: Immediately before use adding 25 x protease inhibitor complete Mini and 10 x Phosphatase Inhibitor, these were diluted with 2 ml H_2O and 1 ml H_2O, separately, before use)
20% SDS	100 g SDS 500 ml H_2O
Stacking Buffer (pH 6.8)	6.05 g Tris-Base 40 ml Distillation-Distillation H_2O adjust pH to 6.8 with 1 M HCl fill up to 100 ml with H_2O add 0.4 g SDS

Separation Buffer (pH 8.8)	91 g Tris-Base 300 ml H_2O adjust pH to 8.8 with 1 M HCl fill up to 500 ml with H_2O add 2 g SDS
15% SDS polyacrylamide gel (1.5 mm) Separation Gel	5.834 ml Rotiphorese® Gel 30 (37, 5:1) 2.917 ml Separation Buffer (pH 8.8) 2.917 ml H_2O 70 µl 10% APS 14 µl TEMED
15% SDS polyacrylamide gel (1.5 mm) Stacking Gel	0.607 ml Rotiphorese® Gel 30 (37, 5:1) 1.167 ml Stacking Buffer (pH 6.8) 2.847 ml H_2O 46.667 µl 10% APS 9.333 µl TEMED
Tris Buffered Saline (10 x TBS)	80 g NaCl 31.5 g Tris HCl adjust pH with 4.5 to 7.6 fill up to 1000 ml with H_2O
Tris Buffered Saline with Tween-20 (1 x TBS-T)	100 ml 10 x TBS 899 ml H_2O 1 ml Tween-20
Tris-Glycine SDS Running Buffer (10 x)	30.2 g Tris 144 g Glycine 50 ml 20% SDS fill up to 1000 ml with H_2O
Tris Glycine Transfer Buffer (10 x)	144 g Glycine 30 g Tris-Base fill up to 1000 ml with H_2O

Tris-Glycine Transfer Buffer (1 x) for use (include 20% Methanol)	100 ml 10 x Tris Glycine Transfer Buffer 200 ml Methanol 700 ml H_2O

2.1.3 Antibodies used in the experiment and their usage

Antibodies for western blot					
Antibody	**Species of Antibodies**	**Protein size (kDa)**	**Blocking**	**Dilution**	**Company**
CAT (14097)	Rabbit	60	5% milk in TBS-T	1 : 1000 in 5% milk	Cell Signaling
GPX1 (ab108427)	Rabbit	22	5% milk in TBS-T	1 : 1000 in 5% milk	Abcam
GPX2 (ab289369)	Rabbit	22	5% milk in TBS-T	1 : 1000 in 5% milk	Abcam
GPX8 (16846-1-AP)	Rabbit	24	5% milk in TBS-T	1 : 1000 in 5% milk	Proteintech
GSTT2 (ab176336)	Rabbit	28	5% milk in TBS-T	1 : 1000 in 5% milk	Abcam
GSTM1 (12412-1-AP)	Rabbit	27	5% milk in TBS-T	1 : 1000 in 5% milk	Proteintech
HSP 90 (4875s)	Rabbit	90	5% BSA in TBS-T	1 : 1000 in 5% BSA	Cell Signaling
PRDX1 (8499)	Rabbit	21	5% BSA in TBS-T	1 : 1000 in 5% BSA	Cell Signaling
PRDX2 (46855)	Rabbit	23	5% BSA in TBS-T	1 : 1000 in 5% BSA	Cell Signaling
PRDX6 (95336)	Rabbit	25	5% BSA in TBS-T	1 : 1000 in 5% BSA	Cell Signaling

TXNRD 1 (M01778)	Rabbit	55	5% milk in TBS-T	1 : 1000 in 5% BSA	Boster
TXNRD2 (180493)	Rabbit	57	5% milk in TBS-T	1 : 1000 in 5% milk	Abcam
Rabbit IgG HRP Linked Whole Ab (second antibody) (NA934V)				1 : 5000 in 5% milk	GE Healthcare

Antibodies for IHC staining				
Antibody	**Species of Antibodies**	**Blocking**	**Dilution**	**Company**
Amylase (A8273)	Rabbit	5% goat serum in PBS	1 : 1000 in blocking solution	Sigma
BrdU (MCA2483T)	Mouse	5% goat serum in PBS	1 : 250 in blocking solution	Bio-rad
Biotinylated anti-rabbit made in goat IgG (H+L) (BA-1000)			1 : 500 in blocking solution	Vector
Biotinylated anti-rat made in Rabbit IgG (H+L) (BA-4000)			1 : 500 in blocking solution	Vector

Biotinylated anti-mouse made in goat IgG (H+L) (BA-9200)			1 : 500 in blocking solution	Vector
Cytokeratin 19 (CK 19) (Troma III)	Rat	5% rabbit serum in PBS	1 : 300 in blocking solution	DSHB
F 4/80 (MF-48000)	Mouse	5% rabbit serum in PBS	1 : 100 in blocking solution	Thermo fisher scientific

2.1.4 Kits

Critical commercial assays	**Source**	**Identifier**
Cytotoxicity detection kit (LDH)	Roche Diagnostics	# 11644793001
GSH / GSSG - Glo™ assay	Promega	# V6612
Pierce BCA Protein assay kit	ThermoFisher	# 23225

2.1.5 Laboratory devices and equipment

Equipment	**Source**	**Identifier**
Centrifuge 5417 R	Eppendorf	# Z366021
Heidolph Brinkmann Homogenizer Silent Crusher	Heidolph	# M 036170020
Infinite® 200 Pro	Tecan	# 200 Pro
Molecular Imager®Gel Doc™ XR system	Bio-rad	# 1708195EDU

Multiscan™ FC Microplate Photometer	ThermoFisher Scientific™	# 51119000
Microvette® 500 Z-Gel (serum gel vial)	Sarstedt	# 20.1344
Sub-Cell GT Horizontal Electrophoresis System	Bio-rad	# 1704402
Thermomixer® compact	Eppendorf	# 5355
T100™ Thermal Cycler	Bio-rad	# 1861096
Tissue processor	Leica	# S300

2.1.6 Software and algorithms

Software and algorithms	**Source**	**Identifier**
GraphPad Prism 9	Version 9.1	GraphPad
QuPath	Version 3.2	Github [110]
ImageJ	Version 2.3.0	NIH [111]

2.2 Methods

2.2.1 Generation of Txnrd1$^{\Delta panc}$ mouse model

For this study, an established C57BL/6 thioredoxin reductase 1 knockout (Txnrd1$^{\Delta panc}$) mouse model was used, including floxed alleles, developed by the Brielmeier group [106]. The LoxP sites flanked exon 15 of the target gene thioredoxin reductase 1, which harbors the coding region for the redox center, including the Sec codon UGA, the selenocysteine insertion sequence (SECIS) element, the AU-riched elements, and the endogenous transcription termination signal [106]. The frt sites flank the neomycin cassette. The Cre-mediated deletion of exon 15 leads to the inactivation of *Txnrd1* (Figure 2.2.1).

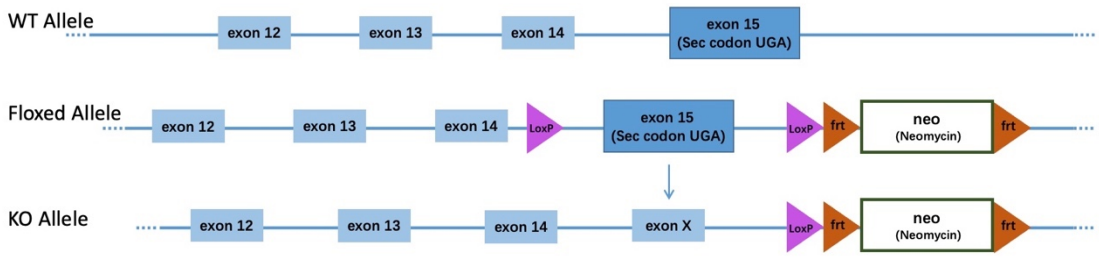

Figure 2.2.1 Generation of floxed *Txnrd1*. Graphical representation general scheme depicting floxed *Txnrd1* mice [106].

To generate mice with a pancreas-specific knockout of *Txnrd1* (Figure 2.2.2), female mice were used which were heterozygous for Ptf1α-Cre^{ex1} [112], and homozygous for the floxed allele of *Txnrd1* (*Txnrd1*$^{flox/flox}$), and a male mouse who did not have a Ptf1α-Cre^{ex1} mutation, but was homozygously floxed for *Txnrd1* (*Txnrd1*$^{flox/flox}$).

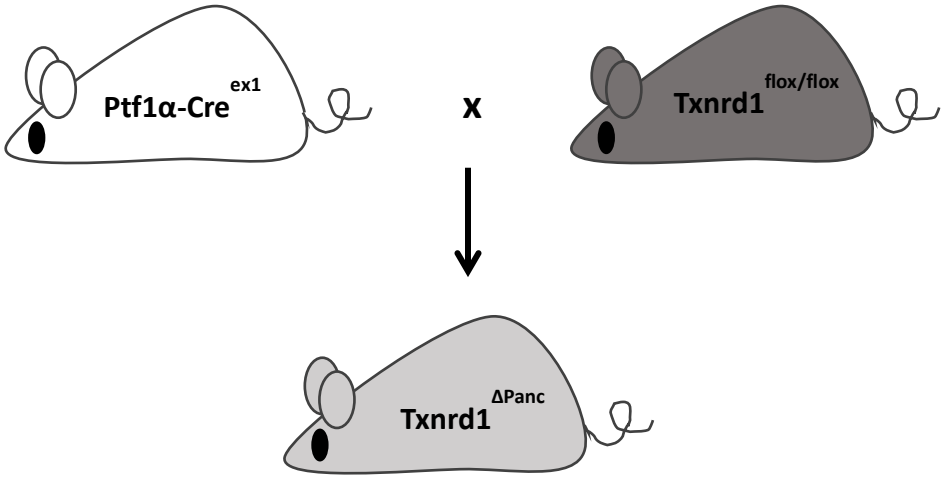

Figure 2.2.2 Mating scheme used to generate Txnrd1$^{\Delta panc}$ mice.

2.2.2 Acute Pancreatitis of Pancreas-specific knockout mouse model

2.2.2.1 Mouse husbandry

Based on the recommendations of the Federation of European Laboratory Animal Science Associations (FELASA), all mice were kept in specific pathogen-free (SPF) conditions at the animal facilities of the Klinikum rechts der Isar University Hospital of the Technische Universität München and housed in groups at 20 to 24°C, 50 to 60% humidity, with 12 hours light/dark cycle, given chow diet (Altromin Spezialfutter) and water *ad libitum*. Mice were maintained using a C57BL / 6 background and breeding was carried out between the 6 - week - old male and 8 - week - old female mice. All mice experiments were conducted in accordance with German federal animal protection Laws and approved by the institutional animal care and use committee on animal experimentation and the Government of Upper Bavaria under the license ROB-55.2-2532.Vet_02-17-32. Male and female mice were not distinguished during the analysis.

Mice were weaned from their mothers at three weeks of age. Their ears were punched with continuous numbers for identification and subsequent genotyping by PCR.

The following genotype and abbreviation were used:

- Txnrd1$^{flox/flox}$; Ptf1atm1(cre)Hnak → Txnrd1$^{\Delta panc}$
- For pancreas-specific deletion of *Txnrd1*, Ptf1a – Cre was used (Ptf1a$^{tm1(cre)Hnak}$) [106, 112]. Mice were born at the expected Mendelian ratios and developed without any problems.

2.2.2.2 Induction of acute pancreatitis in mice by caerulein

To induce acute pancreatitis, 10 – week – old mice were starved for 9 hours and weighed. Eight intraperitoneal (i.p.) of a dose of 50 µg/kg body weight of caerulein were given at hourly intervals. The injection volume was 10 µl/g body weight. Timepoint analyses including serum, histology, immunohistochemistry (IHC), western blot, and gene expression analyses were performed at 0 hours, 8 hours, 24 hours, and 1 week after initiation of acute pancreatitis by caerulein injections, respectively (Figure 2.2.4).

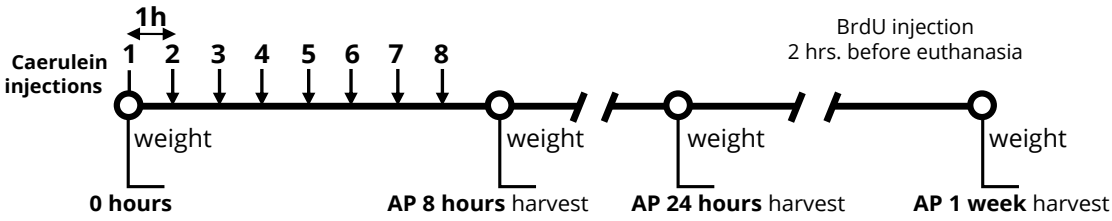

Figure 2.2.3 Scheme of acute pancreatitis. Schedule of AP.

Mice were given preemptive analgesia (Novalgin® Tropfen Metamizole-Natrium 1 H_2O) at a concentration of 200 mg/kg body weight in 0.9% NaCl per os, every four hours, starting 30 minutes before the first injection of caerulein.

2.2.2.3 Dose and time point-finding of BSO treatment in wild-type mice

To determine the dose of BSO in drinking water needed for a significant depletion of glutathione pool, 10 – week – old wild-type mice were treated with different concentrations (0, 5, 10 and 20 mM) of BSO in the drinking water for 24 and 48 hours. Their weight was assessed daily (Figure 2.2.4).

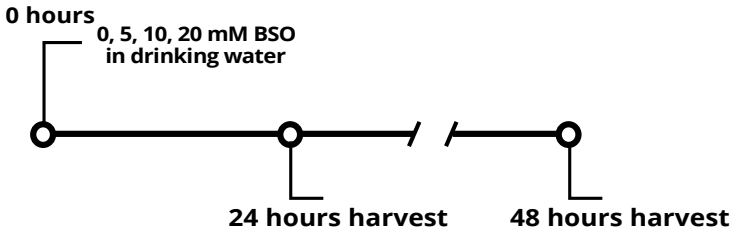

Figure 2.2.4 Dose and time point-finding of BSO treatment. Schedule of BSO treatment in dose-finding experiment.

2.2.2.4 Induction of glutathione depletion in mice by BSO treatment

To induce glutathione depletion, 10 – week – old mice were given BSO in drinking water at the concentration determined in the dose and time point-finding experiment. To monitor the status of the mice, their weight was taken daily. At 0 days, 5 days, or 14 days, the mice were sacrificed, and organs were harvested for further analysis (Figure 2.2.5 A).

To induce glutathione depletion with acute pancreatitis, 10 – week – old mice were given BSO in drinking water at the concentration determined in the dose and time point-finding experiment, at this point, each injected with a dose of 10 µl/g body

weight of caerulein intraperitoneal (i.p) at hourly intervals. At 8 hours, 24 hours, and 1 week the mice were sacrificed, and organs were harvested for further analysis (Figure 2.2.5 B).

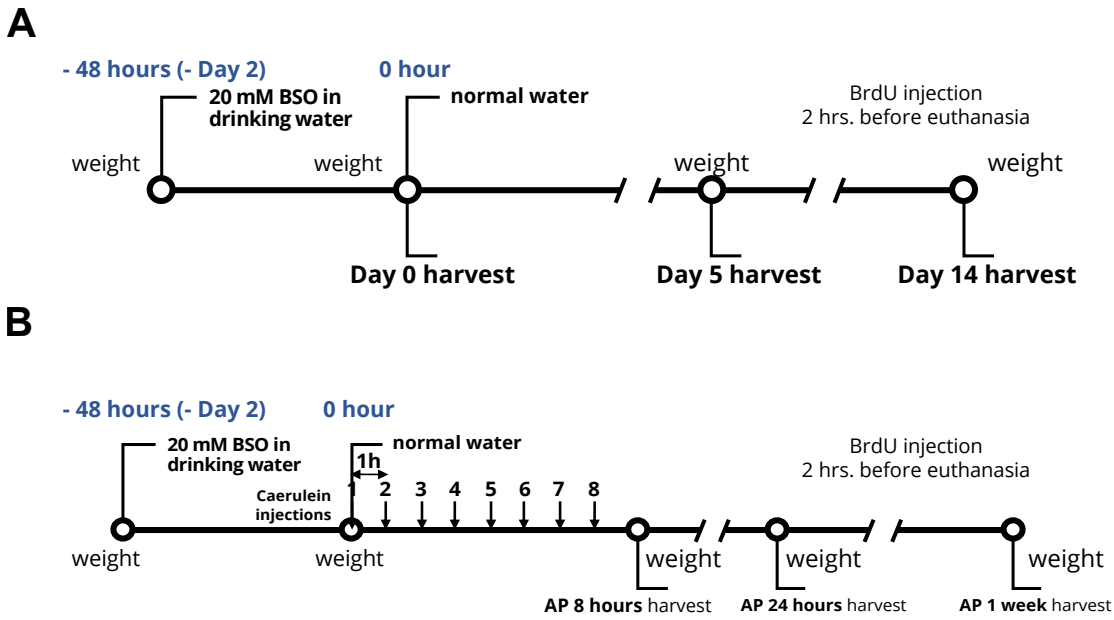

Figure 2.2.5 Scheme of glutathione depletion and glutathione depletion with acute pancreatitis. Schedule of **(A)** glutathione depletion and **(B)** glutathione depletion with acute pancreatitis.

2.2.2.5 Tissue harvesting and preparation of organs

Mice were sacrificed at indicated time points for analysis. At each time point of analysis, 2 hours before euthanasia with isoflurane (cp-pharma), mice were injected with 10 µl/g body weight of 5-Bromo-2-deoxyuridine (BrdU) working solution. The pancreas was removed and divided into three parts, one part for protein isolation, one small part for RNA, and one part for paraffin fixation. Protein samples were snap-frozen in liquid nitrogen. RNA samples were suspended in RNA lysis buffer with 10% 2-Mercaptoethanol and homogenized completely - after that they were snap-frozen in liquid nitrogen and stored at – 80°C.

2.2.2.6 Serum analysis

After euthanizing mice, blood was collected by cardiac puncture, put in a serum gel vial, centrifuged at 10,000 × rpm for 10 minutes at 4°C for further amylase and lipase analysis, and stored at – 80°C.

2.2.2.7 Preparation for paraffin-embedded organ sections

A small part of the liver, lung, spleen, and duodenum were resected from mice and fixed with half of the remaining pancreatic tissue in 4% paraformaldehyde at 4°C overnight. The following day, the organs were dehydrated with increasing concentrations of ethanol, xylol, and paraffin in an S300 tissue processing unit. Finally, organs were embedded in liquid paraffin and stored at room temperature.

2.2.3 Polymerase chain reaction (PCR)

To determine the genotype of transgenic mice PCR was used. Mice ears clip samples were taken to detect mouse genotype. For DNA preparation, 200 µl direct PCR®-Tail (Tail lysis buffer) and 10 µl of recombinant Proteinase K were added to each sample and incubated at 55 °C overnight on a shaker. The following day, samples were incubated at 85°C for 45 minutes to stop the reaction. Then, samples were centrifuged at 14000 x g and 4°C for 1 min, and the supernatant was used as DNA template for genotyping. According to the manufacturer's protocol, GREEN Taq® Ready Mix, PCR reaction mix with $MgCl_2$ was used in a 12 µl volume per sample with target gene primer, the detail are as follows:

- 6 µl GREEN Taq® Ready Mix, PCR Reaction
- 5 µl nuclease of free water
- 0.5 µl primer mix containing of both forward and reverse primers
- 0.5 µl of ears clip sample DNA

Target gene primers (Cre and *Txnrd1*) were obtained from Eurofins company as High Purity Salt Free (HPSF) purified lyophilized oligonucleotides, suspended at 100 mM in 1 x TE buffer and stored at – 20 °C, and diluted with water before use. The primer sequences were shown above. PCR samples were performed by T100™ Thermal cycler with the following program:

95 °C, 1 min
95 °C, 30sec
58 °C, 30sec
72 °C, 1.5mins
} 40 times
72 °C, 10 mins
4 °C, ∞

Using a Sub-Cell GT Horizontal Electrophoresis System with casting gates, PCR products were detected through ROTI® – GelStain - based agarose gel electrophoresis. As mentioned above in method 2.1.2, 2% agarose gel was prepared. For each sample result, the Molecular Imager® Gel Doc™ XR system and the Quantity One software (version 4.5.2 (Basic), Bio-Rad) were used to detect the DNA bands.

2.2.4 Acini and 3D acinar cell culture

4 – week – old mice were sacrificed by isoflurane, and pancreas was quickly resected and transferred into a 60 mm cell culture dish filled with 5 ml of cold sterile PBS washed thrice and transferred into a small new dish containing 4.5 ml of solution 2 (Table 2 and Table 3). The pancreas was perfused by injecting solution 2 with a 20 G needle and cutting it into small pieces with sterile scissors. Primary acini were released by collagenase digestion twice at 37°C, and incubation at 5% CO_2 for 10 mins with gentle shaking every 1 min. After the first-time incubation, the suspension was transferred into a 50 ml Falcon tube and pipetted gently up and down one or two times. Afterward, 10 ml of solution 1 were used to rinse the dish and added to this suspension. The suspension was then centrifuged at 300 x rpm for 5 mins at 18°C and the supernatant was removed. The pellet was mixed with 4.5 ml of solution 2 and aspirated, transferred to a small new dish, and incubated in the incubator for 10 min with gentle shaking every 1 min. Aspirate the sample and filter through the 100 µm nylon cell strainer by centrifuging it at 300 x rpm for 5 mins at 18°C and remove supernatant carefully. To this pellet, 19 ml of solution 1 was added, then transferred to a new 50 ml Falco tube and centrifuged at 300 x rpm for 5 mins at 18°C, and the supernatant was carefully removed. Then the pellet was resuspended twice with 1 ml of culture medium (Table 4) containing 30% FBS and transferred to a cell culture dish. Next, the isolated acini were incubated for 60 minutes for recovery in the incubator (37°C with 5% CO_2).

Table 2 Solution 1 for acinar cell isolation. 50 ml per mouse

Component	Volume
McCoy's 5A Medium	48.5ml
10% BSA	500µl
Soybean trypsin Inhibitor (stored at 4°C)	1000µl

Table 3 Solution 2 for acinar cell isolation. 10 ml per mouse

Component	Volume
Collagenase from *Clostridium histolyticum*, Type VIII	12mg
solution 1	10ml

Table 4 Culture medium for acinar cell. 10 ml per mouse

Component	Stock	Volume	Final Concentration
BSA	10%	100 µl	0.1%
FBS	100%	10 µl	0.1%
Soybean trypsin Inhibitor (stored at 4°C)	100%	100 µl	1%
Insulin-Transferrin-Selenium (stored at 4°C)	100 x	100 µl	1 x
Bovine Pituitary Extract (stored at -20°C)	Depends on LOT	x µl	50 µg/ml
HEPES (stored at 4°C)	1 M	100 µl	10 mM
$NaHCO_3$	N.A.	0.026 g	2.6 g/l
Waymouth's MB 752/1 Medium	N.A.	add to 10 ml	N.A.

For acinar cell culture, 250 µl of cell suspension plus 1750 µl of culture medium were seeded into 6-well cell culture plates to determine a final total of 2 ml per well. The acinar cells were treated with 20 mM BSO and 25 µM H_2O_2 for 24 hours (Figure 2.2.6). The cells for each condition were seeded in duplicates. The medium was collected after 24 hours and further analyzed for LDH assay.

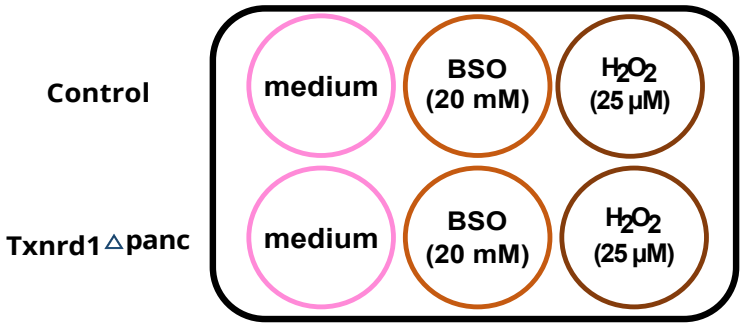

Figure 2.2.6 Layout of isolated acinar cells in 6-well cell culture plate with experimental conditions.

For 3D acinar cell culture, 8-well cell culture plates were coated with first layer collagen which includes 2.5 mg/ml Rat Tail Collagen Type I, 1/10 of the total volume of 10 x PBS, 0.023 times the amount of the collagen volume of 1 M NaOH, and sterile H_2O to dilute the collagen. When the collagen solidified (30 – 40 mins at 37°C with 5% CO_2), the collagen pellet was resuspended in a 3D culture medium for the second layer. This medium includes 0.023 times the collagen volume of 1 M NaOH. Half of the volume of collagen and half of the total volume of acinar cell suspension were mixed (the amount of acinar cell suspension was determined based on the number of acini). The second collagen layer needs to solidify at 37°C and 5% CO_2 incubation for 30 – 40 minutes. The third layer was prepared the same as the first layer and gently added over the second layer. After 30 – 40 minutes, the culture medium was gently added when the third layer of the collagen solidified. For an 8-well chamber slide, 70 µl collagen mixture per layer and 200 µl culture medium were used. The culture medium was changed after 24 hours of incubation. On day 3, the transdifferentiation rate was calculated as the percentage of ductal structures observed per total acinar cell clusters.

To assess the effects of different pathways, various stimulants (Table 5) were added to the culture medium (Figure 2.2.7). The cells in each condition were seeded in duplicates. Medium from day 1 and day 3 were collected for further LDH assay.

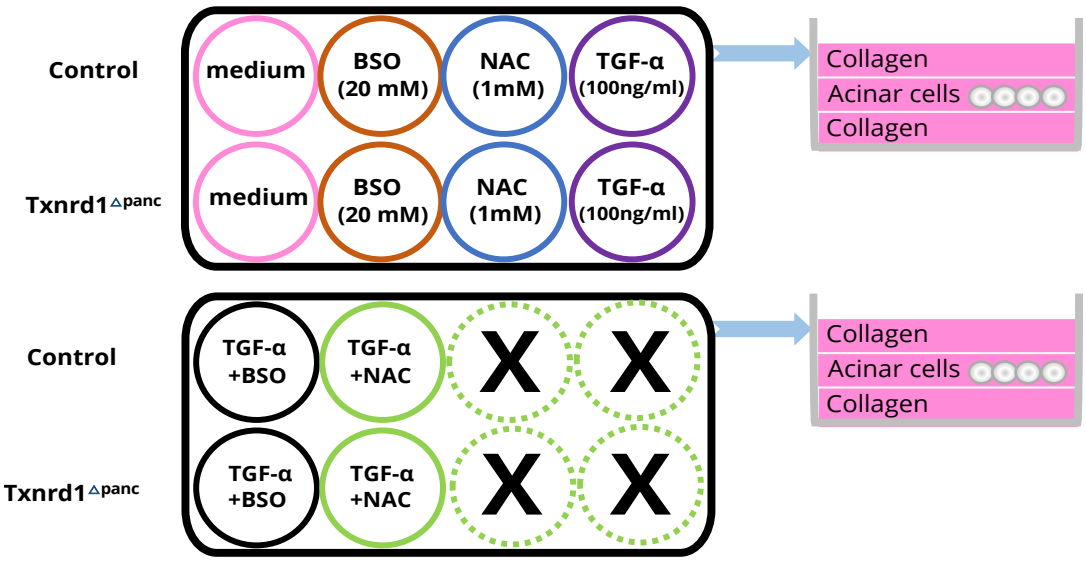

Figure 2.2.7 Scheme of 3D acinar cell culture in 8 – well chamber slide. Schedule of BSO, NAC, TGFα, TGFα + BSO and TGFα + NAC treatment for control and Txnrd1$^{\Delta panc}$ 3D acinar cells experiment in 8-well chamber slide.

As a positive control for the LDH assay, as a positive control, 60 µl of the acinar cell suspension from each sample was mixed with 340 µl of culture medium and lysed with 8 µl Triton®– X–100 for 30 mins at 37°C.

Table 5 Stimulants of signaling pathways for acinar cell culture

Stimulants	Solvent	Stock concentration	Final concentration
BSO	In H_2O	500 mM	20 mM
H_2O_2	In H_2O	9.8 M	25 µM
TGFα	In 10 mM acetic acid	100 µg/ml	100 ng/ml
NAC	In H_2O	100 mM	1 mM

2.2.5 Western blots

Isolated proteins were extracted from frozen pancreas tissues (as described in method 2.2.2.5) using ice-cold RIPA buffer, homogenized in a Heidolph Brinkmann Homogenizer Silent Crusher M 036170020 for 20 seconds and sonicated for 10 seconds on ice. The homogenate was then spun down with centrifuge at max speed for 5 mins at 4°C, and the supernatant was transferred to new reaction tube for protein quantification. To determine protein concentrations, Pierce® BCA Protein Assay Kit was used: 5 µl protein samples were diluted with 20 µl water and 20 µl standards from the BCA protein assay kit were diluted with 5 µl RIPA buffer. Proteins were adjusted to equal concentrations with RIPA buffer and supplemented with 1/5 of the total volume Lämmli sample buffer (6 x SDS) and heated for 5 minutes at 95°C in a Thermomixer® compact (Eppendorf) shaker and put on ice quickly before loading on gels.

Based on the size of the target proteins, 15% SDS polyacrylamide gel was chosen and inserted in the Mini-PROTEAN spacer plates (Bio-Rad) for moist transfer. The total buffer volume for 2 gels was 700 ml, and total buffer volume for 4 gels was 1000 ml, using Tris-Glycine SDS Running Buffer (1 x). The Fermentas Spectra™ Multicolor Broad Range Protein Ladder (10 µl) and 30 µl per sample were loaded into channels of gels. The gels were run at room temperature. First, the voltage was 80 V until the loading of protein samples into separation gel, and then the voltage was increased to 200 V to separate proteins.

Once separated, proteins were transferred to a 0.2 µm nitrocellulose blotting membrane while running the blot in transfer buffer at 100 V for 2 hours on ice. After transfer, the membranes were washed in 1 x TBST for a couple of seconds and blocked in 5% skim milk powder or 5% BSA with 1 x TBST for one hour at room temperature with continuous shaking. Afterwards, membranes were taken out and washed with 1 x TBST for 2 minutes on a shaker. The membranes were put in the

target protein primary antibodies solution and incubated in a cold room (4°C) overnight by shaking. The following day membranes were taken out from primary antibodies solution and washed once for 15 minutes and three times for 5 minutes each time with 1 x TBST on a shaker. Based on the host of primary antibodies, HRP conjugated secondary antibodies solution that matched the primary antibodies were used and diluted 1:5000 in 5% Milk-TBST. Membranes were incubated for one hour at room temperature in a box by shaking. Membranes were taken out from secondary antibodies solution and washed once for 15 minutes and three times for 5 minutes each time with 1 x TBST on a shaker. After washing membranes, Amersham primer ECL Western Blotting Detection Reagent was used for detecting protein bands by Molecular Imager®Gel Doc™ XR system (Figure 2.2.8).

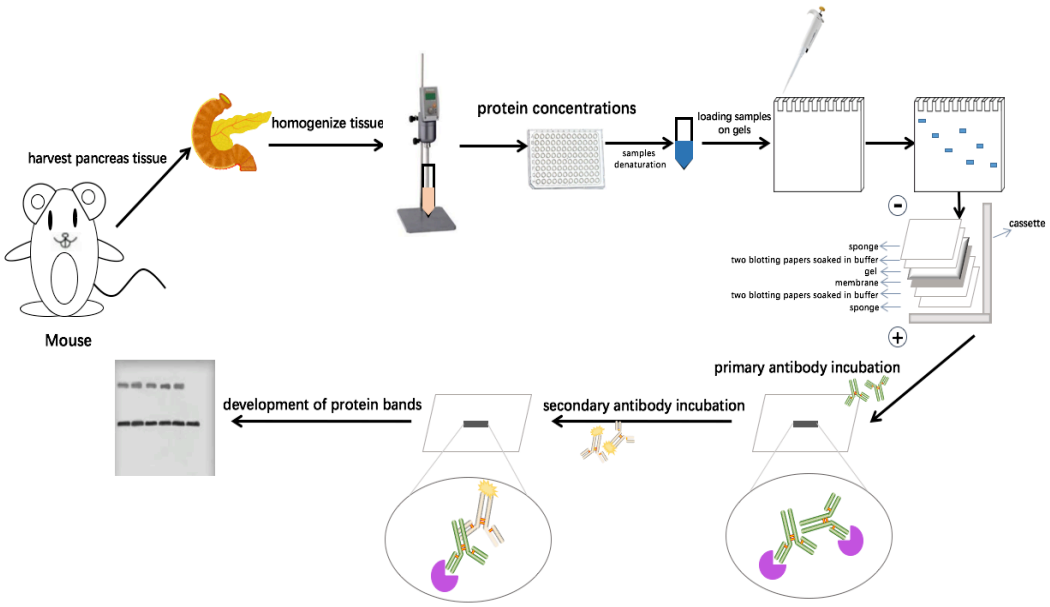

Figure 2.2.8 Detection of pancreatic tissue by western blots. Flow chart of pancreatic tissue by western blots.

2.2.6 Histological analysis

Pancreas tissue samples were harvested from different groups of mice and were locked in an embedding cassette and fixed in 4% paraformaldehyde over night at 4°C, then dehydrated using the S300 tissue processing unit (described in 2.2.2.7) and embedded in Paraffin. Thereafter, the paraffin blocks were cut into sections of 2.5 µm thickness using a Microm HM 355S microtome and transferred onto Superfrost® plus microscope slides. After an air-drying overnight at 37°C, slides were used for hemalaun – Eosin (H&E) and immunohistochemistry (IHC). First, paraffin sections were deparaffinized by incubation in Roti® – Histol twice for 5 mins. Then, the slides were rehydrated in decreasing concentrations of ethanol in demineralized water (100%, 96%, 70%, and 0%) twice for 2 – 3 mins per concentration.
The de-paraffinization and rehydration steps for paraffin sections were applied to the very first parts of H&E and IHC staining. The next steps for H&E and IHC staining were as follows:

2.2.6.1 Hemalaun-Eosin (H&E) Staining

Sections were stained for 3 minutes in Mayer's hemalaun solution and washed for 10 minutes under running tap water. Then, the sections were counterstained in 0.33% eosin for 3.5 min. After staining, slides were dehydrated by consecutive incubation in 96 % ethanol for 25 sec, isopropanol for 25 sec and in Roti®– Histol twice for 3 mins. Finally, the slides were mounted with a Pertex embedding medium and sheeted with coverslips (ThermoFisher, # BB024032A1).

2.2.6.2 Immunohistochemistry (IHC) Staining

CK 19 and BrdU

After the de-paraffinization and rehydration steps of the paraffin sections, the deionized water was removed and the citrate unmasking solution was placed in a black box. The slide was completely covered and placed in a microwave, then heated to boiling at maximum power (900 watts). The power was then changed to 300 watts and maintained for 10 minutes. Afterward, the black box was removed from the microwave and allowed to cool at room temperature for 20 minutes.

Amylase

After the de-paraffinization and rehydration steps of the paraffin sections, the deionized water was removed and the high pH unmasking solution was placed in a black box and the slide should be covered completely, which was placed in a microwave and heated to boiling at maximum power (900 watts), then changed to 300 watts for 10 minutes, after which the black box was removed from the microwave and cooled at room temperature for 20 mins.

F 4/80

20 µg/ml proteinase K (10 µl proteinase K in 9 ml 10 mM Tris/HCl, pH 8.0) solution was added to the slides for 15 mins at room temperature.

Endogenous peroxidases were blocked using the peroxidase blocking solution (3% H_2O_2 in deionized water) for 20 mins at room temperature in a dark and humidified box. Blocking buffers were added on the slides for 1 hour in 5% rabbit serum in PBS for CK 19, BrdU, and F4/80, and 5% goat serum in PBS for amylase. Slides were stained with primary antibodies against Amylase, CK 19, F 4/80, and BrdU overnight in a humidified chamber. The next day, slides were washed with PBS or TBST three times and incubated with secondary antibodies (1:500, anti-rabbit in goat for Amylase, anti-rat in rabbit for CK 19 and F 4/80, anti-mouse in goat for BrdU) in

blocking buffers for 2 hours. Slides were then washed with PBS or TBST three times and then added ABC solution was added for 30 mins. Signal was detected with the DAB Peroxidase Substrate Kit for 1 min (Amylase) and 2.5 mins (CK 19, F 4/80, and BrdU) at room temperature according to the manufacturer's protocol. Tissues were then counterstained by quickly dipping slides into hematoxylin solution and subsequent washing under running tap water for 10 min. Afterwards, slides were dehydrated by increasing concentrations of ethanol in demineralized water (70%, 96%, and 100%) twice for short time per concentration. Finally, the slides were mounted in pertex embedding medium and sheeted with coverslips.
For immunohistochemistry (IHC) staining, antigen retrieval was performed using citrate unmasking solution for CK 19 and BrdU, high pH unmasking solution for Amylase, and 20 µg/ml proteinase K solution for F 4/80.
Slides were scanned at the core facility of animal pathology, TU München, by the laboratory of Katja Steiger. The scanned slides were used for quantification of amylase, CK 19, BrdU, and F 4/80 with QuPath (version 0.3.2).

2.2.7 Enzymatic assays

2.2.7.1 GSH / GSSG assay

For the GSH/GSSG-Glo assay, pancreas and liver tissue samples were rinsed twice in ice-cold PBS. Then, 10 volumes of ice-cold 5% SSA (5 g Sulfosalicylic acid in 100 ml H_2O) were added, and samples were homogenized and centrifuged at 14,000 x g at 4°C for 10 minutes. The supernatant was transferred to new tubes and an equal volume of ice-cold Neutralization Buffer (500 mM HEPES, pH 8) was added. Liver samples were diluted 10 – fold in dilution buffer (250 mM HEPES, pH 7.5) to be measured in the linear detection range, pancreas samples were not diluted for measurement. The 96 – well plate and the dilution buffer were kept on ice. 25 µl tissue lysate per well and 25 µl of either total (Table 6) or oxidized glutathione lysis

reagent (Table 7) per well were added and shaken for 5 minutes in a shaker. Then, 50 µl luciferin generation reagent (Table 8) per well was added and incubating 30 minutes at room temperature. After that, 100 µl luciferin detection reagent per well was added and equilibrated for 15 minutes. Luminescence was measured using Infinite® 200 Pro (Tecan) machine.

Table 6 Total glutathione lysis reagent

Component	**Volume per reaction (96-well plate)**
Luciferin-NT	1.0 µl
Passive lysis buffer, 5x	10.0 µl
Water	14.0 µl
Final volume per reaction	25.0 µl

Note: Use the total glutathione lysis reagent within 30 minutes after preparing it.

Table 7 Oxidized glutathione lysis reagent

Component	**Volume per Reaction (96-well plate)**
Luciferin-NT	1.0 µl
NEM, 25mM	0.5 µl
Passive lysis buffer, 5x	10.0 µl
Water	13.5 µl
Final volume per reaction	25.0 µl

Table 8 Luciferin generation reagent

Component	**Volume per Reaction (96-well plate)**
100mM DTT	1.25 µl
Glutathione-S-Transferase	3.0 µl
Glutathione reaction buffer	45.75 µl
Final volume per reaction	50.0 µl

2.2.7.2 Lactate dehydrogenase (LDH) assay

LDH activity was measured using Roche LDH Cytotoxicity detection kit to estimate the amount of cell death during acinar cell culture following the manufacturer's protocol. Briefly, all supernatants from acinar cell culture were collected at day 1 and day 3 were combined from each sample. For positive control, 60 µl of acinar cell suspension was mixed with 340 µl of culture medium and lysed with 8 µl Triton®X – 100 for 30 mins at 37°C at day 0. Absorbance was measured at a wavelength of 490 nm on a Multiscan™ FC Microplate Photometer (ThermoFisher Scientific™) machine.

The number of dead cells was determined using equation (1), where PC is the average absorption of the total positive control value in control and Txnrd1$^{\Delta panc}$ groups separately, BC is the average absorption of the background control value.

$$\text{Cytotoxicity rate (LDH release rate)} = \frac{\text{Sample} - \text{BC}}{\text{PC} - \text{BC}} \qquad (1)$$

2.2.8 Statistical analysis

Statistical analysis was performed using GraphPad Prism version 9. Unpaired t-test was used for comparison between the control group and the knockout group. Statistical significance was considered when the p-value was less than 0.05.

3. RESULTS

3.1 Experimentally induced acute pancreatitis in *Txnrd1* deficient pancreas

Pancreas-specific knockout of Thioredoxin reductase 1 (Txnrd1$^{\Delta panc}$) in mice was previously generated. Txnrd1$^{\Delta panc}$ mice were generated by crossbreeding Txnrd1$^{flox/flox}$ mice to Ptf1α-Cre^{ex1} mice. Knockout of *Txnrd1* in these mice was confirmed at the level of DNA and protein (Figure 3.1). Absence of *Txnrd1* in pancreas in these mice did not show any major differences in growth, pancreatic gross-morphology, and other parameters, as compared to control mice (described in introduction 1.5) [109].

A

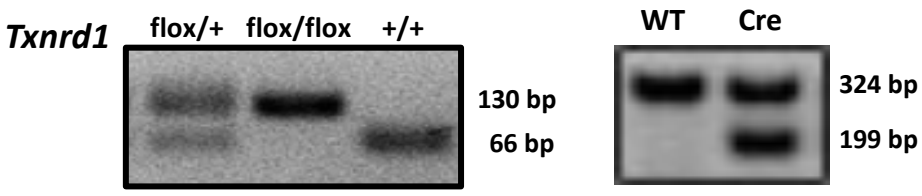

B

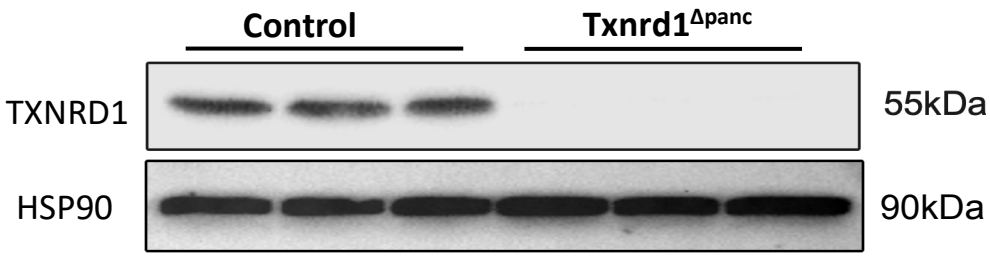

Figure 3.1 Generation of Txnrd1$^{\Delta panc}$ mice. (A) PCR results for *Txnrd1*$^{flox/flox}$ or Ptf1α-Cre^{ex1} recombinase in ear biopsies. Only the combination *Txnrd1*$^{flox/flox}$, Ptf1α-Cre^{ex1} leads to Txnrd1$^{\Delta panc}$ mouse. **(B)** Representative western blot from pancreatic tissue of control (*Txnrd1*$^{flox/flox}$) (left) and Txnrd1$^{\Delta panc}$ (right) mice. HSP90 served as loading control.

To investigate the changes after acute pancreatitis in control and Txnrd1$^{\Delta panc}$ animals, caerulein-induced acute pancreatitis was performed in 10 – week – old control and Txnrd1$^{\Delta panc}$ animals, and organs were harvested at 0 hours, 8 hours, 24 hours, and 1 week time points (described in method 2.2.2.2). The pancreas to bodyweight ratio of *Txnrd1* deficient pancreas was found to be decreased at 1-week after caerulein administration (Figure 3.2).

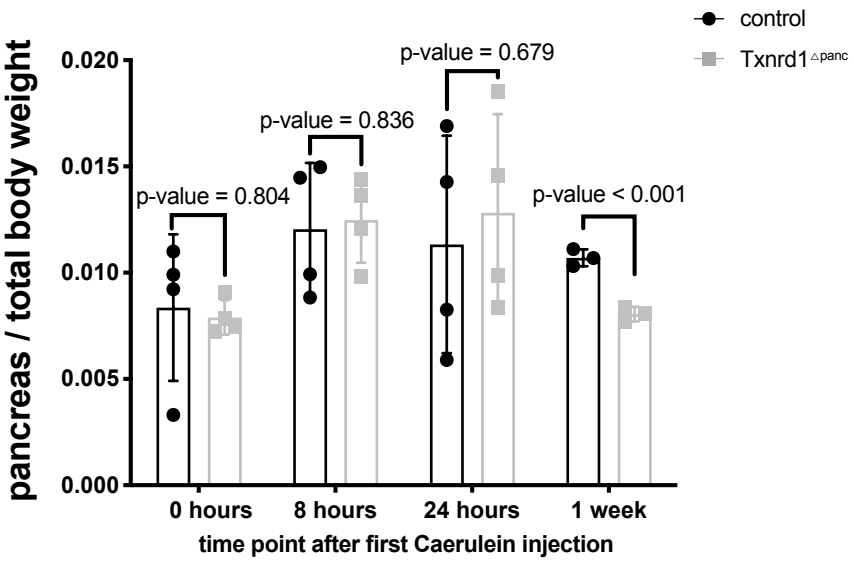

Figure 3.2 Pancreas to bodyweight ratio after caerulein administration. Pancreas to bodyweight ratio in 10 – week – old control and Txnrd1$^{\Delta panc}$ mice at 0 hours (control: n=4 & Txnrd1$^{\Delta panc}$: n=4), 8 hours (control: n=4 & Txnrd1$^{\Delta panc}$: n=4), 24 hours (control: n=4 & Txnrd1$^{\Delta panc}$: n=4), and 1 week (control: n=3 & Txnrd1$^{\Delta panc}$: n=3) after caerulein administration. Data are shown as mean ± standard deviation (SD). Differences were considered statistically significant at $p < 0.05$ using unpaired t-test.

Amylase and lipase released into the circulation were detected at their highest levels 8 hours after first caerulein injection, indicating that the acute pancreatitis was successfully induced, and levels of these enzymes returned to basal levels after 1 week (Figure 3.3). AP is diagnosed and monitored elevated serum amylase and lipase levels [113].

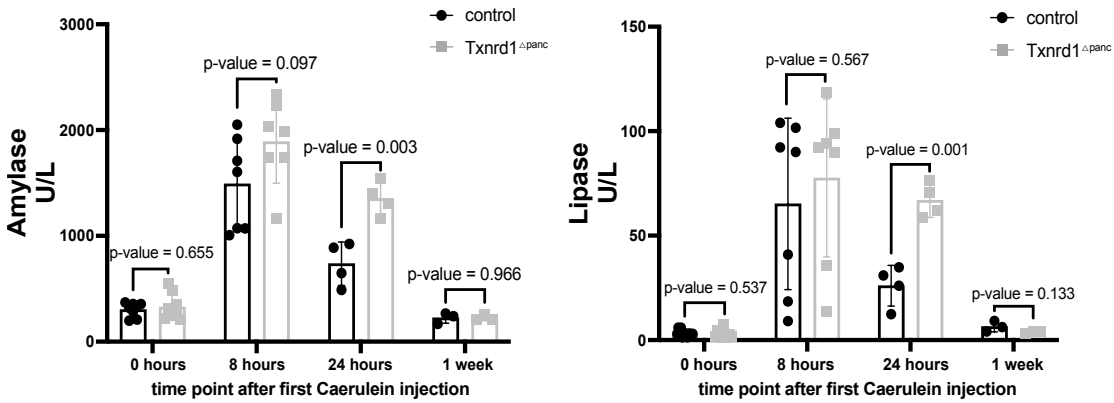

Figure 3.3 Serum amylase and lipase after caerulein administration. Serum amylase and lipase levels in 10 – week – old control and Txnrd1$^{\Delta panc}$ mice at 0 hours (control: n=4 & Txnrd1$^{\Delta panc}$: n=4), 8 hours (control: n=4 & Txnrd1$^{\Delta panc}$: n=4), 24 hours (control: n=4 & Txnrd1$^{\Delta panc}$: n=4), and 1 week (control: n=3 & Txnrd1$^{\Delta panc}$: n=3) after caerulein administration. Data are shown as mean ± SD. Differences were considered statistically significant at $p < 0.05$ using unpaired t-test.

Next, the ratio of edema to total pancreas area was analyzed on histological slides. Significantly increased ratios in Txnrd1$^{\Delta panc}$ at 8 hours and 24 hours (Figure 3.4) were observed compared to control group, indicating increased inflammation. To investigate the status of acinar cell compartment, histological slides were stained for amylase using immuhistochemistry. In line with circulating levels, amylase expression in pancreatic tissue was similar between the groups at all time points (Figure 3.5). To determine any changes in acinar-ductal metaplasia (ADM) program, pancreatic tissue was stained with CK19, no statistically significant differences between groups were found at all time points (Figure 3.6). Furthermore, pancreatic tissue was analyzed for macrophage infiltration using F 4/80 as a marker, which was found to be increased in Txnrd1$^{\Delta panc}$ at 24 hours and 1 week compared to control group but was not statistically significant (Figure 3.7). Taken together, these data suggest that caerulein-induced acute pancreatitis in Txnrd1$^{\Delta panc}$ mice results in a mild phenotype with increased edema and decreased pancreatic weight compared to control mice.

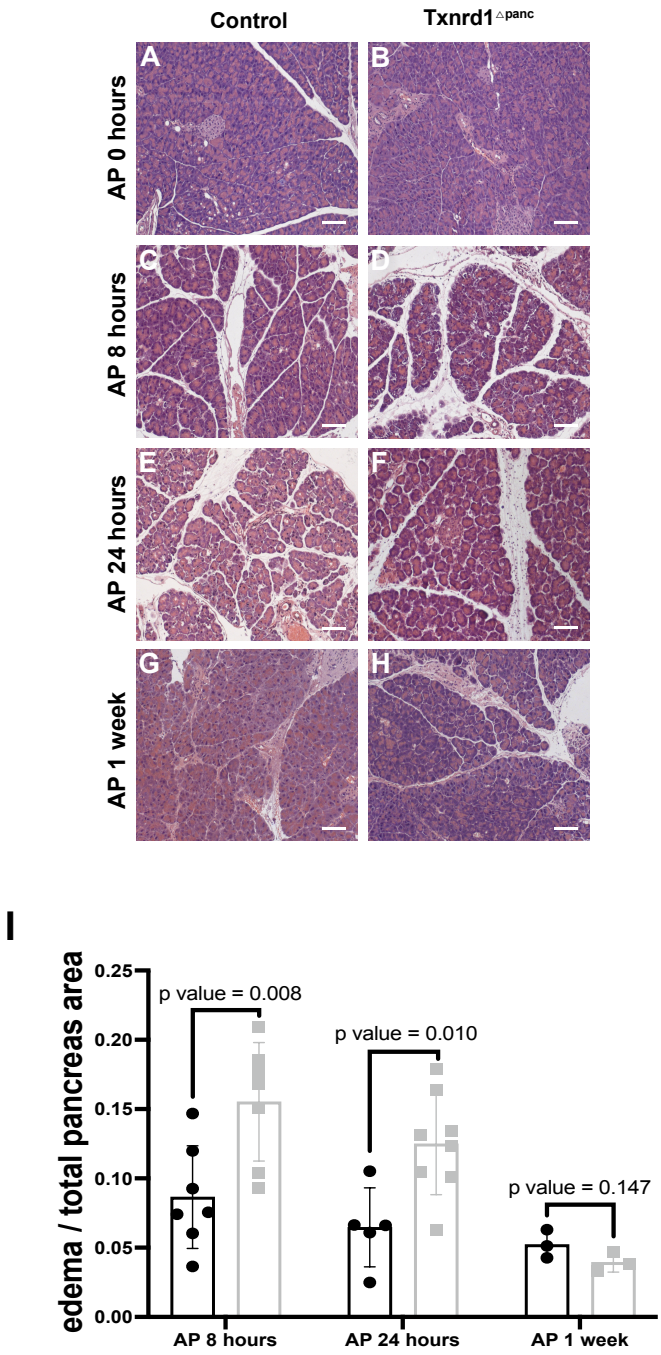

Figure 3.4 Edema to pancreas area after induction of acute pancreatitis. Representative images of H&E staining of pancreatic tissues in 10 – week – old control and Txnrd1$^{\Delta panc}$ mice at **(A, B)** 0 hours (control: n=4 & Txnrd1$^{\Delta panc}$: n=4), **(C, D)** 8 hours (control: n=7 & Txnrd1$^{\Delta panc}$: n=7), **(E, F)** 24 hours (control: n=5 & Txnrd1$^{\Delta panc}$: n=8), and **(G, H)** 1 week (control: n=3 & Txnrd1$^{\Delta panc}$: n=3) after caerulein administration and quantification thereof in **(I)**. Scale bar, 100 µm. Data are shown as mean ± SD. Differences were considered statistically significant at $p < 0.05$ using unpaired t-test.

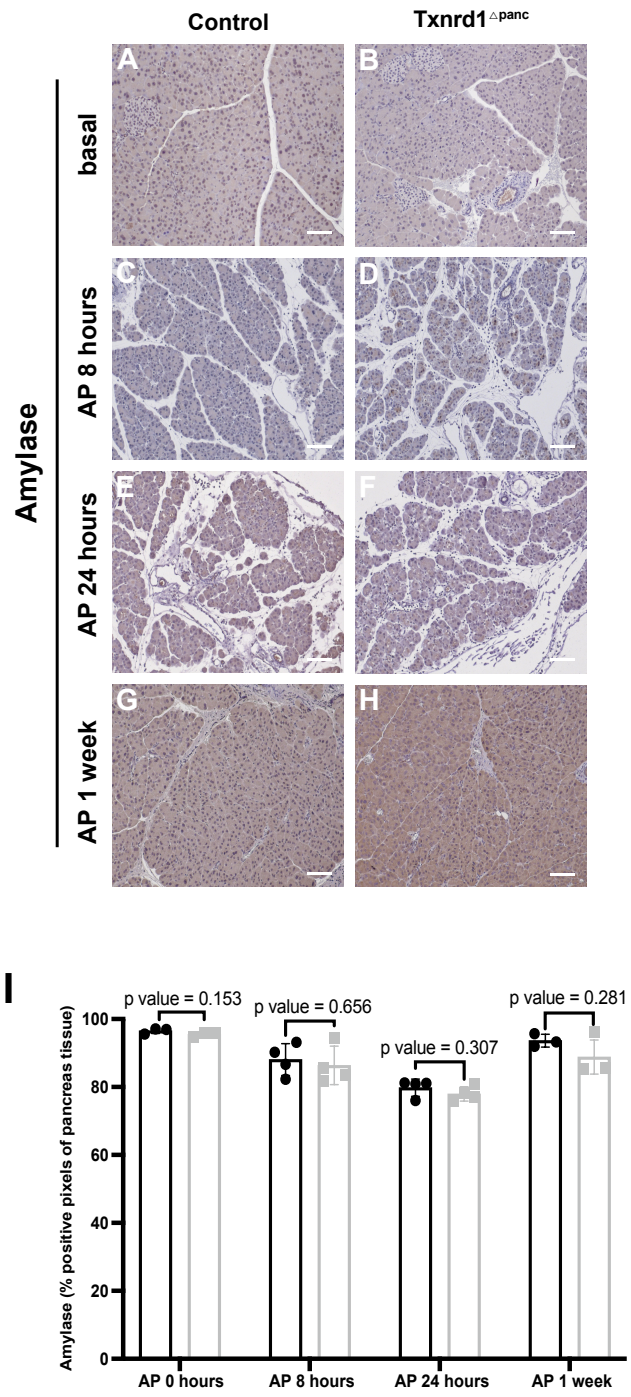

Figure 3.5 Amylase expression in pancreatic tissue after induction of acute pancreatitis. Representative images of IHC staining of amylase in pancreatic tissues of 10 – week – old control and Txnrd1$^{\Delta panc}$ mice at **(A, B)** 0 hours (control: n=3 & Txnrd1$^{\Delta panc}$: n=3), **(C, D)** 8 hours (control: n=4 & Txnrd1$^{\Delta panc}$: n=4), **(E, F)** 24 hours (control: n=4 & Txnrd1$^{\Delta panc}$: n=4), and **(G, H)** 1 week (control: n=3 & Txnrd1$^{\Delta panc}$: n=3) after caerulein administration. Scale bar, 100 µm. **I** Pancreas amylase pixel positive area/total pancreas area quantification of **A-H.** Data are shown as mean ± SD. Differences were considered statistically significant at $p < 0.05$ using unpaired t-test.

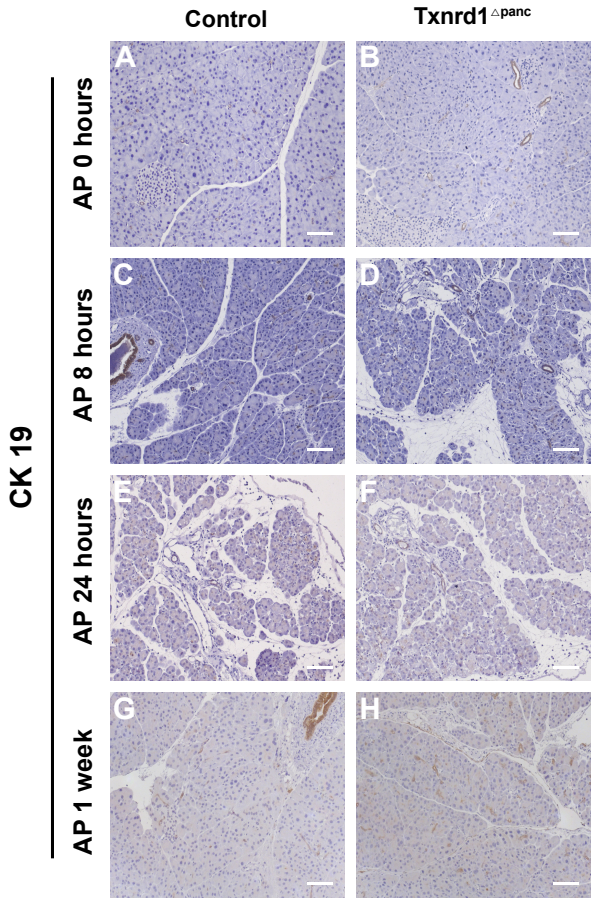

I

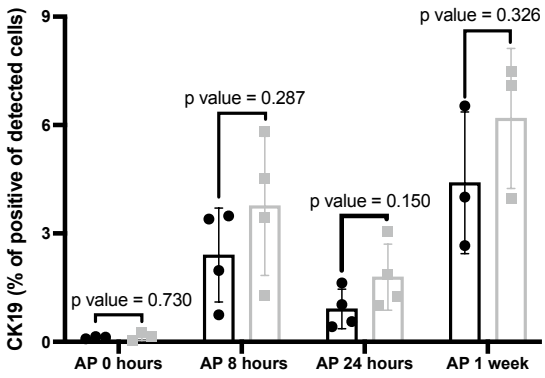

Figure 3.6 CK19 expression in pancreatic tissue after induction of acute pancreatitis. Representative images of IHC staining of CK19 in pancreatic tissues of 10 – week – old control and Txnrd1$^{\Delta panc}$ mice at **(A, B)** 0 hours (control: n=3 & Txnrd1$^{\Delta panc}$: n=3), **(C, D)** 8 hours (control: n=4 & Txnrd1$^{\Delta panc}$: n=4), **(E, F)** 24 hours (control: n=4 & Txnrd1$^{\Delta panc}$: n=4), and **(G, H)** 1 week (control: n=3 & Txnrd1$^{\Delta panc}$: n=3) after caerulein administration. Scale bar, 100 µm. **I** Pancreas CK19 positive cells/total pancreas area quantification of **A-H.** Data are shown as mean ± SD. Differences were considered statistically significant at $p < 0.05$ using unpaired t-test.

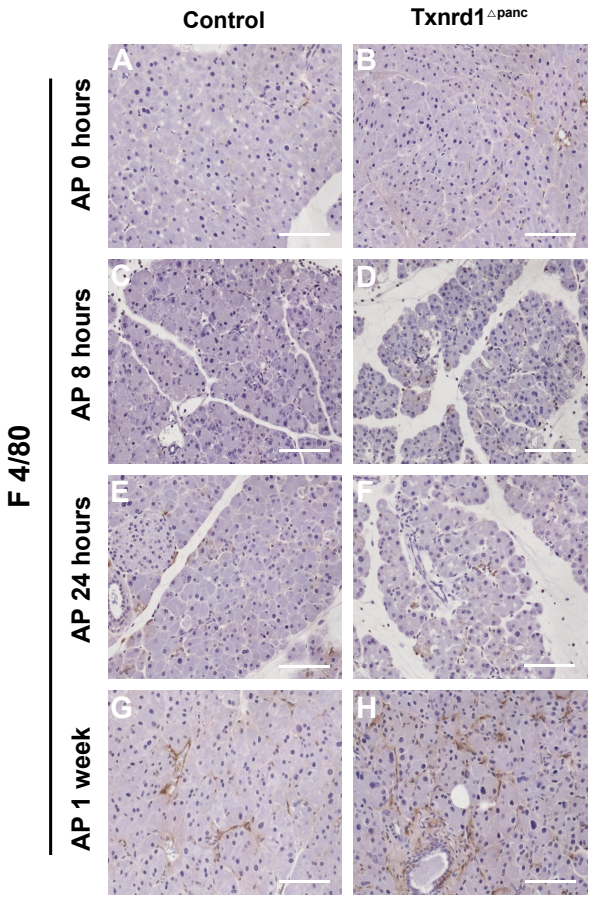

I

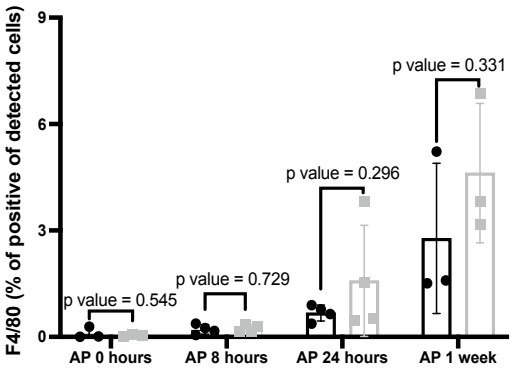

Figure 3.7 F 4/80 expression in pancreatic tissue after induction of acute pancreatitis. Representative images of IHC staining of F 4/80 in pancreatic tissues of 10 – week – old control and Txnrd1$^{\Delta panc}$ mice at **(A, B)** 0 hours (control: n=3 & Txnrd1$^{\Delta panc}$: n=3), **(C, D)** 8 hours (control: n=4 & Txnrd1$^{\Delta panc}$: n=4), **(E, F)** 24 hours (control: n=4 & Txnrd1$^{\Delta panc}$: n=4), and **(G, H)** 1 week (control: n=3 & Txnrd1$^{\Delta panc}$: n=3) after caerulein administration. Scale bar, 100 µm. **I** Pancreas F 4/80 positive cells/total pancreas area quantification of **A-H**. Data are shown as mean ± SD. Differences were considered statistically significant at $p < 0.05$ using unpaired t-test.

3.2 The glutathione system is upregulated in *Txnrd1* deficient pancreas

Induction of AP in Txnrd1$^{\Delta panc}$ mice resulted in a mild phenotype without major changes to the acinar compartment. To gain further insight into possible changes, RNA sequencing (RNA-Seq) of pancreatic tissue was performed from 0, 3, 8, and 24 hours after caerulein administration. Interestingly, a significantly increased expression of *Gstm1* in Txnrd1$^{\Delta panc}$ mice (Figure 3.8 A) was observed at all time points. This gene belongs to the glutathione system, which is important for cellular redox balance. Next, glutathione levels in pancreata were determined. We observed a significant increase in the total glutathione (GSH + GSSG) level and GSH/GSSG ratio in Txnrd1$^{\Delta panc}$ at basal condition compared to control group (Figure 3.8 B).

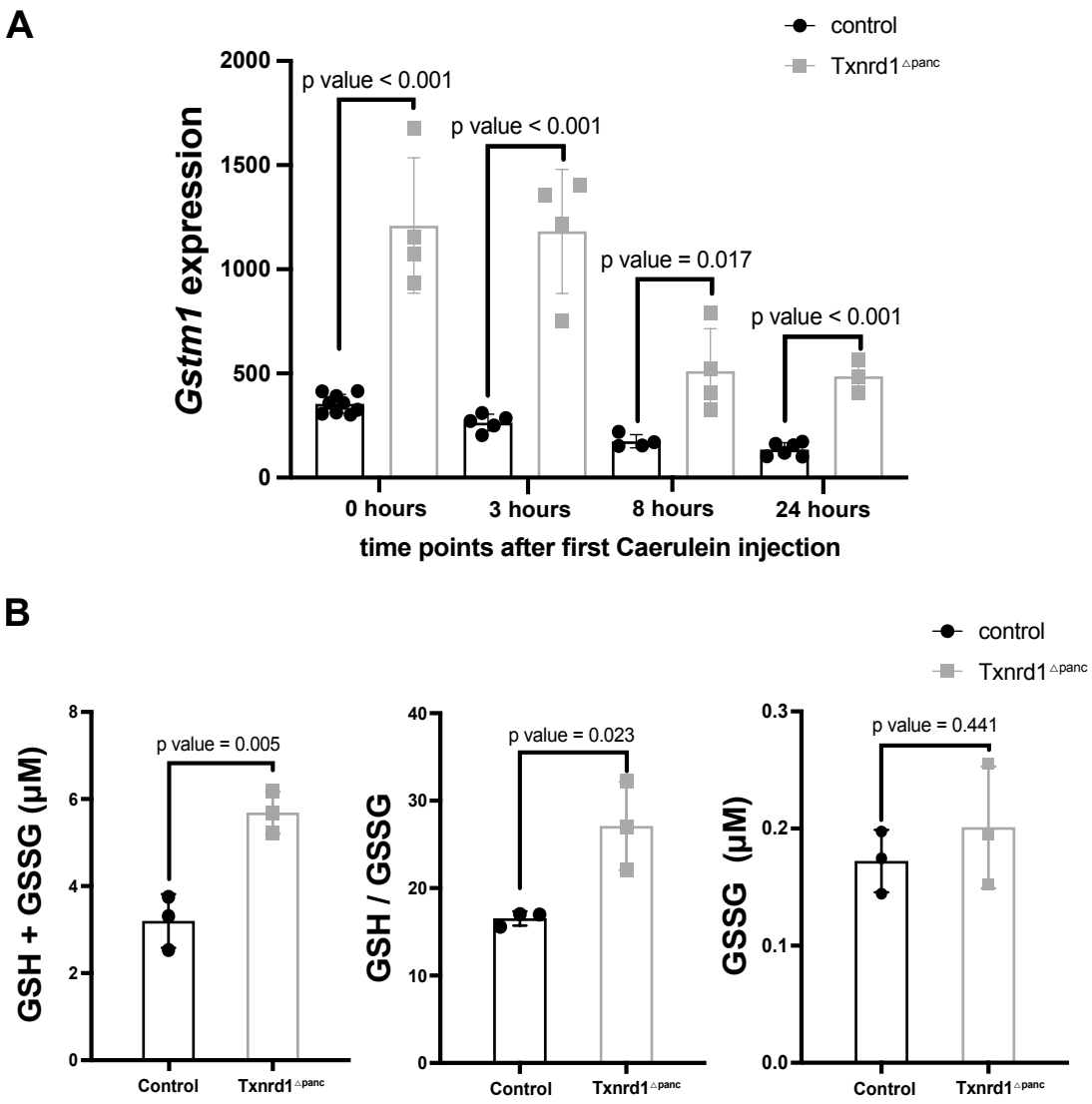

Figure 3.8 Status of GSH system in Txnrd1$^{\Delta panc}$ mice. A *Gstm1* expression as determined by RNA sequencing in pancreas after caerulein administration. 0 hours (control: n=9 & Txnrd1$^{\Delta panc}$: n=4), 3 hours (control: n=5 & Txnrd1$^{\Delta panc}$: n=4), 8 hours (control: n=4 & Txnrd1$^{\Delta panc}$: n=4), 24 hours (control: n=6 & Txnrd1$^{\Delta panc}$: n=3) **B** GSH and GSSG concentrations in pancreatic tissue for basal condition. Control: n=3 & Txnrd1$^{\Delta panc}$: n=3. Data are shown as mean ± SD. Differences were considered statistically significant at $p < 0.05$ using unpaired t-test.

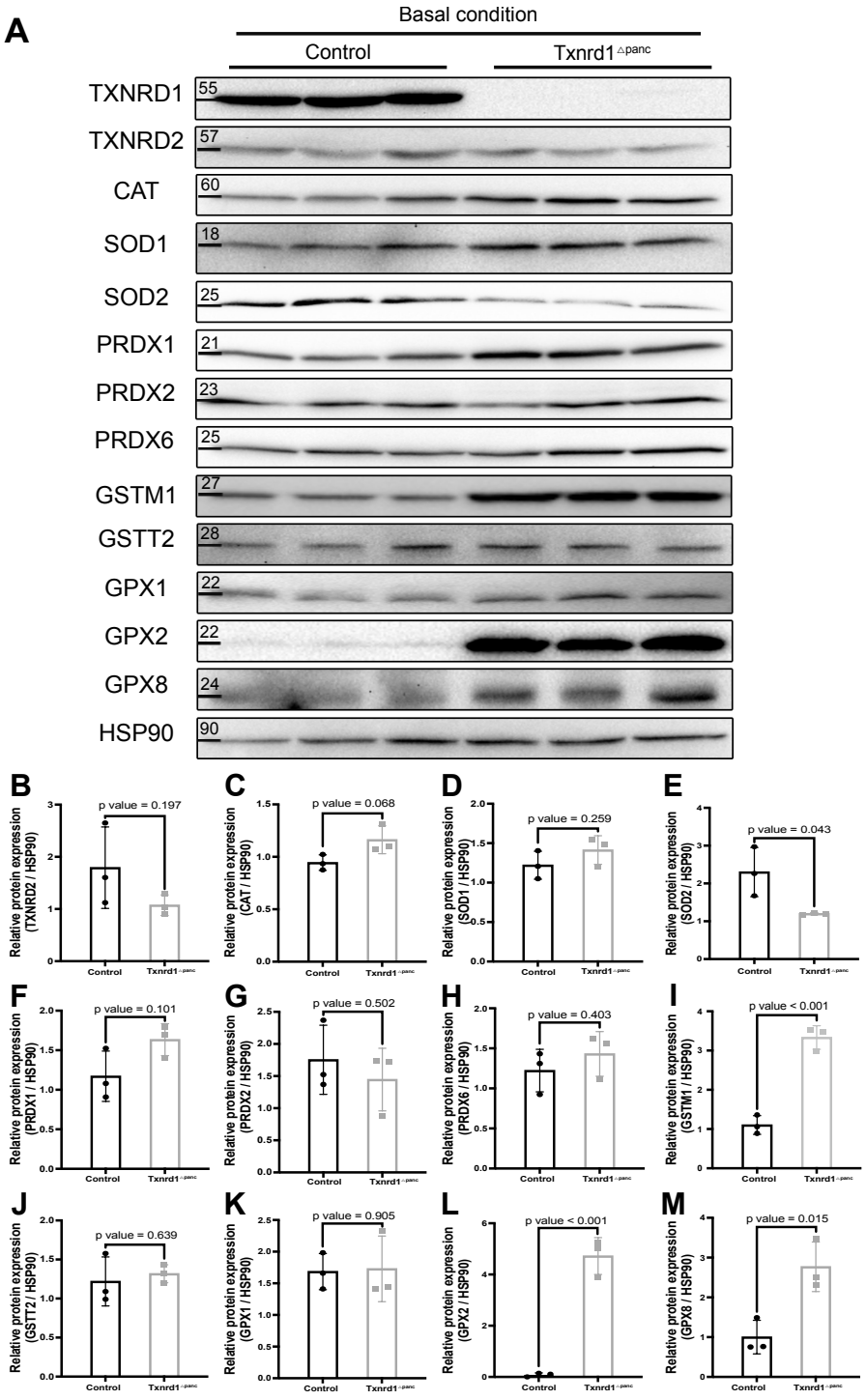

Figure 3.9 Expression of selected antioxidant proteins in unstimulated control and Txnrd$^{\Delta panc}$ mice. A Western blot for antioxidant proteins in pancreas tissue in 10-week-old unstimulated mice. HSP90 served as a loading control. **B-M** Quantification of **A**. Control: n=3 & Txnrd1$^{\Delta panc}$: n=3. Data are shown as mean ± standard deviation (SD). Differences were considered statistically significant at $p < 0.05$ using unpaired t-test.

To validate increase in GSH levels and *Gstm1* expression, and to explore changes in other antioxidant systems on the protein level in Txnrd1$^{\Delta panc}$ mice at basal condition, western blots were carried out. In accordance to increased glutathione levels, higher expression of enzymes GSTM1, GPX2, and GPX8 were observed, which were significantly increased in Txnrd1$^{\Delta panc}$ at basal condition (Figure 3.9).

Thus, these data show that glutathione system is upregulated in pancreas of *Txnrd1* deficient mice.

3.3 Investigation of the glutathione system as a compensatory mechanism in Txnrd1$^{\Delta panc}$ mice

3.3.1 Dose and time point finding for BSO treatment in wild-type mice

The indication of a possible compensation by the glutathione system in *Txnrd1* deficient mice needed further investigation. BSO treatment was employed to interfere with the rate-limiting enzyme of glutathione synthesis, glutamate-cysteine ligase (GCL), also known as γ-glutamyl transferase synthase. To determine the dose of BSO in drinking water needed for a significant and sufficient depletion of glutathione pools, wild-type mice were treated with different concentrations (0, 5, 10 and 20 mM) of BSO in the drinking water for 24 and 48 hours. Total glutathione (GSH + GSSG) level and the ratio of GSH / GSSG were significantly decreased at all concentrations at every time point (Figure 3.10), the most pronounced effect was observed with 20 mM. Moreover, the decrease of total glutathione (GSH + GSSG) and the ratio of GSH / GSSG caused by 20 mM BSO concentration was significantly more pronounced at 48 hours compared to 24 hours. The behavior and activity of wild-type mice was normal following BSO treatments.

Finally, a concentration of 20 mM BSO in drinking water for 48 hours was chosen for

further experiments.

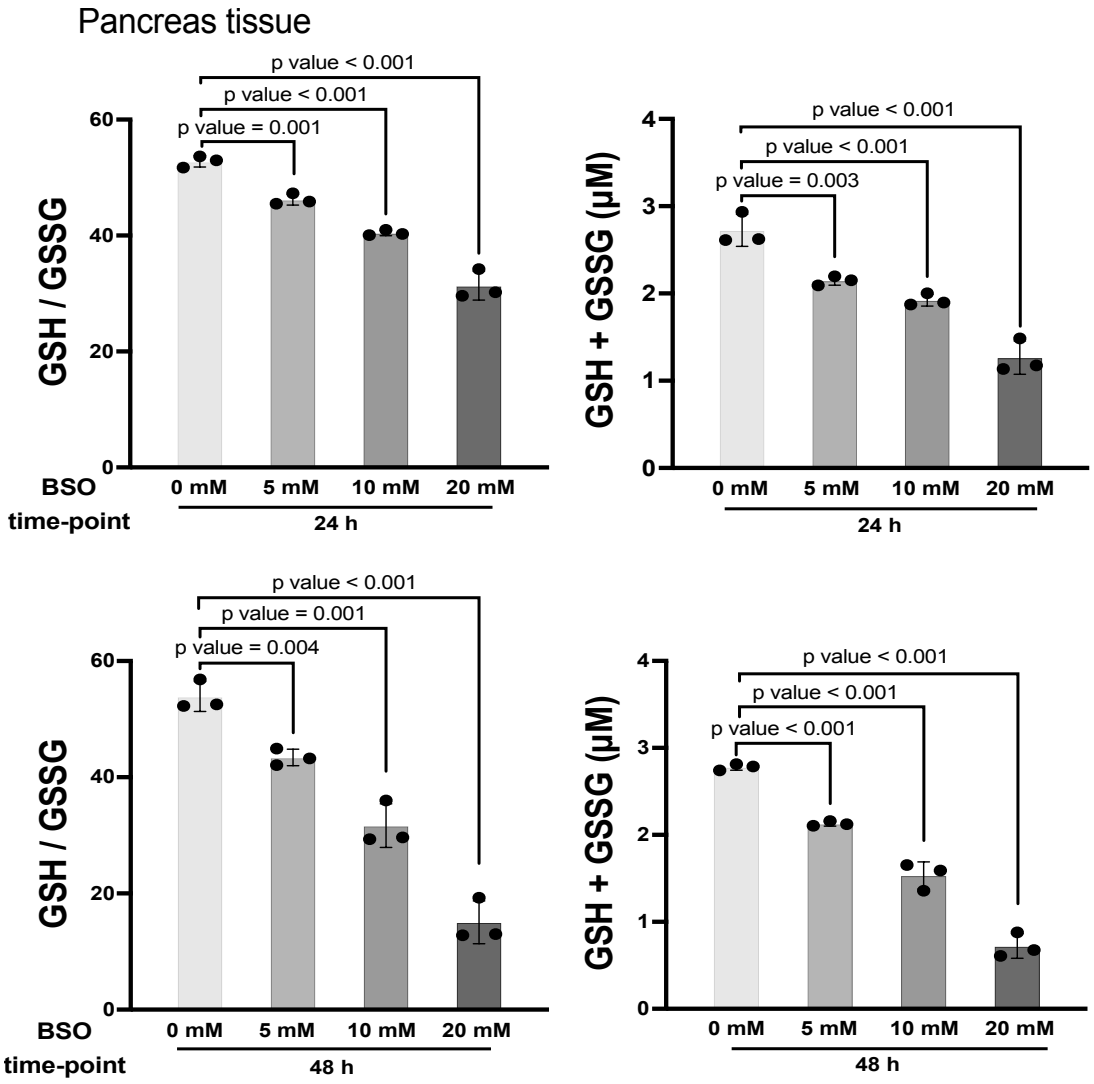

Figure 3.10 Dose and time point-finding of BSO treatment. The GSH and GSSG concentrations and the GSH / GSSG ratio in pancreata of wild-type animals. n=3 per group. Data are shown as mean ± SD. Differences were considered statistically significant at $p < 0.05$ using unpaired t-test.

3.3.2 Investigation of the potential role of GSH in *Txnrd1* deficient pancreas

Txnrd1$^{\Delta panc}$ and control mice were treated with 20 mM of BSO in drinking water for 48 hours and protein expression of the glutathione system were determined using western blotting. Interestingly, GSTM1, GSST2, GPX1, GPX2 and GPX8 were significantly decreased in pancreas of Txnrd1$^{\Delta panc}$ mice after BSO treatment compared to basal condition. In addition, we detected a higher amount of TXNRD1 protein in wild-type mice given BSO treatment compared to basal condition. This indicates that TXNRD1 might compensate for the reduced GSH levels in the control group (Figure 3.11).

To understand the long-term effect of glutathione depletion in Txnrd1$^{\Delta panc}$ animals, mice were treated with 20 mM concentration of BSO for 48 hours and then kept under normal conditions for 5 days or 14 days before harvesting organs. 5 and 14 days after administration of BSO treatment, a significant decrease in pancreas to body weight ratio (Figure 3.12 A) and a change in body weight after glutathione depletion in Txnrd1$^{\Delta panc}$ mice were observed (Figure 3.12 B).

Next, GSH levels in pancreatic and liver tissues were analyzed. In pancreatic tissue, total GSH level and GSH / GSSG ratio, were significantly decreased in Txnrd1$^{\Delta panc}$ mice after 48 hours of BSO treatment, while 5 days after BSO treatment, they increased and again, decreased after 14 days. In liver, total GSH level and GSH / GSSG ratio prior to BSO treatment, tended to be higher in Txnrd1$^{\Delta panc}$. However, a significant increase in Txnrd1$^{\Delta panc}$ mice at 48 hours after BSO treatment was observed, while at 5 and 14 days there was an elevated trend in the control group and no statistically significant change in Txnrd1$^{\Delta panc}$ mice (Figure 3.13 A-B).

Additionally, the ratio of edema to total pancreas area was analyzed, there were no significant differences detectable between the groups at any time point (Figure 3.14). Next, immunohistochemistry for amylase was performed. Surprisingly,

amylase positive cell area was significantly decreased in Txnrd1$^{\Delta panc}$ after 48 hours BSO treatment, but after 5 days and 14 days, no significant differences could be detected (Figure 3.15). To determine changes in ADM formation, pancreatic tissue was stained for CK19 and a significant increase at 14 days in Txnrd1$^{\Delta panc}$ mice (Figure 3.16) was found. In addition, when pancreatic tissue was analyzed for macrophage infiltration using F 4/80 as a marker, a significant increase in Txnrd1$^{\Delta panc}$ mice after BSO treatment was observed (Figure 3.17).

Taken together, BSO treatment for 48 hours caused a significant decrease in glutathione in Txnrd1$^{\Delta panc}$ mice and induced an overall mild phenotype with increased ADM formation, a decrease of acinar tissue and increased macrophage infiltration.

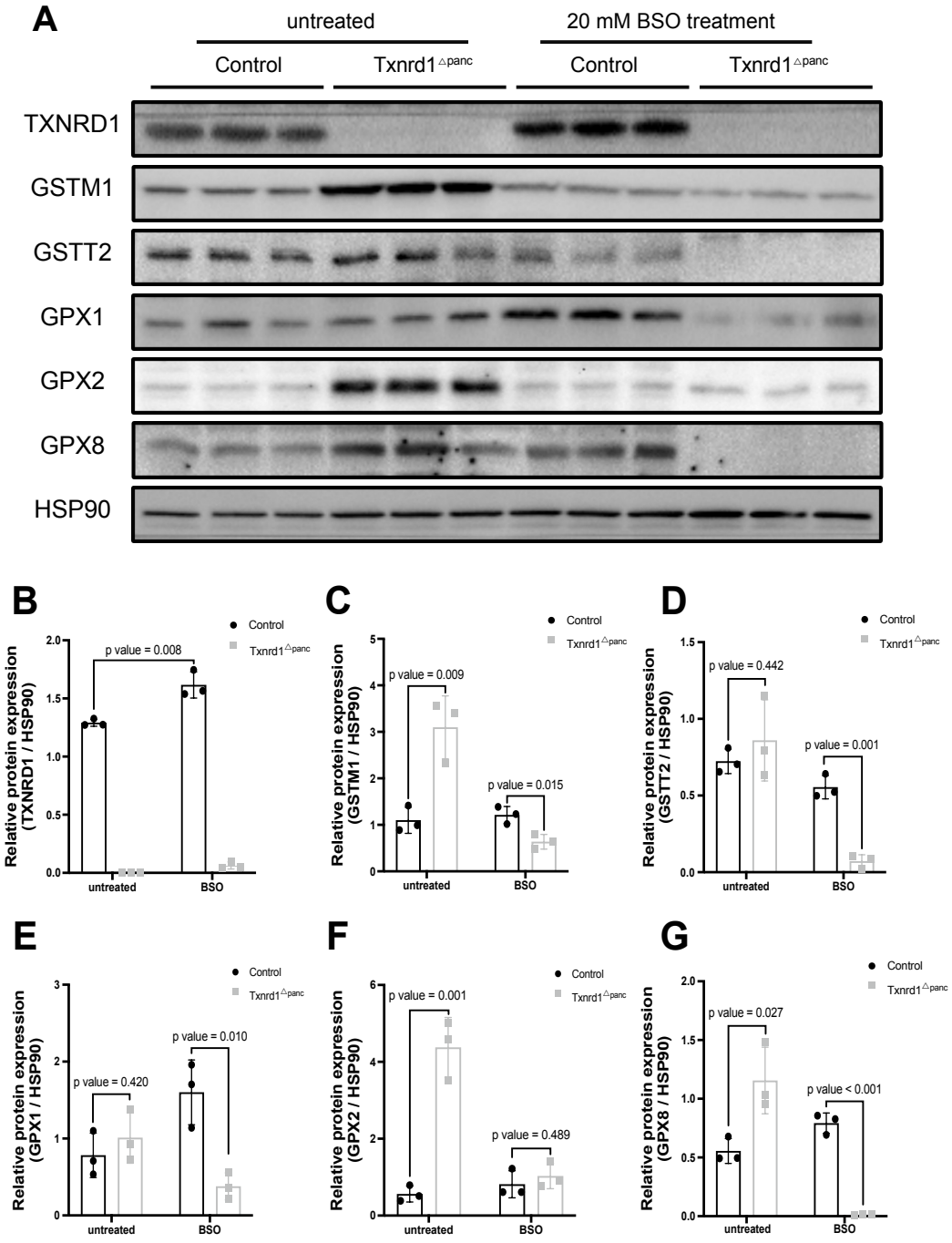

Figure 3.11 Influence of glutathione system on proteins level after BSO treatment. **A** Western blot for antioxidant systems of pancreas tissue on 20 mM concentration of BSO treatment. HSP90 served as a loading control. **B-G** Quantification of **A**. Control: n=3 & Txnrd1$^{\Delta panc}$: n=3. Data are shown as mean ± SD. Differences were considered statistically significant at $p < 0.05$ using unpaired t-test.

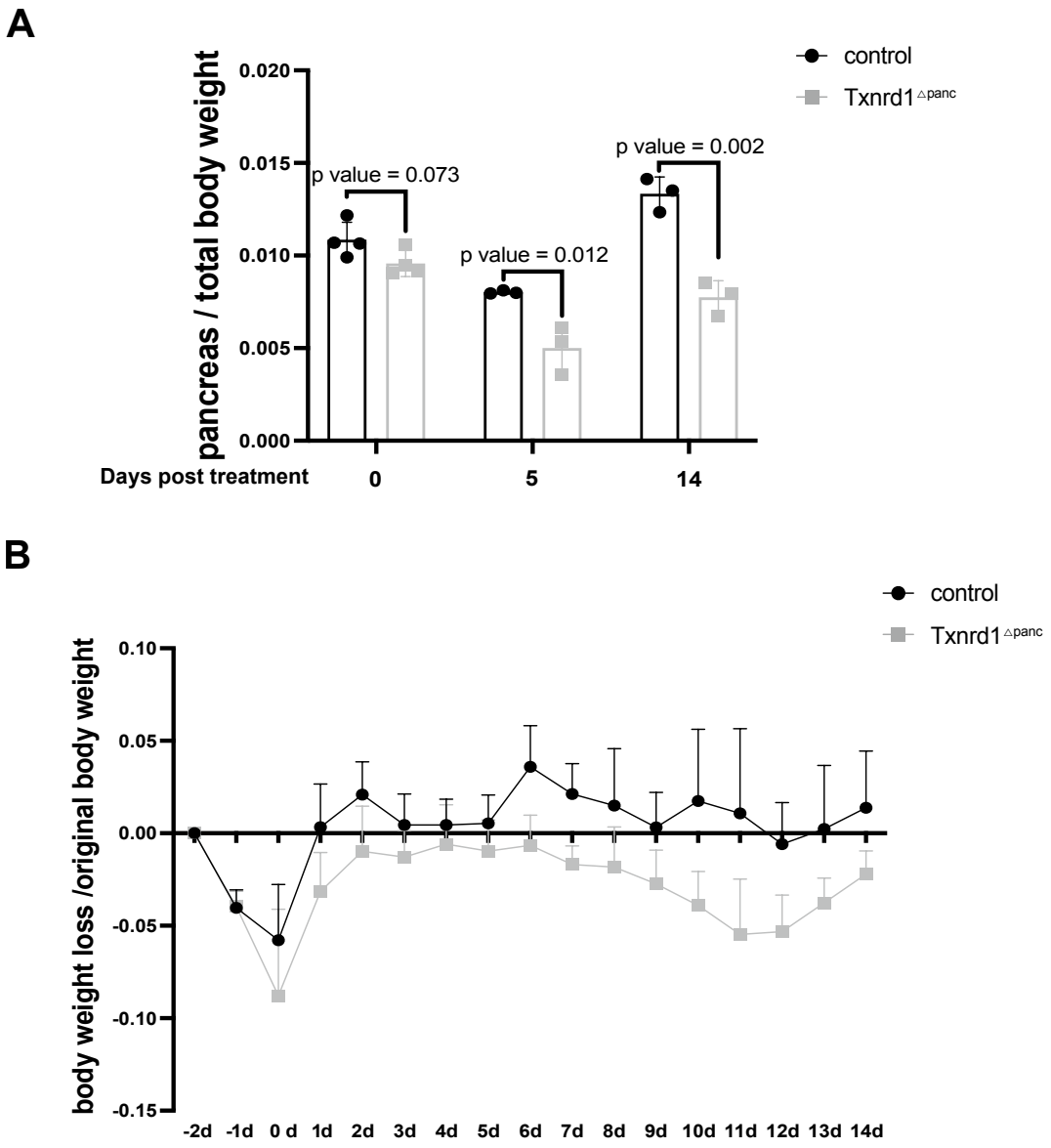

Figure 3.12 Pancreas and body weight during and after BSO treatment. A Pancreas to body weight and **B** change in body weight after BSO treatment. 0 days after end of 48 hours BSO treatment (control: n=4 & Txnrd1$^{\Delta panc}$: n=4), 5 days after end of 48 hours BSO treatment (control: n=3 & Txnrd1$^{\Delta panc}$: n=3), 14 days after end of 48 hours BSO treatment (control: n=3 & Txnrd1$^{\Delta panc}$: n=3). Data are shown as mean ± SD. Differences were considered statistically significant at $p < 0.05$ using unpaired t-test.

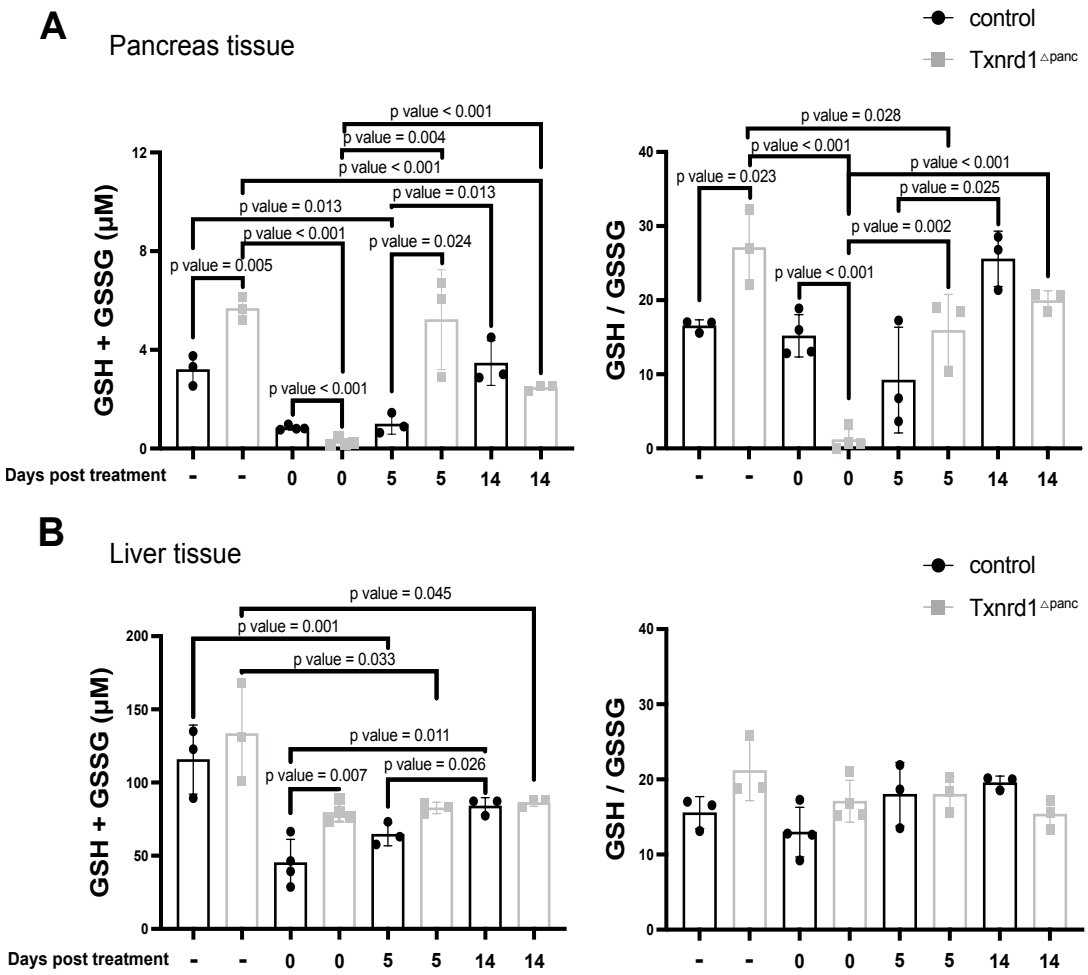

Figure 3.13 Glutathione levels in pancreas and liver after BSO treatment. A The GSH and GSSG concentrations and **B** GSH / GSSG ratio in pancreata and liver tissues. Untreated (control: n=3 & Txnrd1$^{\Delta panc}$: n=3), 0 days after end of 48 hours BSO treatment (control: n=4 & Txnrd1$^{\Delta panc}$: n=4), 5 days after end of 48 hours BSO treatment (control: n=3 & Txnrd1$^{\Delta panc}$: n=3), 14 days after end of 48 hours BSO treatment (control: n=3 & Txnrd1$^{\Delta panc}$: n=3). Data are shown as mean ± SD. Differences were considered statistically significant at $p < 0.05$ using unpaired t-test.

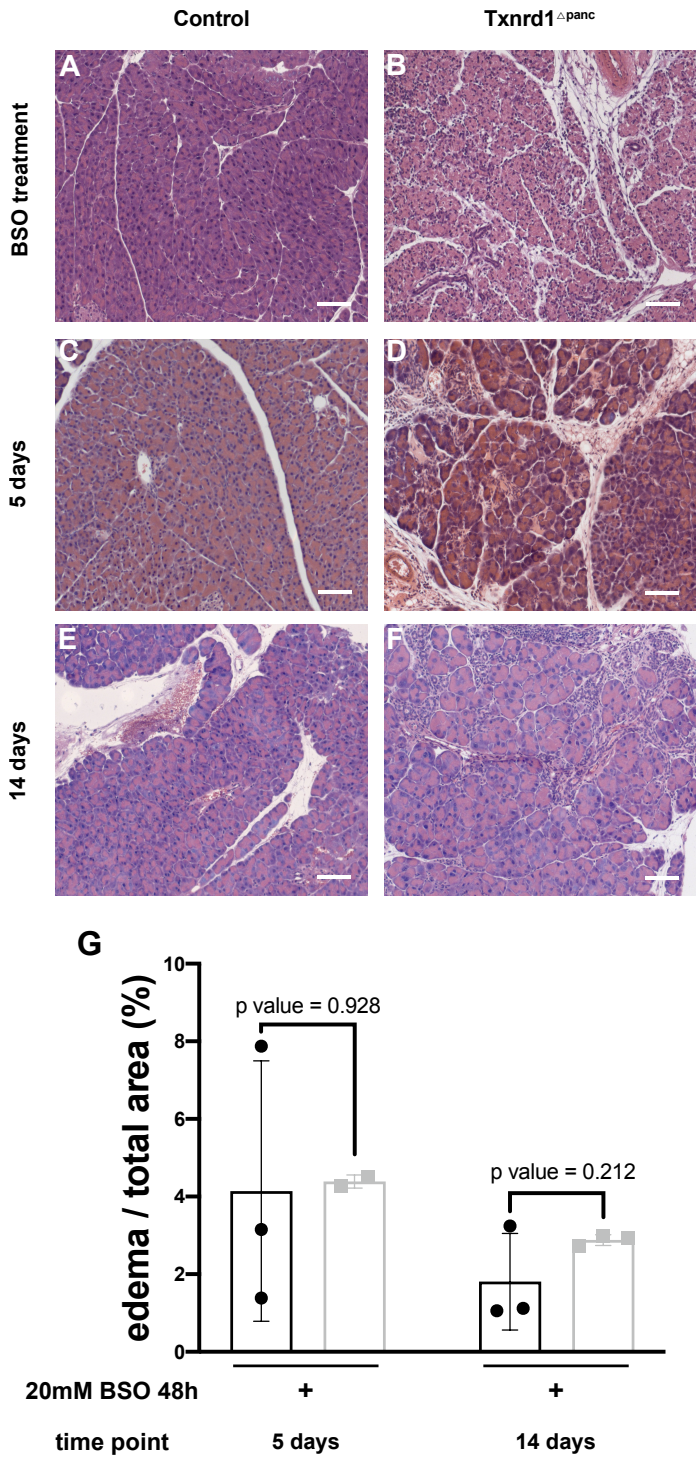

Figure 3.14 Edema to pancreas area after BSO treatment. Representative images of H&E staining of pancreatic tissues in control and Txnrd1$^{\Delta panc}$ mice at **(A, B)** 0 days after end of 48 hours BSO treatment (control: n=4 & Txnrd1$^{\Delta panc}$: n=4), **(C, D)** 5 days after end of 48 hours BSO treatment (control: n=3 & Txnrd1$^{\Delta panc}$: n=2), **(E, F)** 14 days after end of 48 hours BSO treatment (control: n=3 & Txnrd1$^{\Delta panc}$: n=3). Scale bar, 100 µm. **G** Edema quantification of **C-F.** Data are shown as mean ± SD. Differences were considered statistically significant at $p < 0.05$ using unpaired t-test.

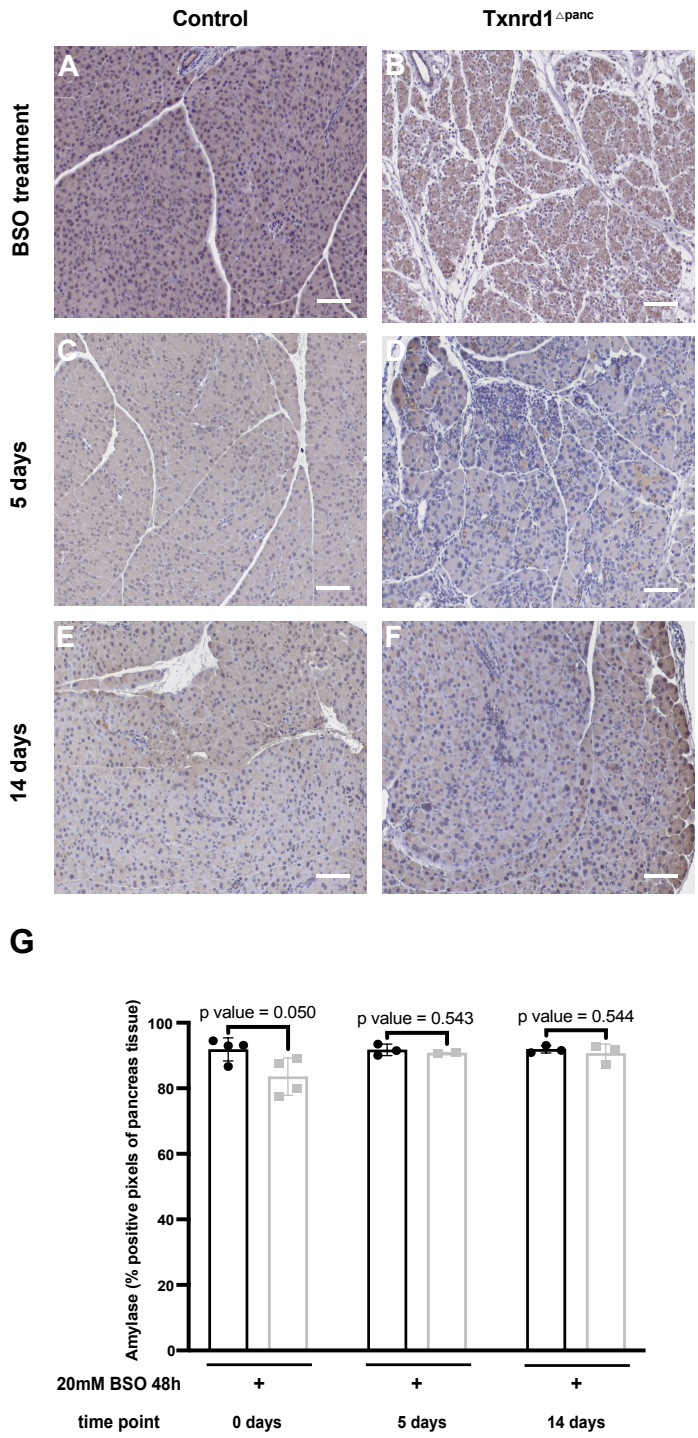

Figure 3.15 Amylase expression in pancreas after BSO treatment. Representative images of pancreata stained for amylase in control and Txnrd1$^{\Delta panc}$ mice at **(A, B)** 0 days after end of 48 hours BSO treatment (control: n=4 & Txnrd1$^{\Delta panc}$: n=4), **(C, D)** 5 days after end of 48 hours BSO treatment (control: n=3 & Txnrd1$^{\Delta panc}$: n=2)**, (E, F)** 14 days after end of 48 hours BSO treatment (control: n=3 & Txnrd1$^{\Delta panc}$: n=3). Scale bar, 100 µm. **G** Quantification of **A-F.** Data are shown as mean ± SD. Differences were considered statistically significant at $p < 0.05$ using unpaired t-test.

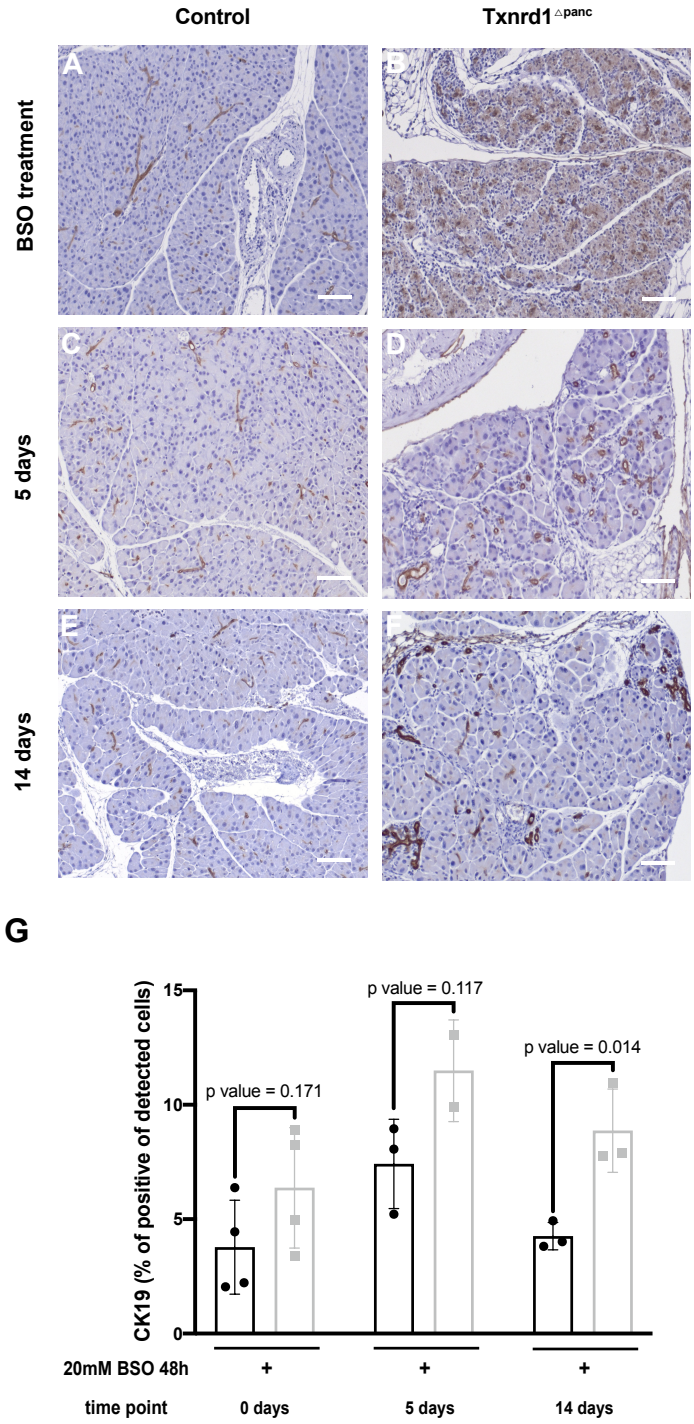

Figure 3.16 CK 19 expression in pancreas after BSO treatment. Representative images of pancreata stained for CK 19 in control and Txnrd1$^{\Delta panc}$ mice at **(A, B)** 0 days after end of 48 hours BSO treatment (control: n=4 & Txnrd1$^{\Delta panc}$: n=4), **(C, D)** 5 days after end of 48 hours BSO treatment (control: n=3 & Txnrd1$^{\Delta panc}$: n=2), **(E, F)** 14 days after end of 48 hours BSO treatment (control: n=3 & Txnrd1$^{\Delta panc}$: n=3). Scale bar, 100 µm. **G** Quantification of **A-F.** Data are shown as mean ± SD. Differences were considered statistically significant at $p < 0.05$ using unpaired t-test.

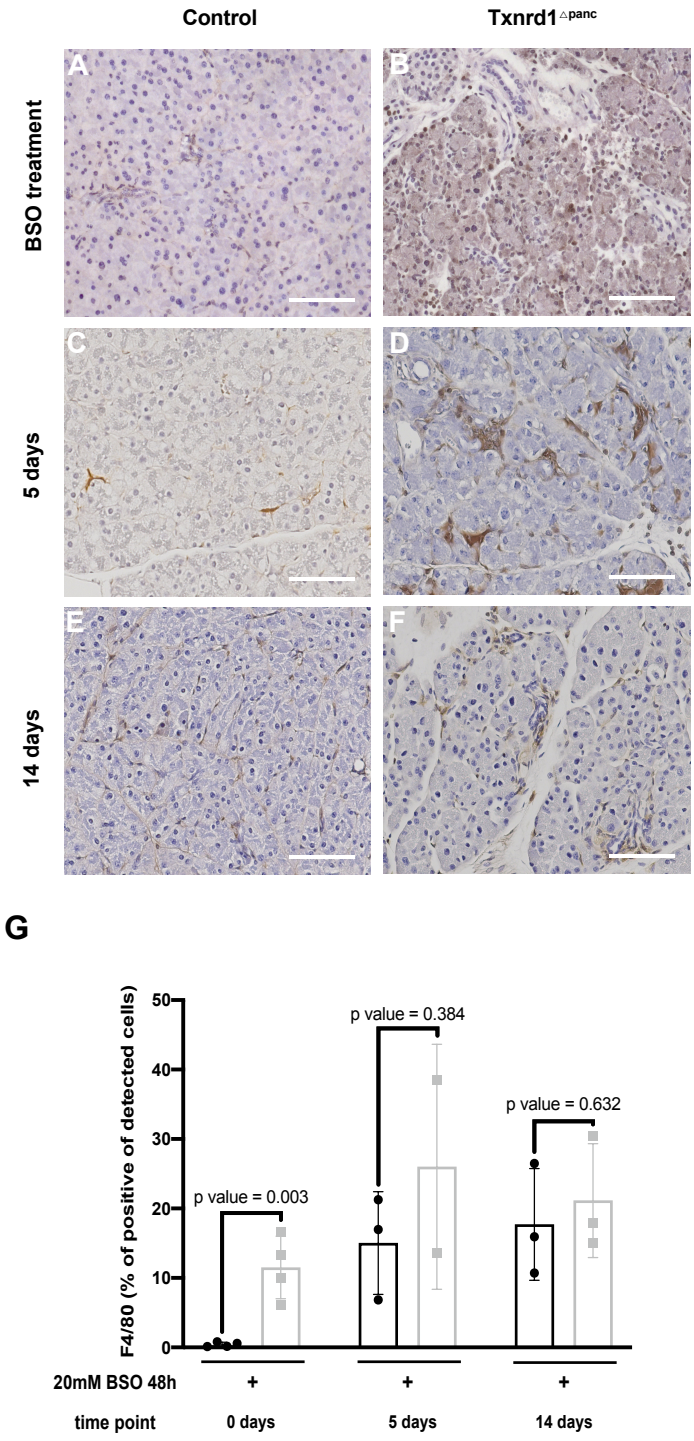

Figure 3.17 F 4/80 expression in pancreas after BSO treatment. Representative images of pancreata stained for F 4/80 in control and Txnrd1$^{\Delta panc}$ mice at **(A, B)** 0 days after end of 48 hours BSO treatment (control: n=4 & Txnrd1$^{\Delta panc}$: n=4), **(C, D)** 5 days after end of 48 hours BSO treatment (control: n=3 & Txnrd1$^{\Delta panc}$: n=2)**, (E, F)** 14 days after end of 48 hours BSO treatment (control: n=3 & Txnrd1$^{\Delta panc}$: n=3). Scale bar, 100 µm. **G** Quantification of **A-F.** Data are shown as mean ± SD. Differences were considered statistically significant at $p < 0.05$ using unpaired t-test.

3.4 Glutathione in *Txnrd1* deficient pancreas protects against pancreatitis-induced injury.

Txnrd1-deficient pancreata showed only mild changes after induction of acute pancreatitis. Although, treating Txnrd1$^{\Delta panc}$ mice with BSO in drinking water resulted in significant differences in glutathione levels, we observed not significant changes in pancreatic morphology, suggesting compensatory relationship between the glutathione system and thioredoxin-reductase activity.

To test this hypothesis, mice were given BSO for 48 hours and directly afterwards, AP was induced. Mice were analyzed at 8 hours, 24 hours and 1 week after caerulein administration. During this experiment, a significant decrease in body weight after BSO treatment was noticed and AP induction that persisted after one week in Txnrd1$^{\Delta panc}$ mice (Figure 3.18 A). Amylase and lipase serum levels were at their highest level 8 hours after the first injection at control group, indicating that the acute pancreatitis was successfully induced (Figure 3.18 B). In addition, a significant decrease in pancreas to body weight ratio in Txnrd1$^{\Delta panc}$ mice compared to control mice was observed, with increasing severity at each later timepoint (Figure 3.18 C).

The liver is the major organ for GSH synthesis and metabolism [114, 115]. To determine changes in GSH levels in pancreatic and liver tissues, total GSH levels and GSH/GSSG were analyzed. In pancreatic tissue, total GSH level and GSH/GSSG ratio were significantly decreased in Txnrd1$^{\Delta panc}$ mice 48 hours post-BSO treatment, while an increase was found in these mice 8 hours after AP (Figure 3.19 A). Interestingly, the total GSH levels were similar between the groups 24 hours after AP induction, and GSH / GSSG ratio in Txnrd1$^{\Delta panc}$ mice was reduced (Figure 3.19 A). In liver tissues, the total GSH level, and GSH / GSSG ratio, showed a decreasing trend for two groups 48 hours after BSO treatment, but a significant increase in Txnrd1$^{\Delta panc}$ mice while at AP 24 hours after BSO treatment, there was a significant decrease in Txnrd1$^{\Delta panc}$ mice (Figure 3.19 B).

In line with the dramatic decrease in pancreas weight, pancreatic morphology was immensely altered in *Txnrd1* knockout mice (Figure 3.20). Moreover, amylase positive area was greatly reduced after AP induction in Txnrd1$^{\Delta panc}$ mice, with increasing severity along time points analyzed (Figure 3.21). To determine any changes in the acinar-ductal metaplasia (ADM), pancreatic tissue was stained for CK19 and a significant increase 8 hours and 1 week after AP was found (Figure 3.22). Furthermore, when pancreatic tissue was analyzed for macrophage infiltration using F4/80 as a marker, a significant increase in Txnrd1$^{\Delta panc}$ mice at all time points was observed (Figure 3.23). When pancreatic tissue was analyzed for proliferation using BrdU as a marker, it showed a significant increase in Txnrd1$^{\Delta panc}$ mice at all time points except for 1-week post-AP (Figure 3.24).

Taken together, pancreatic glutathione depletion in addition to acute pancreatitis caused a severe phenotype in Txnrd1$^{\Delta panc}$ mice.

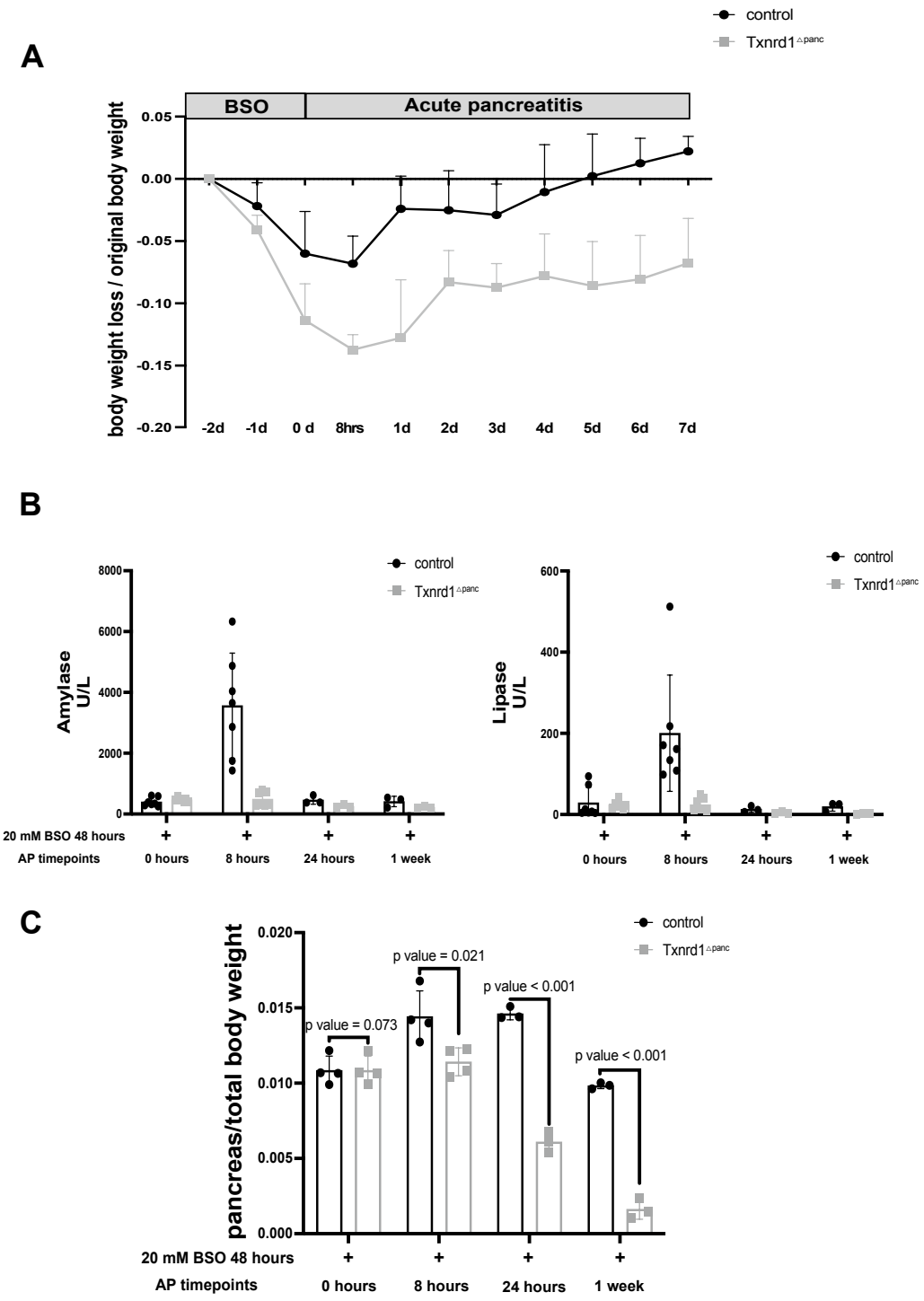

Figure 3.18 Effect of glutathione in *Txnrd1* deficient pancreas on pancreatitis-induced injury. A Change body weight, **B** serum amylase and lipase and **C** pancreas to body weight ratio after glutathione depletion with acute pancreatitis. After end of 48 hours BSO treatment (control: n=4 & Txnrd1$^{\Delta panc}$: n=4), acute pancreatitis 8 hours after end of 48 hours BSO treatment (control: n=4 & Txnrd1$^{\Delta panc}$: n=4), acute pancreatitis 24 hours after end of 48 hours BSO treatment (control: n=3 & Txnrd1$^{\Delta panc}$: n=3), acute pancreatitis 1 week after end of 48 hours BSO treatment

(control: n=3 & Txnrd1$^{\Delta panc}$: n=3). Data are shown as mean ± SD. Differences were considered statistically significant at $p < 0.05$ using unpaired t-test.

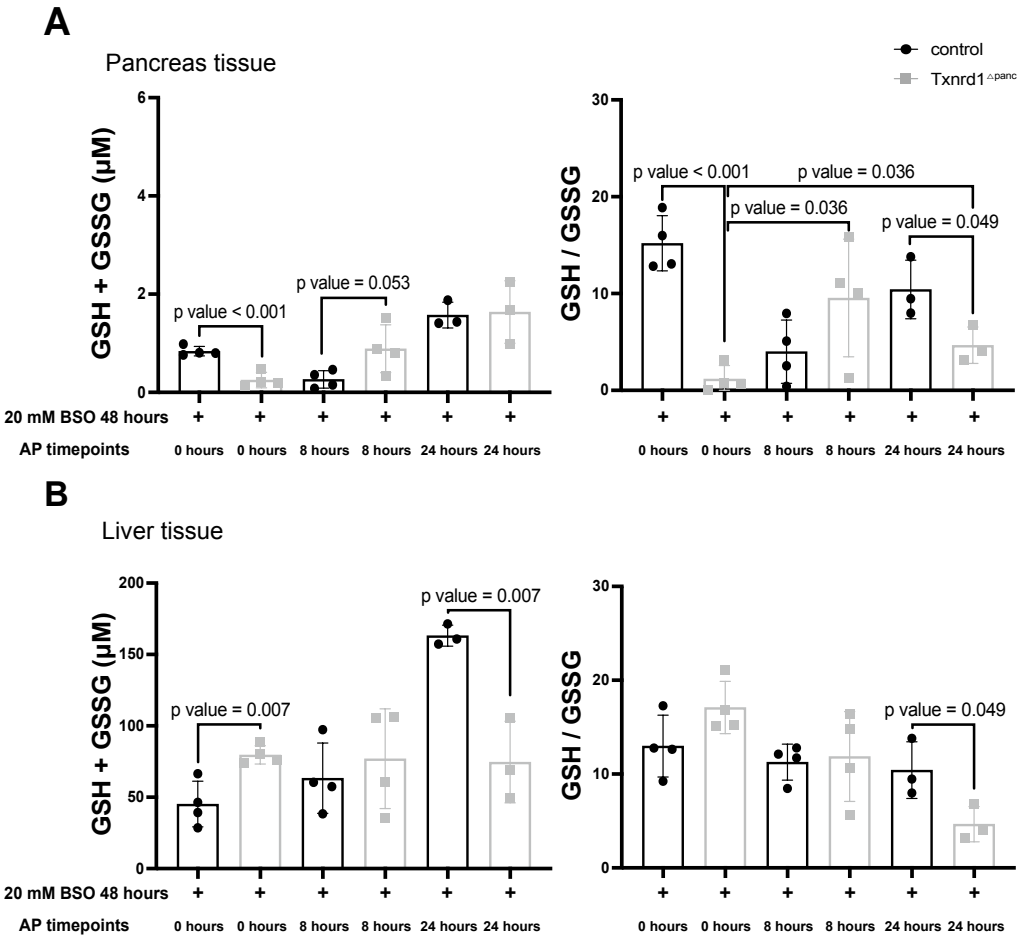

Figure 3.19 Effect on glutathione in *Txnrd1* deficient pancreas post pancreatitis-induced injury. The GSH and GSSG concentrations and GSH / GSSG ratio in **A** pancreata and **B** liver tissues. After end of 48 hours BSO treatment (control: n=4 & Txnrd1$^{\Delta panc}$: n=4), acute pancreatitis 8 hours after end of 48 hours BSO treatment (control: n=4 & Txnrd1$^{\Delta panc}$: n=4), acute pancreatitis 24 hours after end of 48 hours BSO treatment (control: n=3 & Txnrd1$^{\Delta panc}$: n=3), acute pancreatitis 1 week after end of 48 hours BSO treatment (control: n=3 & Txnrd1$^{\Delta panc}$: n=3). Data are shown as mean ± SD. Differences were considered statistically significant at $p < 0.05$ using unpaired t-test.

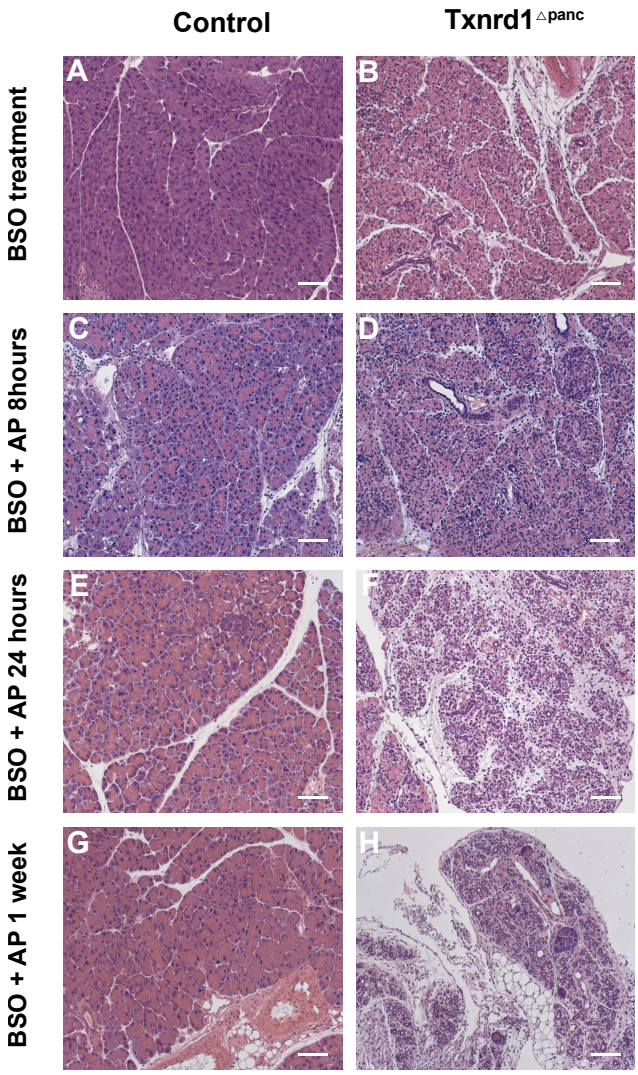

Figure 3.20 Gross morphology of pancreas after BSO treatment and AP induction. Representative images of H & E staining of pancreatic tissues in control and Txnrd1$^{\Delta panc}$ mice at **(A, B)** after end of 48 hours BSO treatment (control: n=4 & Txnrd1$^{\Delta panc}$: n=4), **(C, D)** acute pancreatitis 8 hours after end of 48 hours BSO treatment (control: n=4 & Txnrd1$^{\Delta panc}$: n=4), **(E, F)** acute pancreatitis 24 hours after end of 48 hours BSO treatment (control: n=3 & Txnrd1$^{\Delta panc}$: n=3), **(G, H)** acute pancreatitis 1 week after end of 48 hours BSO treatment (control: n=3 & Txnrd1$^{\Delta panc}$: n=3). Scale bar, 100 µm.

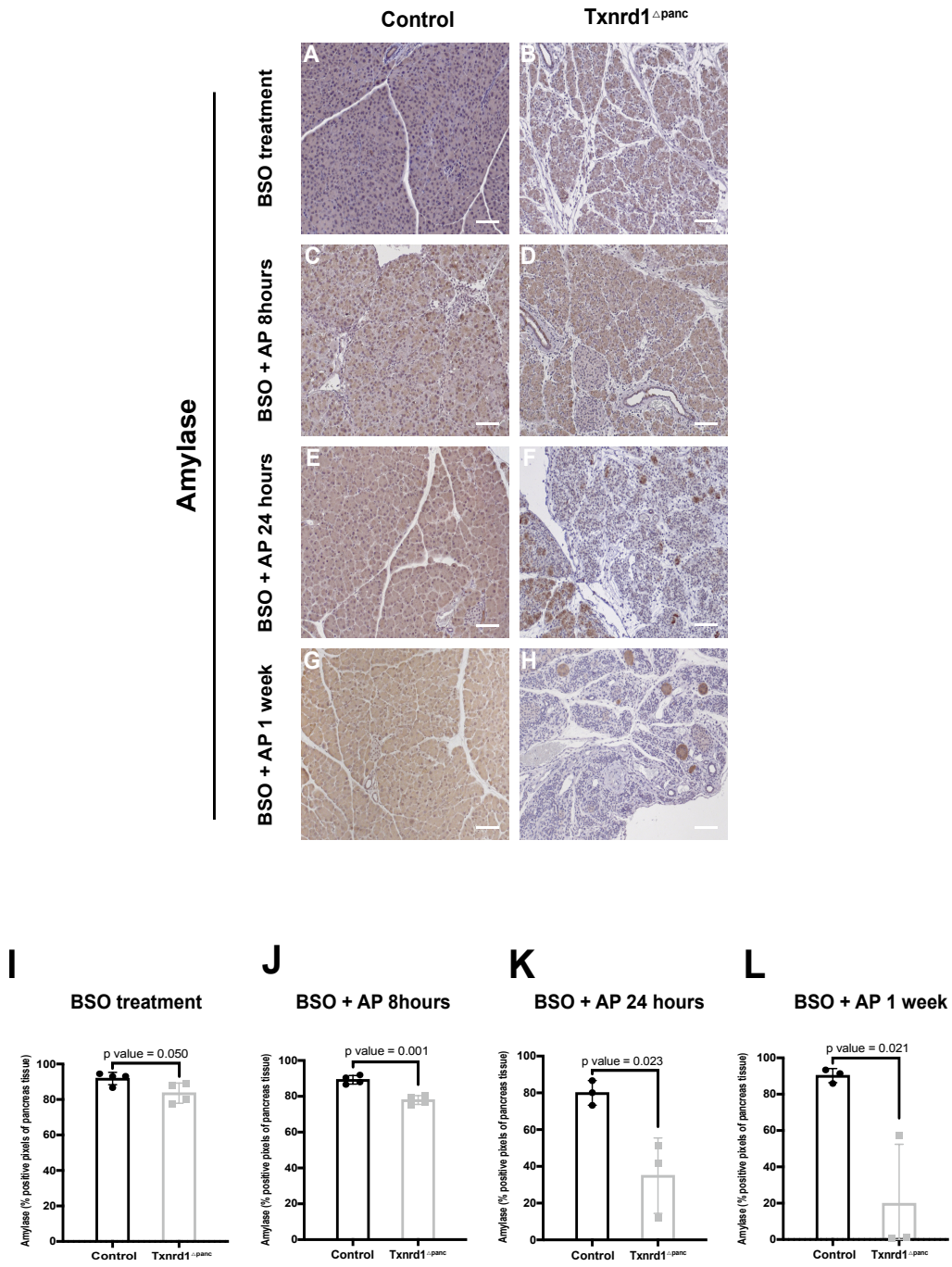

Figure 3.21 Amylase expression in pancreas after BSO treatment and AP induction. Representative images of pancreata stained for amylase in control and Txnrd1$^{\Delta panc}$ mice at **(A, B)** after end of 48 hours BSO treatment (control: n=4 & Txnrd1$^{\Delta panc}$: n=4), **(C, D)** acute pancreatitis 8 hours after end of 48 hours BSO treatment (control: n=4 & Txnrd1$^{\Delta panc}$: n=4), **(E, F)** acute pancreatitis 24 hours after end of 48 hours BSO treatment (control: n=3 & Txnrd1$^{\Delta panc}$: n=3), **(G, H)** acute pancreatitis 1 week after end of 48 hours BSO treatment (control: n=3 & Txnrd1$^{\Delta panc}$: n=3). Scale bar, 100 µm. **I** Quantification of **A, B**. **J** Quantification of **C, D**. **K** Quantification of **E, F**. **L** Quantification of **G, H**. Data are shown as mean ± SD. Differences were considered statistically significant at $p < 0.05$ using unpaired t-test.

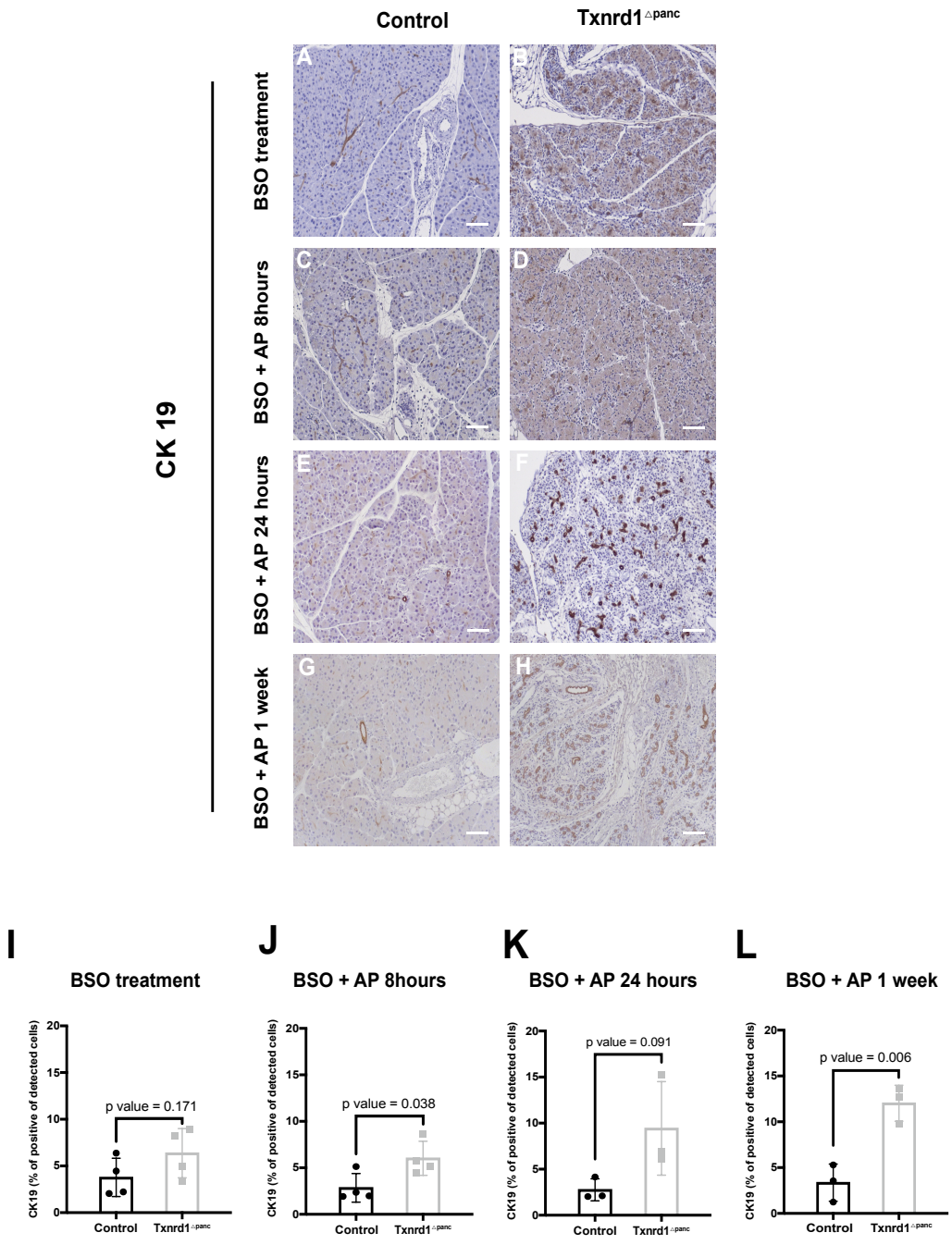

Figure 3.22 CK 19 expression in pancreas after BSO treatment and AP induction. Representative IHC images of pancreata stained for CK 19 in control and Txnrd1$^{\Delta panc}$ mice at **(A, B)** after end of 48 hours BSO treatment (control: n=4 & Txnrd1$^{\Delta panc}$: n=4), **(C, D)** acute pancreatitis 8 hours after end of 48 hours BSO treatment (control: n=4 & Txnrd1$^{\Delta panc}$: n=4), **(E, F)** acute pancreatitis 24 hours after end of 48 hours BSO treatment (control: n=3 & Txnrd1$^{\Delta panc}$: n=3), **(G, H)** acute pancreatitis 1 week after end of 48 hours BSO treatment (control: n=3 & Txnrd1$^{\Delta panc}$: n=3). Scale bar, 100 µm. **I** Quantification of **A, B**. **J** Quantification of **C, D**. **K** Quantification of **E, F**. **L** Quantification of **G, H**. Data are shown as mean ± SD. Differences were considered statistically significant at $p < 0.05$ using unpaired t-test.

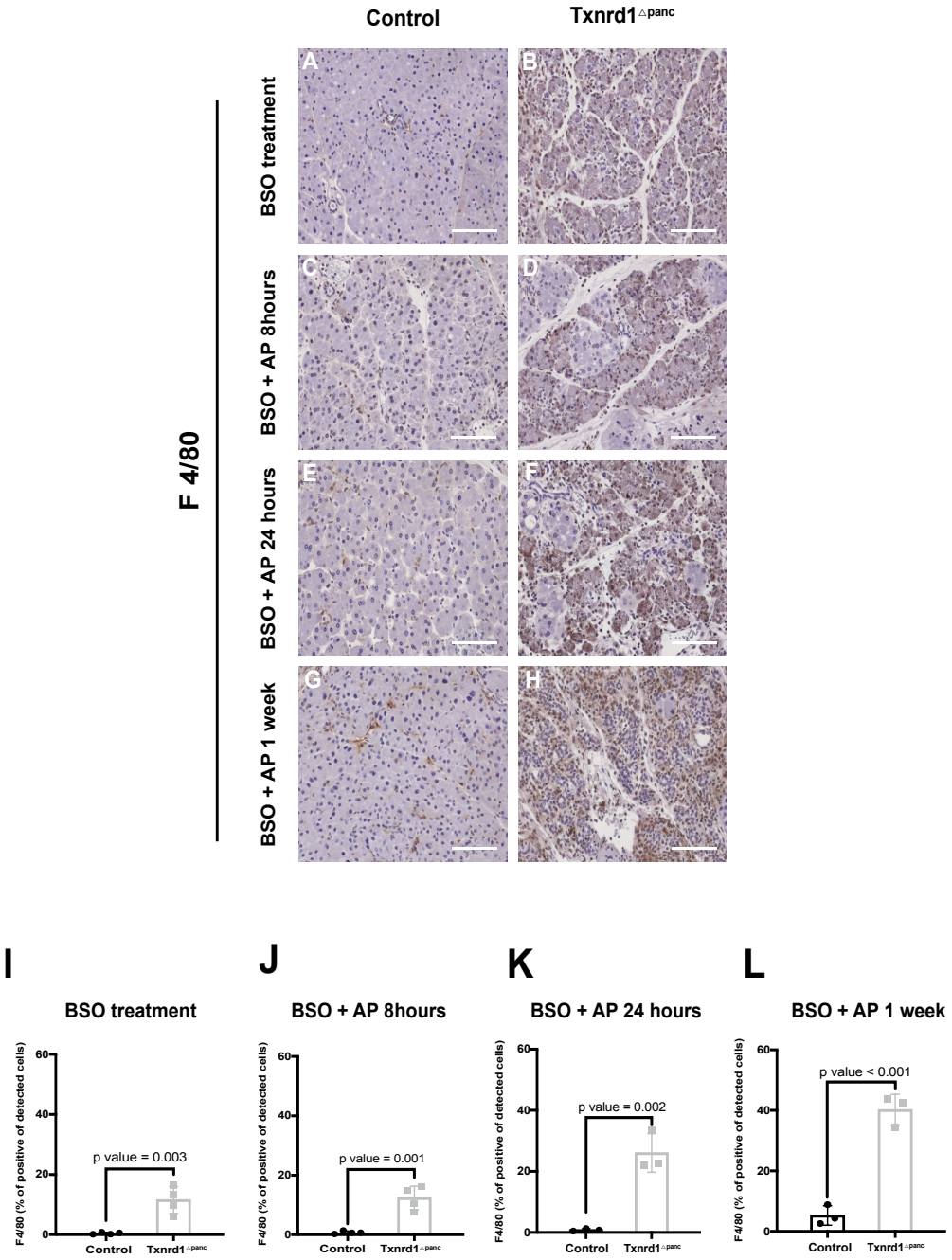

Figure 3.23 F 4/80 expression in pancreas after BSO treatment and AP induction. Representative IHC images of pancreata stained for F 4/80 in control and Txnrd1$^{\Delta panc}$ mice at **(A, B)** after end of 48 hours BSO treatment (control: n=4 & Txnrd1$^{\Delta panc}$: n=4), **(C, D)** acute pancreatitis 8 hours after end of 48 hours BSO treatment (control: n=4 & Txnrd1$^{\Delta panc}$: n=4), **(E, F)** acute pancreatitis 24 hours after end of 48 hours BSO treatment (control: n=3 & Txnrd1$^{\Delta panc}$: n=3), **(G, H)** acute pancreatitis 1 week after end of 48 hours BSO treatment (control: n=3 & Txnrd1$^{\Delta panc}$: n=3). Scale bar, 100 µm. **I** Quantification of **A, B**. **J** Quantification of **C, D**. **K** Quantification of **E, F**. **L** Quantification of **G, H**. Data are shown as mean ± SD. Differences were considered statistically significant at $p < 0.05$ using unpaired t-test.

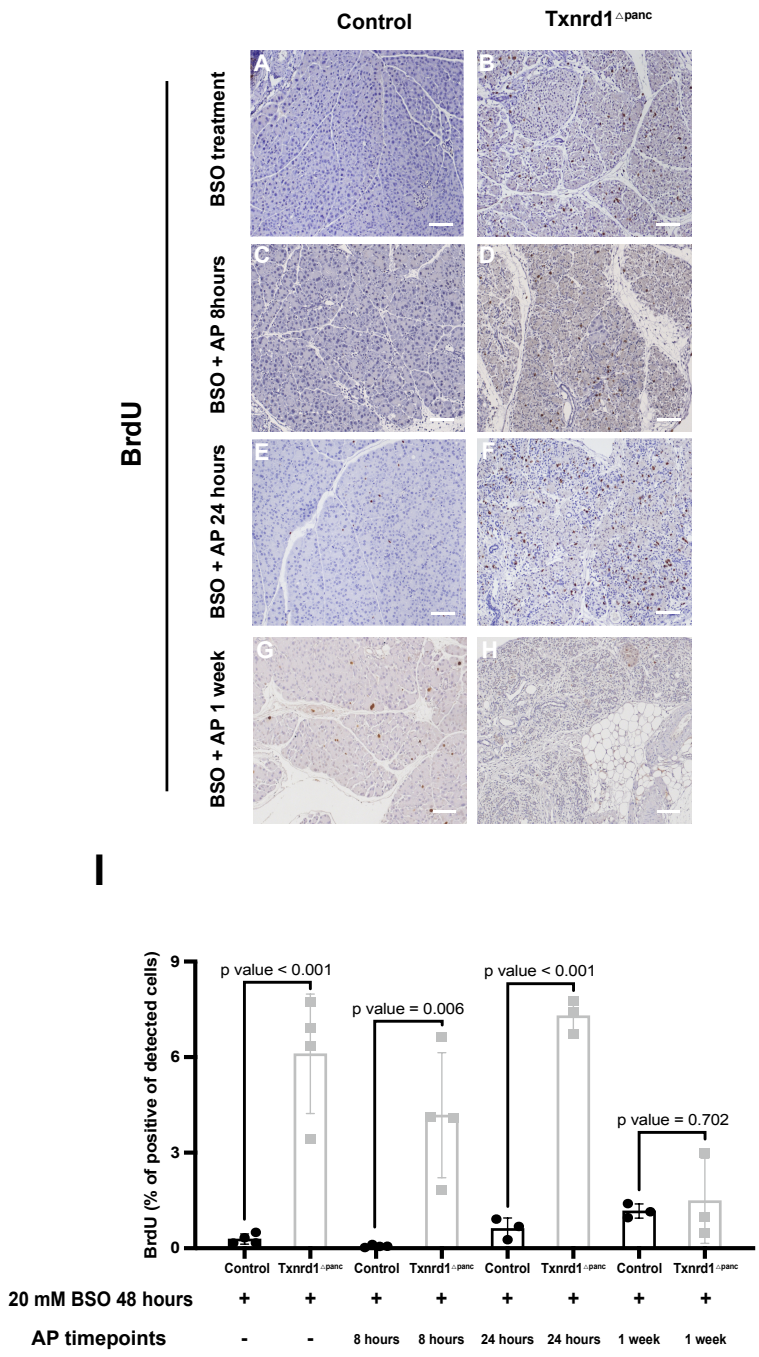

Figure 3.24 BrdU expression in pancreas after BSO treatment and AP induction. Representative IHC images of pancreata stained for BrdU in control and Txnrd1$^{\Delta panc}$ mice at **(A, B)** after end of 48 hours BSO treatment (control: n=4 & Txnrd1$^{\Delta panc}$: n=4), **(C, D)** acute pancreatitis 8 hours after end of 48 hours BSO treatment (control: n=4 & Txnrd1$^{\Delta panc}$: n=4), **(E, F)** acute pancreatitis 24 hours after end of 48 hours BSO treatment (control: n=3 & Txnrd1$^{\Delta panc}$: n=3), **(G, H)** acute pancreatitis 1 week after end of 48 hours BSO treatment (control: n=3 & Txnrd1$^{\Delta panc}$: n=3). Scale bar, 100 µm. **I** Quantification of **A-H**. Data are shown as mean ± SD. Differences were considered statistically significant at $p < 0.05$ using unpaired t-test.

3.5 *In vitro* glutathione depletion does not influence acinar integrity in Txnrd1$^{\Delta panc}$ animals

To investigate the effect of glutathione depletion on acinar clusters *in vitro*, pancreatic acinar clusters from 4 – week – old Txnrd1$^{\Delta panc}$ and wild-type mice were isolated and treated with 20 mM BSO in culture.

Since hydrogen peroxide (H_2O_2) is one of the most important ROS, H_2O_2 was used as a ROS control independent of glutathione [116]. Acinar clusters were either treated with BSO (20 mM), or with H_2O_2 (25 µM) for 24 hours. As compared to the untreated control group, no major change in morphology of isolated clusters was detected after treatment with BSO (Figure 3.25 E-H) or H_2O_2 (Figure 3.25 I-L). Moreover, there were no major changes in LDH release between treatment groups or genotypes, suggesting that there was no significant difference in cell death between groups (Figure 3.25 M).

Taken together, and in stark contrast to the *in vivo* situation, *in vitro* glutathione depletion does not seem to influence acinar integrity in Txnrd1$^{\Delta panc}$ acinar clusters.

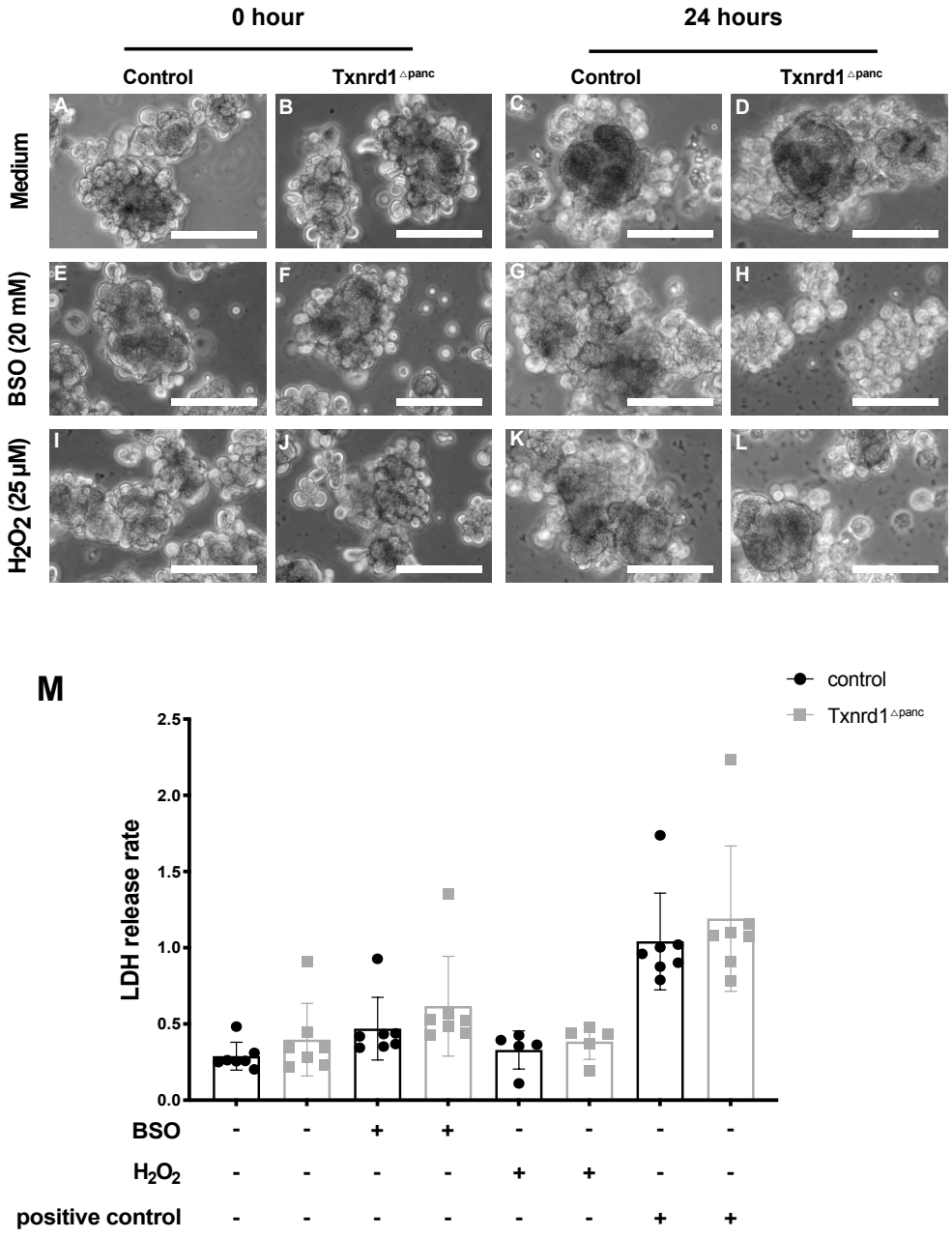

Figure 3.25 ***In vitro*** **glutathione depletion does not influence acinar integrity in** ***Txnrd1*** **deficient acinar cells.** Imaging of acinar clusters in **(A-D) control** medium, **(E-H)** medium with BSO, and **(I-L)** medium with H_2O_2 (at indicated concentrations) at 0 hours and 24 hours. Scale bar = 100 µm. **M** LDH release expressed as a rate of the positive control determined after 24 hours treatment of medium (control: n=7 & Txnrd1$^{\Delta panc}$: n=7), BSO (control: n=7 & Txnrd1$^{\Delta panc}$: n=7) and H_2O_2 (control: n=5 & Txnrd1$^{\Delta panc}$: n=5) from control and *Txnrd1* deficient acinar cells. At day 0, control or Txnrd1 deficient acinar cells were lysed with 2% Triton®X-100 for 30 mins at 37°C as positive control. Data are shown as mean ± SD. Differences were considered statistically significant at $p < 0.05$ using unpaired t-test.

3.6 *In vitro* glutathione depletion inhibited ADM transdifferentiation in *Txnrd1* deficient animals

Since glutathione depletion showed mild changes in CK19 expression *in vivo* while indicating an increased ADM program, it was investigated whether acinar transdifferentiation into duct-like cells could be observed *in vitro*.

Acinar clusters isolated from 4-week-old pancreas of Txnrd1$^{\Delta panc}$ and control mice were used to study the cell-autonomous effects of *Txnrd1* deletion on the transdifferentiation potential of acinar cells.

To determine ADM potential *in vitro*, acinar clusters were treated with BSO (20 mM), NAC (1 mM), which acts as an antioxidant, TGFα (100 ng/ml), which is an ADM inducer, BSO plus TGFα and NAC plus TGFα. Next, a transdifferentiation rate in control and Txnrd1$^{\Delta panc}$ acini under untreated conditions and upon stimulation with TGFα, NAC, and NAC plus TGFα treated conditions were monitored.

As shown in Figure 3.26, acinar clusters isolated from Txnrd1$^{\Delta panc}$ mice did not show a significant change as compared to controls. This indicates that *Txnrd1* deletion does not affect transdifferentiation, similar to *in vivo* observations (Figure 3.5 & 3.6) Moreover, no transdifferentiation was found in control and Txnrd1$^{\Delta panc}$ acini after BSO treatment or BSO plus TGFα treatment, indicating that BSO treatment can inhibit transdifferentiation. Likewise, no major changes in LDH release between treatment groups or genotypes were found, suggesting that there is no significant difference in cell death (Figure 3.26).

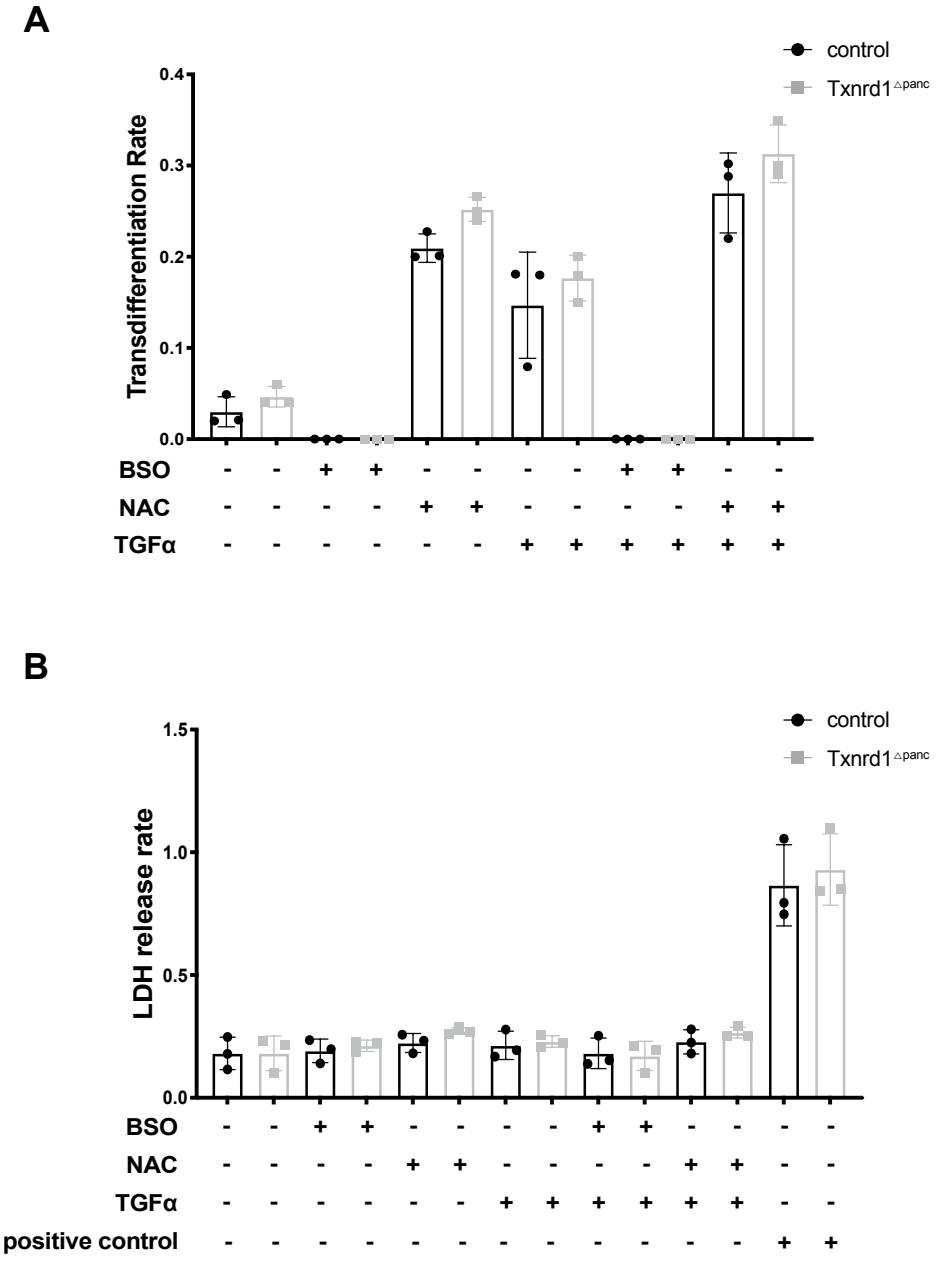

Figure 3.26 ***In vitro*** **glutathione depletion inhibited ADM transdifferentiation in control and** ***Txnrd1*** **deficient acinar cells. A** ADM transdifferentiation rate and **B** effect of BSO, NAC, TGFα, TGFα + BSO and TGFα + NAC treatment on LDH release from control and *Txnrd1* deficient acinar cells. At day 0, control or *Txnrd1* deficient acinar cells were lysed with 2% Triton®X-100 for 30 mins at 37°C as positive control. Control: n=3 & Txnrd1$^{\Delta panc}$: n=3. Data are shown as mean ± SD. Differences were considered statistically significant at $p < 0.05$ using unpaired t-test.

4. DISCUSSION

Despite the progress in understanding the molecular mechanisms leading to pancreatitis, this inflammatory disease can still be fatal when accompanied by necrosis and systemic complications [1-3, 117, 118]. For many years, it was suspected that oxidative stress affects the disease process in patients [15, 73, 119]. Therefore, investigating oxidant and antioxidant systems during AP is essential.

Previously, our group performed gene expression analysis on pancreatic tissue after AP and found *Txnrd1* as one of the highest upregulated oxidoreductases. TXNRD1 is an essential component of the thioredoxin system that can catalyze the NADPH-dependent reduction of thioredoxin as well as a variety of small-molecule substrates such as hydrogen peroxide (H_2O_2), selenite, and lipoic acid [120]. Our group generated mice harboring *Txnrd1* knockout allele in the pancreas (Txnrd1$^{\Delta panc}$), which showed normal growth, normal relative pancreatic weight, normal pancreatic morphology, and normal exocrine function. When AP was induced with caerulein , 24 hours after AP, Txnrd1$^{\Delta panc}$ mice showed increased relative pancreatic weight and a significant increase in edema. After one week, a significantly decreased pancreatic weight without a significant difference in edema was observed compared to wild-type mice. For inflammatory manifestations, macrophages can be used as response equivalents [121], and in our study macrophage infiltration of pancreatic tissue was analyzed using F 4/80 as a marker, and no significant differences between groups were found at any time point. This indicates that experimentally induced AP in Txnrd1$^{\Delta panc}$ mice causes a mild phenotype and Txnrd1$^{\Delta panc}$ mice which recovered to a great extent after one week.

Under basal conditions, total GSH level and *Gstm1* RNA expression were significantly increased in Txnrd1$^{\Delta panc}$ pancreata compared to control pancreata. Components of the glutathione system, including GSTM1, GPX2 and GPX8, were upregulated at the protein level in pancreas of Txnrd1$^{\Delta panc}$ mice. GPX1 is a selenoprotein, a member of

the peroxidase family [122], whose main function is to reduce H_2O_2 and other soluble hydroperoxides at the expense of GSH [123]. GPX2 is an antioxidant enzyme that uses glutathione as an electron source to reduce peroxides in the cytoplasm [124]. Stancill et al. found nuclear factor erythroid 2-related factor 2 (Nrf2)-regulated genes were significantly increased in *Txnrd1*-deficient pancreatic β-cells, including *Gpx2* [125], which is consistent with our results. GPX8 is a cysteine-rich glutathione peroxidase that is anchored to the endoplasmic reticulum membrane and can prevent the leakage of H_2O_2 into the cytoplasm and thus control the redox state of the cell [126]. Our results suggest that pancreatic acinar cells respond to the loss of *Txnrd1* by increasing components of glutathione system (especially GSTM1, GPX2 and GPX8), and thereby glutathione-based antioxidant mechanisms, indicating compensation.

GSH synthesis includes two pathways. On the one hand, GSH biosynthesis occurs via γ-glutamylcysteine synthetase (GCL) [127], which is the rate-limiting enzyme that can be inhibited by BSO [128]. On the other hand, NADPH-depend reduction of GSSG to GSH is catalyzed by glutathione reductase (GR) [60, 129]. Extensive work has been done to determine the turnover, transport, and processing of GSH inter- and intra-organ, illustrating that the liver is the central organ for inter-organ GSH homeostasis [130-133]. In our study, it was found that total GSH dramatically decreased in pancreatic tissues of control and Txnrd1$^{\Delta panc}$ mice after BSO treatment, and the decrease was significant in the Txnrd1$^{\Delta panc}$ group compared to control group. Interestingly, the decrease in total GSH was more pronounced in liver tissues of control group than in the Txnrd1$^{\Delta panc}$ group. At day 5 after BSO treatment, total GSH level in the Txnrd1$^{\Delta panc}$ group in pancreatic tissues was significantly increased compared to control group. There are multiple possible explanations for this, mainly: (1) pancreatic acinar cells from Txnrd1$^{\Delta panc}$ mice respond to the loss of *Txnrd1* by increasing components of glutathione system. After BSO treatment, total GSH dramatically decreased in pancreatic tissue of Txnrd1$^{\Delta panc}$ mice, but the decrease in total GSH in the liver was not as pronounced as in the control group, probably to

compensate for the lack of GSH in the pancreas. (2) In Txnrd1$^{\Delta panc}$ group, total GSH in the liver was not changed at day 5 and day 14 after BSO treatment, whereas total GSH in pancreatic tissue was significantly increased, possibly compensating for the absence of GSH in the pancreas through inter-organ transfer from the liver [130-133].

Stenson, et al. found that depletion of glutathione inhibits amylase release in guinea pig pancreatic acini [134]. Yu, et al. found that BSO induced depletion of glutathione and inhibited pancreatic amylase release during AP [135]. However, our results showed that glutathione depletion in Txnrd1$^{\Delta panc}$ mice caused early pancreatic acinar cell necrosis and amylase-positive area was reduced, but no big changes in serum amylase levels compared to control group were observed. In combination with acute pancreatitis, pancreatic amylase release and amylase-positive area were greatly reduced, with increasing severity along time points analyzed, but not in the control group. Glutathione and thioredoxin-dependent metabolism are the major cellular thiol-dependent pathways for scavenging hydrogen peroxide, allowing maintenance of the cellular redox potential while preventing and repairing oxidative damage [136, 137]. Yu, et al. found that rather than depletion of protein thiols a decrease in caerulein induced Ca^{2+} mobilization might participate in the inhibition of pancreatic amylase release. However, these mechanisms warrant further examination.

To what extent each antioxidant system can compensate for the loss of the other, has not been fully elucidated yet. Kiebala et al. showed that simultaneous inhibition of Txn system and GSH system synergistically induced apoptosis in malignant B-cells [138]. Sang et al. showed inhibition of TXNRD1 and depletion of GSH may induce excessive ROS production [139]. Moreover, Stancill et al. group reported normal islet architecture and found that *Txnrd1*-deficient β-cells may utilize glutathione metabolism as protective mechanism against oxidative damage [125]. Meanwhile, our results showed that inhibition of GSH synthesis by administration of BSO in Txnrd1$^{\Delta panc}$ mice during AP leads to severe changes in the pancreas. This

demonstrates that GSH and *Txnrd1* play a mutually complementary role in pancreatic homeostasis.

To determine whether the effects observed in vivo were due to an increased vulnerability of acinar cells, explanted acinar cluster of wild-type (control) and Txnrd1$^{\Delta panc}$ animals were investigated in vitro. First, we applied 20 mM of BSO to isolated pancreatic acinar clusters and monitored changes in morphology. All in all, no significant loss or damage of acinar cell was found in any group upon BSO treatment for 24 hours and there were no major changes in LDH release between treatment groups or genotypes, suggesting that there was no significant difference in cell death between groups. However, we did not do pathological analysis to observe senescence, apoptosis, or autophagy. Perhaps, acinar cells maintain their morphological structure but lose their original functions of synthesizing, storing and secreting digestive enzymes, which needs to be further investigated. Meanwhile, *in vivo*, we only found slight pancreatic necrosis in Txnrd1$^{\Delta panc}$ mice after 48 hours of 20 mM BSO treatment. Probably, we need to observe acinar clusters for 48 hours to see the changes in the *in vitro* set up.

In addition, after tissue injury or stress, acinar cells undergo a process of transdifferentiation into duct-like cells in 3D collagen model [140-142]. Furthermore, exogenous treatment with TGFα of collagen-embedded acinar explants is a well-established method for studying *in vitro* ADM [143-145]. To better understand the simultaneous changes mediated by glutathione and *Txnrd1* during ADM, acinar explants were treated with BSO, the antioxidant NAC, which can reduce ROS by increasing glutathione levels, the established ADM inducer TGFα, or a combination of them. Surprisingly, no transdifferentiation was found in control and Txnrd1$^{\Delta panc}$ acini after BSO alone or with TGFα treatment, indicating that 20 mM BSO treatment can inhibit the transdifferentiation process. However, Radyk et al showed that treatment of wild-type acinar cells with BSO increased ROS and accelerated ADM *in vitro* [146], whereas we don't know the details of their BSO treatment, which might

explain part of the differences. Sato et al showed that inhibition of γ-glutamyl cysteine synthetase by 100 µM BSO treatment for 24 hours reduced GSH levels [147], but in our experiments a 200 times higher concentration (20 mM) of BSO was used. It is possible that the concentration of BSO needs to be adjusted and tested for a dose-dependent response to compare results with those seen *in vivo*.
Liou et al. and Nelson et al. showed that administration of 5 mM concentration of NAC was effective in reducing ADM at day 5 in mouse strain [148, 149]. In contrast, our results demonstrated an increase in ADM after administration of 1 mM concentration of NAC at day 3. It is possible that NAC may have a dose or time dependent effect and that its concentration in our *in vitro* assay was too low, or treatment time too short to act as an antioxidant. This may increase pancreatic acinar cell plasticity thus promoting the conversion of pancreatic acinar cells to ductal cells [150, 151], and contributing to regeneration of acinar cells [150, 152, 153].

Taken together, *Txnrd1* is required for the protection of acinar cells integrity from oxidative stress. When *Txnrd1* is depleted, the glutathione system plays a dominant role and is upregulated to maintain homeostasis.

The presented results give new insight into the Txn and glutathione antioxidant systems in pancreatic acinar cells, which is that TXNRD1 and the glutathione system are central to pancreatic homeostasis. Additionally, whether the simultaneous administration of caerulein and BSO *in vitro* shows the same results as *in vivo* need further analysis. Meanwhile, to investigate the mechanism of compensated, in-depth analysis of RNA sequencing may be needed.

5. SUMMARY

In this thesis, the following aspects were systematically studied mainly on animal models:

1. Expression of the glutathione system in the *Txnrd1*-deficient pancreas.
2. Investigation of glutathione system as a compensatory mechanism in Txnrd1$^{\Delta panc}$ mice.
3. Glutathione in *Txnrd1* deficient pancreas protects against pancreatitis-induced injury.
4. The effect of *in vitro* glutathione depletion on acinar integrity, and the effect of ADM formation in Txnrd1$^{\Delta panc}$ acinar cells.

The above study led to the following main conclusions:

1. components of thioredoxin reductase 1 and glutathione systems are altered during AP.
2. the glutathione system is upregulated in the *Txnrd1*-deficient pancreas, suggesting a possible compensatory mechanism.
3. glutathione depletion with acute pancreatitis resulted in a severe phenotype in Txnrd1$^{\Delta panc}$ mice with loss of acinar tissue due to necrosis, proliferation, and macrophage infiltration.

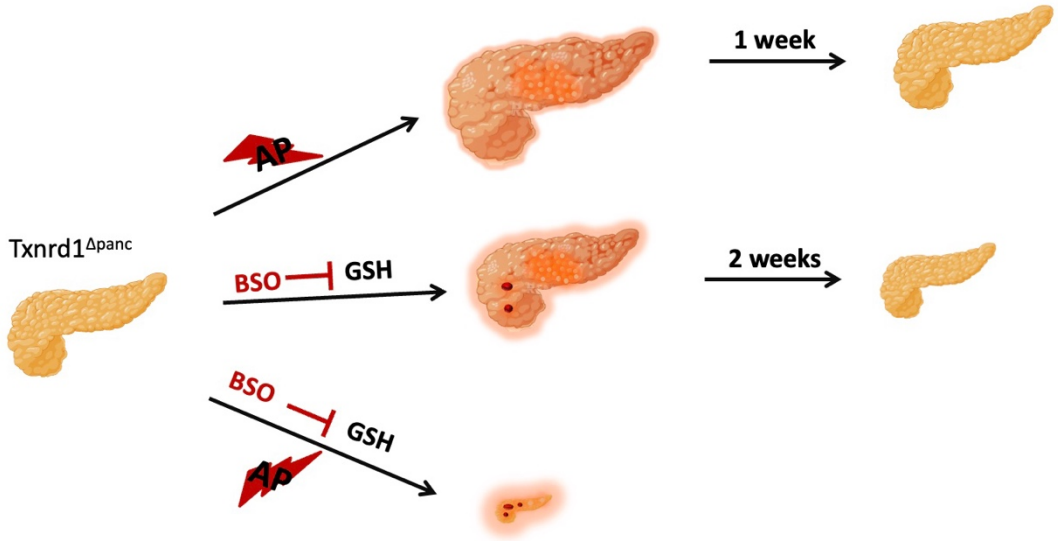

Figure 5.1 Models illustrating pancreas-specific *Txnrd1* depletion in mice induce AP, BSO treatment to inhibit glutathione synthesis, or induced AP + BSO treatments.

In conclusion, these data indicate that TXNRD1 and the glutathione system are central to pancreatic homeostasis.

6. REFERENCES

1. Pandol, S.J., et al., *Acute pancreatitis: bench to the bedside.* Gastroenterology, 2007. **132**(3): p. 1127-51.
2. Vege, S.S., et al., *Initial Medical Treatment of Acute Pancreatitis: American Gastroenterological Association Institute Technical Review.* Gastroenterology, 2018. **154**(4): p. 1103-1139.
3. Xiao, A.Y., et al., *Global incidence and mortality of pancreatic diseases: a systematic review, meta-analysis, and meta-regression of population-based cohort studies.* Lancet Gastroenterol Hepatol, 2016. **1**(1): p. 45-55.
4. Unger, R.H., et al., *Studies of pancreatic alpha cell function in normal and diabetic subjects.* J Clin Invest, 1970. **49**(4): p. 837-48.
5. Unger, R.H. and L. Orci, *The essential role of glucagon in the pathogenesis of diabetes mellitus.* Lancet, 1975. **1**(7897): p. 14-6.
6. Lat, J. and S. Caprio, *Understanding the Pathophysiology of Youth-Onset Type 2 Diabetes (T2D): Importance of Alpha-Cell Function.* J Clin Endocrinol Metab, 2022. **107**(9): p. e3957-e3958.
7. Haedersdal, S., et al., *The Role of Glucagon in the Pathophysiology and Treatment of Type 2 Diabetes.* Mayo Clin Proc, 2018. **93**(2): p. 217-239.
8. Padureanu, V., et al., *Role of antioxidants and oxidative stress in the evolution of acute pancreatitis (Review).* Exp Ther Med, 2022. **23**(3): p. 197.
9. Schulz, H.U., et al., *Oxidative stress in acute pancreatitis.* Hepatogastroenterology, 1999. **46**(29): p. 2736-50.
10. Closa, D., *Free radicals and acute pancreatitis: much ado about ... something.* Free Radic Res, 2013. **47**(11): p. 934-40.
11. Sanfey, H., G.B. Bulkley, and J.L. Cameron, *The role of oxygen-derived free radicals in the pathogenesis of acute pancreatitis.* Ann Surg, 1984. **200**(4): p. 405-13.
12. Rau, B., et al., *Pathophysiologic role of oxygen free radicals in acute pancreatitis: initiating event or mediator of tissue damage?* Ann Surg, 2000. **231**(3): p. 352-60.
13. Urunuela, A., et al., *Time-course of oxygen free radical production in acinar cells during acute pancreatitis induced by pancreatic duct obstruction.* Biochim Biophys Acta, 2002. **1588**(2): p. 159-64.
14. Chvanov, M., O.H. Petersen, and A. Tepikin, *Free radicals and the pancreatic acinar cells: role in physiology and pathology.* Philos Trans R Soc Lond B Biol Sci, 2005. **360**(1464): p. 2273-84.
15. Park, B.K., et al., *Role of oxygen free radicals in patients with acute pancreatitis.* World J Gastroenterol, 2003. **9**(10): p. 2266-9.
16. Petrov, M.S. and D. Yadav, *Global epidemiology and holistic prevention of pancreatitis.* Nat Rev Gastroenterol Hepatol, 2019. **16**(3): p. 175-184.
17. Jia, W., et al., *Application of nanotechnology in the diagnosis and treatment of acute pancreatitis.* Nanoscale Adv, 2022. **4**(8): p. 1949-1961.

18. Pendharkar, S.A., J. Mathew, and M.S. Petrov, *Age- and sex-specific prevalence of diabetes associated with diseases of the exocrine pancreas: A population-based study.* Dig Liver Dis, 2017. **49**(5): p. 540-544.
19. Pendharkar, S.A., et al., *Ethnic and geographic variations in the incidence of pancreatitis and post-pancreatitis diabetes mellitus in New Zealand: a nationwide population-based study.* N Z Med J, 2017. **130**(1450): p. 55-68.
20. Xu, C., et al., *Influence of Fatty Liver on the Severity and Clinical Outcome in Acute Pancreatitis.* PLoS One, 2015. **10**(11): p. e0142278.
21. Petrov, M.S., *Editorial: abdominal fat: a key player in metabolic acute pancreatitis.* Am J Gastroenterol, 2013. **108**(1): p. 140-2.
22. Yadav, D., G.I. Papachristou, and D.C. Whitcomb, *Alcohol-associated pancreatitis.* Gastroenterol Clin North Am, 2007. **36**(2): p. 219-38, vii.
23. Whitcomb, D.C., *Gene-environment factors that contribute to alcoholic pancreatitis in humans.* J Gastroenterol Hepatol, 2006. **21 Suppl 3**: p. S52-5.
24. Matta, B., et al., *Worldwide Variations in Demographics, Management, and Outcomes of Acute Pancreatitis.* Clin Gastroenterol Hepatol, 2020. **18**(7): p. 1567-1575 e2.
25. Hanck, C. and D.C. Whitcomb, *Alcoholic pancreatitis.* Gastroenterol Clin North Am, 2004. **33**(4): p. 751-65.
26. Buchler, M., et al., *Clinical relevance of experimental acute pancreatitis.* Eur Surg Res, 1992. **24 Suppl 1**: p. 85-8.
27. Berent, A., et al., *Initial experience with endoscopic retrograde cholangiography and endoscopic retrograde biliary stenting for treatment of extrahepatic bile duct obstruction in dogs.* J Am Vet Med Assoc, 2015. **246**(4): p. 436-46.
28. Werner, J., et al., *Pancreatic injury in rats induced by fatty acid ethyl ester, a nonoxidative metabolite of alcohol.* Gastroenterology, 1997. **113**(1): p. 286-94.
29. Pandol, S.J., et al., *Ethanol diet increases the sensitivity of rats to pancreatitis induced by cholecystokinin octapeptide.* Gastroenterology, 1999. **117**(3): p. 706-16.
30. Manabe, T. and M.L. Steer, *Protective effects of PGE2 on diet-induced acute pancreatitis in mice.* Gastroenterology, 1980. **78**(4): p. 777-81.
31. Yang, X., et al., *Experimental Acute Pancreatitis Models: History, Current Status, and Role in Translational Research.* Front Physiol, 2020. **11**: p. 614591.
32. Bertola, A., et al., *Mouse model of chronic and binge ethanol feeding (the NIAAA model).* Nat Protoc, 2013. **8**(3): p. 627-37.
33. Lombardi, B., L.W. Estes, and D.S. Longnecker, *Acute hemorrhagic pancreatitis (massive necrosis) with fat necrosis induced in mice by DL-ethionine fed with a choline-deficient diet.* Am J Pathol, 1975. **79**(3): p. 465-80.
34. Wang, J., et al., *Relationship of strain-dependent susceptibility to experimentally induced acute pancreatitis with regulation of Prss1 and Spink3 expression.* Lab Invest, 2010. **90**(5): p. 654-64.

35. Lampel, M. and H.F. Kern, *Acute interstitial pancreatitis in the rat induced by excessive doses of a pancreatic secretagogue.* Virchows Arch A Pathol Anat Histol, 1977. **373**(2): p. 97-117.
36. Niederau, C., L.D. Ferrell, and J.H. Grendell, *Caerulein-induced acute necrotizing pancreatitis in mice: protective effects of proglumide, benzotript, and secretin.* Gastroenterology, 1985. **88**(5 Pt 1): p. 1192-204.
37. Sies, H., *Oxidative eustress: On constant alert for redox homeostasis.* Redox Biol, 2021. **41**: p. 101867.
38. Durackova, Z., *Some current insights into oxidative stress.* Physiol Res, 2010. **59**(4): p. 459-469.
39. Serafini, S. and C. O'Flaherty, *Redox Regulation to Modulate Phosphorylation Events in Human Spermatozoa.* Antioxid Redox Signal, 2021.
40. Drevet, J.R., et al., *Reactive oxygen species and their consequences on the structure and function of mammalian spermatozoa.* Antioxid Redox Signal, 2021.
41. Malorni, W., et al., *Redox features of the cell: a gender perspective.* Antioxid Redox Signal, 2007. **9**(11): p. 1779-801.
42. Darenskaya, M.A., L.I. Kolesnikova, and S.I. Kolesnikov, *Oxidative Stress: Pathogenetic Role in Diabetes Mellitus and Its Complications and Therapeutic Approaches to Correction.* Bull Exp Biol Med, 2021. **171**(2): p. 179-189.
43. Leung, P.S. and Y.C. Chan, *Role of oxidative stress in pancreatic inflammation.* Antioxid Redox Signal, 2009. **11**(1): p. 135-65.
44. Escobar, J., et al., *Cross-talk between oxidative stress and pro-inflammatory cytokines in acute pancreatitis: a key role for protein phosphatases.* Curr Pharm Des, 2009. **15**(26): p. 3027-42.
45. Donthaisong, C., et al., *Infectivity and development of Opisthorchis viverrini metacercariae in immunosuppressed Barbonymus gonionotus fingerlings (Cyprinidae).* Acta Trop, 2016. **162**: p. 107-113.
46. Collins, A.E., T.M. Saleh, and B.E. Kalisch, *Naturally Occurring Antioxidant Therapy in Alzheimer's Disease.* Antioxidants (Basel), 2022. **11**(2).
47. Sharifi-Rad, M., et al., *Lifestyle, Oxidative Stress, and Antioxidants: Back and Forth in the Pathophysiology of Chronic Diseases.* Front Physiol, 2020. **11**: p. 694.
48. Zelko, I.N., T.J. Mariani, and R.J. Folz, *Superoxide dismutase multigene family: a comparison of the CuZn-SOD (SOD1), Mn-SOD (SOD2), and EC-SOD (SOD3) gene structures, evolution, and expression.* Free Radic Biol Med, 2002. **33**(3): p. 337-49.
49. Kim, C.H., E.J. Kim, and Y.K. Nam, *Superoxide Dismutase Multigene Family from a Primitive Chondrostean Sturgeon, Acipenser baerii: Molecular Characterization, Evolution, and Antioxidant Defense during Development and Pathogen Infection.* Antioxidants (Basel), 2021. **10**(2).
50. Culotta, V.C., M. Yang, and T.V. O'Halloran, *Activation of superoxide dismutases: putting the metal to the pedal.* Biochim Biophys Acta, 2006. **1763**(7): p. 747-58.

51. Boyd, S.D., et al., *The yeast copper chaperone for copper-zinc superoxide dismutase (CCS1) is a multifunctional chaperone promoting all levels of SOD1 maturation.* J Biol Chem, 2019. **294**(6): p. 1956-1966.
52. Kicinski, P., et al., *The level of extracellular superoxide dismutase in the first week of life in very and extremely low birth weight infants and the risk of developing bronchopulmonary dysplasia.* J Perinat Med, 2019. **47**(6): p. 671-676.
53. MacMillan-Crow, L.A., J.P. Crow, and J.A. Thompson, *Peroxynitrite-mediated inactivation of manganese superoxide dismutase involves nitration and oxidation of critical tyrosine residues.* Biochemistry, 1998. **37**(6): p. 1613-22.
54. Weisiger, R.A. and I. Fridovich, *Mitochondrial superoxide simutase. Site of synthesis and intramitochondrial localization.* J Biol Chem, 1973. **248**(13): p. 4793-6.
55. Kirkman, H.N. and G.F. Gaetani, *Mammalian catalase: a venerable enzyme with new mysteries.* Trends Biochem Sci, 2007. **32**(1): p. 44-50.
56. Kumar, M., et al., *Copper-induced Genotoxicity, Oxidative Stress, and Alteration in Transcriptional Level of Autophagy-associated Genes in Snakehead Fish Channa punctatus.* Biol Trace Elem Res, 2022.
57. Pizzorno, J., *Glutathione!* Integr Med (Encinitas), 2014. **13**(1): p. 8-12.
58. Huang, K.P. and F.L. Huang, *Glutathionylation of proteins by glutathione disulfide S-oxide.* Biochem Pharmacol, 2002. **64**(5-6): p. 1049-56.
59. Pompella, A., et al., *The changing faces of glutathione, a cellular protagonist.* Biochem Pharmacol, 2003. **66**(8): p. 1499-503.
60. Kosower, N.S. and E.M. Kosower, *The glutathione status of cells.* Int Rev Cytol, 1978. **54**: p. 109-60.
61. Chatterji, A., K. Sachin, and R. Sengupta, *Glutathione-dependent thioredoxin reduction and lipoamide system support in-vitro mammalian ribonucleotide reductase catalysis: a possible antioxidant redundancy.* Mol Biol Rep, 2022.
62. Obrador, E., et al., *Intertissue flow of glutathione (GSH) as a tumor growth-promoting mechanism: interleukin 6 induces GSH release from hepatocytes in metastatic B16 melanoma-bearing mice.* J Biol Chem, 2011. **286**(18): p. 15716-27.
63. Ballatori, N. and J.F. Rebbeor, *Roles of MRP2 and oatp1 in hepatocellular export of reduced glutathione.* Semin Liver Dis, 1998. **18**(4): p. 377-87.
64. Arthur, J.R., *The glutathione peroxidases.* Cell Mol Life Sci, 2000. **57**(13-14): p. 1825-35.
65. Rinaldi, R., et al., *Reactive intermediates and the dynamics of glutathione transferases.* Drug Metab Dispos, 2002. **30**(10): p. 1053-8.
66. Mariotti, M., et al., *Composition and evolution of the vertebrate and mammalian selenoproteomes.* PLoS One, 2012. **7**(3): p. e33066.
67. Buday, K. and M. Conrad, *Emerging roles for non-selenium containing ER-resident glutathione peroxidases in cell signaling and disease.* Biol Chem, 2021. **402**(3): p. 271-287.

68. Chae, H.Z., et al., *Characterization of three isoforms of mammalian peroxiredoxin that reduce peroxides in the presence of thioredoxin.* Diabetes Res Clin Pract, 1999. **45**(2-3): p. 101-12.
69. Wu, M., et al., *Peroxiredoxin, Senescence, and Cancer.* Cells, 2022. **11**(11).
70. Perez, S., et al., *Redox signaling in acute pancreatitis.* Redox Biol, 2015. **5**: p. 1-14.
71. Sevillano, S., et al., *N-acetylcysteine prevents intra-acinar oxygen free radical production in pancreatic duct obstruction-induced acute pancreatitis.* Biochim Biophys Acta, 2003. **1639**(3): p. 177-84.
72. Tsai, K., et al., *Oxidative stress: an important phenomenon with pathogenetic significance in the progression of acute pancreatitis.* Gut, 1998. **42**(6): p. 850-5.
73. Solakoglu, T., et al., *Association between antioxidants and mild acute pancreatitis.* Arab J Gastroenterol, 2017. **18**(4): p. 201-205.
74. Baser, H., et al., *Evaluation of oxidant/anti-oxidants status in patients with mild acute -pancreatitis.* Acta Gastroenterol Belg, 2016. **79**(1): p. 23-8.
75. Dabrowski, A., et al., *Oxygen-derived free radicals in cerulein-induced acute pancreatitis.* Scand J Gastroenterol, 1988. **23**(10): p. 1245-9.
76. Dabrowski, A. and M. Chwiecko, *Oxygen radicals mediate depletion of pancreatic sulfhydryl compounds in rats with cerulein-induced acute pancreatitis.* Digestion, 1990. **47**(1): p. 15-9.
77. Schoenberg, M.H., et al., *Oxygen free radicals in acute pancreatitis of the rat.* Gut, 1990. **31**(10): p. 1138-43.
78. Schoenberg, M.H., et al., *Effect of antioxidant treatment in rats with acute hemorrhagic pancreatitis.* Dig Dis Sci, 1994. **39**(5): p. 1034-40.
79. Neuschwander-Tetri, B.A., et al., *Glutathione monoethyl ester ameliorates caerulein-induced pancreatitis in the mouse.* J Clin Invest, 1992. **89**(1): p. 109-16.
80. Hatfield, D.L. and V.N. Gladyshev, *How selenium has altered our understanding of the genetic code.* Mol Cell Biol, 2002. **22**(11): p. 3565-76.
81. Rayman, M.P., *Selenium and human health.* Lancet, 2012. **379**(9822): p. 1256-68.
82. Arner, E.S. and A. Holmgren, *Physiological functions of thioredoxin and thioredoxin reductase.* Eur J Biochem, 2000. **267**(20): p. 6102-9.
83. Gromer, S., R.H. Schirmer, and K. Becker, *News and views on thioredoxin reductases.* Redox Rep, 1999. **4**(5): p. 221-8.
84. Marteyn, B., et al., *The thioredoxin reductase-glutaredoxins-ferredoxin crossroad pathway for selenate tolerance in Synechocystis PCC6803.* Mol Microbiol, 2009. **71**(2): p. 520-32.
85. Powis, G. and W.R. Montfort, *Properties and biological activities of thioredoxins.* Annu Rev Biophys Biomol Struct, 2001. **30**: p. 421-55.
86. Arner, E.S., *Focus on mammalian thioredoxin reductases--important selenoproteins with versatile functions.* Biochim Biophys Acta, 2009. **1790**(6): p. 495-526.

87. Gencheva, R. and E.S.J. Arner, *Thioredoxin Reductase Inhibition for Cancer Therapy.* Annu Rev Pharmacol Toxicol, 2022. **62**: p. 177-196.
88. Miranda-Vizuete, A., et al., *Human mitochondrial thioredoxin reductase cDNA cloning, expression and genomic organization.* Eur J Biochem, 1999. **261**(2): p. 405-12.
89. Miranda-Vizuete, A., A.E. Damdimopoulos, and G. Spyrou, *The mitochondrial thioredoxin system.* Antioxid Redox Signal, 2000. **2**(4): p. 801-10.
90. Miranda-Vizuete, A., et al., *The mammalian testis-specific thioredoxin system.* Antioxid Redox Signal, 2004. **6**(1): p. 25-40.
91. Gasdaska, J.R., et al., *Human thioredoxin reductase gene localization to chromosomal position 12q23-q24.1 and mRNA distribution in human tissue.* Genomics, 1996. **37**(2): p. 257-9.
92. Rundlof, A.K., et al., *Prominent expression of the selenoprotein thioredoxin reductase in the medullary rays of the rat kidney and thioredoxin reductase mRNA variants differing at the 5 ' untranslated region.* Biochemical Journal, 2000. **347**: p. 661-668.
93. Rozell, B., A. Holmgren, and H.A. Hansson, *Ultrastructural demonstration of thioredoxin and thioredoxin reductase in rat hepatocytes.* Eur J Cell Biol, 1988. **46**(3): p. 470-7.
94. Rozell, B., et al., *Immunohistochemical localization of thioredoxin and thioredoxin reductase in adult rats.* Eur J Cell Biol, 1985. **38**(1): p. 79-86.
95. Selenius, M., et al., *Selenium and the selenoprotein thioredoxin reductase in the prevention, treatment and diagnostics of cancer.* Antioxid Redox Signal, 2010. **12**(7): p. 867-80.
96. Holmgren, A. and J. Lu, *Thioredoxin and thioredoxin reductase: current research with special reference to human disease.* Biochem Biophys Res Commun, 2010. **396**(1): p. 120-4.
97. Becker, K., et al., *Thioredoxin reductase as a pathophysiological factor and drug target.* European Journal of Biochemistry, 2000. **267**(20): p. 6118-6125.
98. Watson, W.H., et al., *Thioredoxin and its role in toxicology.* Toxicol Sci, 2004. **78**(1): p. 3-14.
99. Nordberg, J. and E.S. Arner, *Reactive oxygen species, antioxidants, and the mammalian thioredoxin system.* Free Radic Biol Med, 2001. **31**(11): p. 1287-312.
100. Miranda-Vizuete, A., A.E. Damdimopoulos, and G. Spyrou, *cDNA cloning, expression and chromosomal localization of the mouse mitochondrial thioredoxin reductase gene(1).* Biochim Biophys Acta, 1999. **1447**(1): p. 113-8.
101. Rigobello, M.P., et al., *Purification of mitochondrial thioredoxin reductase and its involvement in the redox regulation of membrane permeability.* Free Radic Biol Med, 1998. **24**(2): p. 370-6.
102. Sun, Q.A., et al., *Redox regulation of cell signaling by selenocysteine in mammalian thioredoxin reductases.* J Biol Chem, 1999. **274**(35): p. 24522-30.
103. Rundlof, A.K., et al., *Prominent expression of the selenoprotein thioredoxin reductase in the medullary rays of the rat kidney and thioredoxin reductase*

mRNA variants differing at the 5' untranslated region. Biochem J, 2000. **347 Pt 3**: p. 661-8.
104. Watabe, S., et al., *Mitochondrial thioredoxin reductase in bovine adrenal cortex its purification, properties, nucleotide/amino acid sequences, and identification of selenocysteine.* Eur J Biochem, 1999. **264**(1): p. 74-84.
105. Conrad, M., et al., *Essential role for mitochondrial thioredoxin reductase in hematopoiesis, heart development, and heart function.* Mol Cell Biol, 2004. **24**(21): p. 9414-23.
106. Jakupoglu, C., et al., *Cytoplasmic thioredoxin reductase is essential for embryogenesis but dispensable for cardiac development.* Mol Cell Biol, 2005. **25**(5): p. 1980-8.
107. Sun, Q.A., et al., *Selenoprotein oxidoreductase with specificity for thioredoxin and glutathione systems.* Proc Natl Acad Sci U S A, 2001. **98**(7): p. 3673-8.
108. Bondareva, A.A., et al., *Effects of thioredoxin reductase-1 deletion on embryogenesis and transcriptome.* Free Radic Biol Med, 2007. **43**(6): p. 911-23.
109. Aichler, M., et al., *Selenium status alters tumour differentiation but not incidence or latency of pancreatic adenocarcinomas in Ela-TGF-alpha p53+/ mice.* Carcinogenesis, 2007. **28**(9): p. 2002-7.
110. Bankhead, P., et al., *QuPath: Open source software for digital pathology image analysis.* Sci Rep, 2017. **7**(1): p. 16878.
111. Schindelin, J., et al., *Fiji: an open-source platform for biological-image analysis.* Nat Methods, 2012. **9**(7): p. 676-82.
112. Nakhai, H., et al., *Ptf1a is essential for the differentiation of GABAergic and glycinergic amacrine cells and horizontal cells in the mouse retina.* Development, 2007. **134**(6): p. 1151-60.
113. Ismail, O.Z. and V. Bhayana, *Lipase or amylase for the diagnosis of acute pancreatitis?* Clin Biochem, 2017. **50**(18): p. 1275-1280.
114. Chen, Y., et al., *Glutathione defense mechanism in liver injury: insights from animal models.* Food Chem Toxicol, 2013. **60**: p. 38-44.
115. Lin, Y., et al., *The hepatoprotective role of reduced glutathione and its underlying mechanism in oxaliplatin-induced acute liver injury.* Oncol Lett, 2018. **15**(2): p. 2266-2272.
116. Olowe, R., et al., *Approaches for Reactive Oxygen Species and Oxidative Stress Quantification in Epilepsy.* Antioxidants (Basel), 2020. **9**(10).
117. Garg, P.K., et al., *Association of extent and infection of pancreatic necrosis with organ failure and death in acute necrotizing pancreatitis.* Clin Gastroenterol Hepatol, 2005. **3**(2): p. 159-66.
118. Beyer, G., et al., *Acute and Chronic Pancreatitis.* Dtsch Arztebl Int, 2022. **119**(29-30): p. 495-501.
119. Berber, A., et al., *Effect of different polishing systems and drinks on the color stability of resin composite.* J Contemp Dent Pract, 2013. **14**(4): p. 662-7.
120. Zhang, J., et al., *Targeting the Thioredoxin System for Cancer Therapy.* Trends Pharmacol Sci, 2017. **38**(9): p. 794-808.

121. Lundberg, A.H., et al., *Trypsin stimulates production of cytokines from peritoneal macrophages in vitro and in vivo.* Pancreas, 2000. **21**(1): p. 41-51.
122. Handy, D.E., et al., *Glutathione peroxidase-1 regulates mitochondrial function to modulate redox-dependent cellular responses.* J Biol Chem, 2009. **284**(18): p. 11913-21.
123. Brigelius-Flohe, R. and L. Flohe, *Regulatory Phenomena in the Glutathione Peroxidase Superfamily.* Antioxid Redox Signal, 2020. **33**(7): p. 498-516.
124. Chu, F.F., J.H. Doroshow, and R.S. Esworthy, *Expression, characterization, and tissue distribution of a new cellular selenium-dependent glutathione peroxidase, GSHPx-GI.* J Biol Chem, 1993. **268**(4): p. 2571-6.
125. Stancill, J.S., et al., *Deletion of Thioredoxin Reductase Disrupts Redox Homeostasis and Impairs beta-Cell Function.* Function (Oxf), 2022. **3**(4): p. zqac034.
126. Bosello Travain, V., et al., *Lack of glutathione peroxidase-8 in the ER impacts on lipid composition of HeLa cells microsomal membranes.* Free Radic Biol Med, 2020. **147**: p. 80-89.
127. Lu, S.C., *Glutathione synthesis.* Biochim Biophys Acta, 2013. **1830**(5): p. 3143-53.
128. Harris, I.S., et al., *Deubiquitinases Maintain Protein Homeostasis and Survival of Cancer Cells upon Glutathione Depletion.* Cell Metab, 2019. **29**(5): p. 1166-1181 e6.
129. Forman, H.J., H. Zhang, and A. Rinna, *Glutathione: overview of its protective roles, measurement, and biosynthesis.* Mol Aspects Med, 2009. **30**(1-2): p. 1-12.
130. Anderson, M.E. and A. Meister, *Dynamic state of glutathione in blood plasma.* J Biol Chem, 1980. **255**(20): p. 9530-3.
131. Estrela, J.M., A. Ortega, and E. Obrador, *Glutathione in cancer biology and therapy.* Crit Rev Clin Lab Sci, 2006. **43**(2): p. 143-81.
132. Ookhtens, M., A.V. Mittur, and N.A. Erhart, *Changes in plasma glutathione concentrations, turnover, and disposal in developing rats.* Am J Physiol, 1994. **266**(3 Pt 2): p. R979-88.
133. Lushchak, V.I., *Glutathione homeostasis and functions: potential targets for medical interventions.* J Amino Acids, 2012. **2012**: p. 736837.
134. Stenson, W.F., E. Lobos, and H.J. Wedner, *Glutathione depletion inhibits amylase release in guinea pig pancreatic acini.* Am J Physiol, 1983. **244**(3): p. G273-7.
135. Yu, H., H. Klonowski-Stumpe, and R. Luthen, *Glutathione might exert an important function in caerulein-stimulated amylase release in isolated rat pancreatic acini.* Pancreas, 2002. **24**(1): p. 53-62.
136. Krauth-Siegel, R.L., H. Bauer, and R.H. Schirmer, *Dithiol proteins as guardians of the intracellular redox milieu in parasites: old and new drug targets in trypanosomes and malaria-causing plasmodia.* Angew Chem Int Ed Engl, 2005. **44**(5): p. 690-715.

137. Rodman, S.N., et al., *Enhancement of Radiation Response in Breast Cancer Stem Cells by Inhibition of Thioredoxin- and Glutathione-Dependent Metabolism.* Radiat Res, 2016. **186**(4): p. 385-395.
138. Kiebala, M., et al., *Dual targeting of the thioredoxin and glutathione antioxidant systems in malignant B cells: a novel synergistic therapeutic approach.* Exp Hematol, 2015. **43**(2): p. 89-99.
139. Sang, J., et al., *Jolkinolide B targets thioredoxin and glutathione systems to induce ROS-mediated paraptosis and apoptosis in bladder cancer cells.* Cancer Lett, 2021. **509**: p. 13-25.
140. Husain, S. and E. Thrower, *Molecular and cellular regulation of pancreatic acinar cell function.* Curr Opin Gastroenterol, 2009. **25**(5): p. 466-71.
141. Greer, R.L., et al., *Numb regulates acinar cell dedifferentiation and survival during pancreatic damage and acinar-to-ductal metaplasia.* Gastroenterology, 2013. **145**(5): p. 1088-1097 e8.
142. Jensen, J.N., et al., *Recapitulation of elements of embryonic development in adult mouse pancreatic regeneration.* Gastroenterology, 2005. **128**(3): p. 728-41.
143. Ardito, C.M., et al., *EGF receptor is required for KRAS-induced pancreatic tumorigenesis.* Cancer Cell, 2012. **22**(3): p. 304-17.
144. Scotti, M.L., et al., *Protein kinase C iota regulates pancreatic acinar-to-ductal metaplasia.* PLoS One, 2012. **7**(2): p. e30509.
145. Liou, G.Y., et al., *Protein kinase D1 drives pancreatic acinar cell reprogramming and progression to intraepithelial neoplasia.* Nat Commun, 2015. **6**: p. 6200.
146. Radyk, M.D., et al., *Abstract 2176: NADPH production and redox homeostasis regulate acinar to ductal metaplasia.* Cancer Research, 2022. **82**(12_Supplement): p. 2176-2176.
147. Sato, H., et al., *Induction of cystine transport via system x-c and maintenance of intracellular glutathione levels in pancreatic acinar and islet cell lines.* Biochim Biophys Acta, 1998. **1414**(1-2): p. 85-94.
148. Liou, G.Y., et al., *Mutant KRas-Induced Mitochondrial Oxidative Stress in Acinar Cells Upregulates EGFR Signaling to Drive Formation of Pancreatic Precancerous Lesions.* Cell Rep, 2016. **14**(10): p. 2325-36.
149. Nelson, B., *Defining Roles of Metabolic Reprogramming in Pancreatic Tumorigenesis and Tumor Maintenance*. 2020.
150. Tekin, C., et al., *Protease-activated receptor 1 drives and maintains ductal cell fates in the premalignant pancreas and ductal adenocarcinoma.* Mol Oncol, 2021. **15**(11): p. 3091-3108.
151. Demcollari, T.I., A.M. Cujba, and R. Sancho, *Phenotypic plasticity in the pancreas: new triggers, new players.* Curr Opin Cell Biol, 2017. **49**: p. 38-46.
152. Liou, G.Y., et al., *Macrophage-secreted cytokines drive pancreatic acinar-to-ductal metaplasia through NF-kappaB and MMPs.* J Cell Biol, 2013. **202**(3): p. 563-77.

153. Houbracken, I., et al., *Lineage tracing evidence for transdifferentiation of acinar to duct cells and plasticity of human pancreas.* Gastroenterology, 2011. **141**(2): p. 731-41, 741 e1-4.

ACKNOWLEDGES

It's been almost four years since I started my doctoral study at Technical University of Munich**, AG Schmid / Einwächter**. Now, I am very much looking forward to closing this chapter and start a new challenge for my life. Looking back on these years, the people who helped me and guided me to the pinnacle of knowledge have always been engraved in my heart.

I would like to thank my main scientific advisor **Dr. Henrik Einwächter** for enlightening me when I was confused about my project. I can still remember when I first joined the group, Dr. Henrik Einwächter introduced me to each member of the group and explained to me carefully the specific research direction and focus of our group. Since I was an attending plastic surgeon in China before, I knew very little about pancreatic research, so Dr. Henrik Einwächter showed great patience to support me. Thank you for all your ideas, valuable feedback, for improving my research skills and for giving me more opportunities to practice and present.

I would like to thank my supervisor **Prof. Dr. Roland M. Schmid** for accepting me into AG Schmid / Einwächter as doctoral student. Your profound expertise, rigorous academic approach, and dedication to excellence have had a profound impact on me. I truly benefited from your guidance, support, and your valuable advice and ideas.

Also, I would like to thank **Prof. Dr. Ihsan Ekin Demir** for being my mentor. Thanks for his ongoing support, guidance, and encouragement.

Furthermore, many thanks to all my co-workers, AG Schmid / Einwächter: **Nirav Florian Chhabra, Thorsten Neuß, Sankaranarayanan Ramasubramanian, Leeanne Mundle, Min-Chun Chen, Chao Wu, Ali Altaee, Judit Desztics, Andrea Stroppiana, Mathilde Neuhofer, Anke Bettenbrock, Melanie Höcker and Anja Motz**, who helped

me with my doctoral work. Special thanks to **Thorsten and Nirav** for taking the time to revise my thesis manuscript. Your comments have been very valuable and helpful.

Finally, I would like to express my deep gratitude to my family members.
Thanks to my mother, **Ms. Ju**, who has always supported and helped me in my life, both spiritually and materially.
Without my mother, I would not be who I am today.

Thanks to my husband, **Thomas Roth**, for always cheering me up when I was down, giving me a strong shoulder to lean on, and encouraging me to move forward.
Thanks to his lasting support and understanding, I was able to work and live more easily in Germany. I would also like to thank him for helping me with the German translation of my abstract and resume.